CCMS-88-02
VPI-E-88-5

VIRGINIA TECH

CENTER FOR COMPOSITE MATERIALS AND STRUCTURES

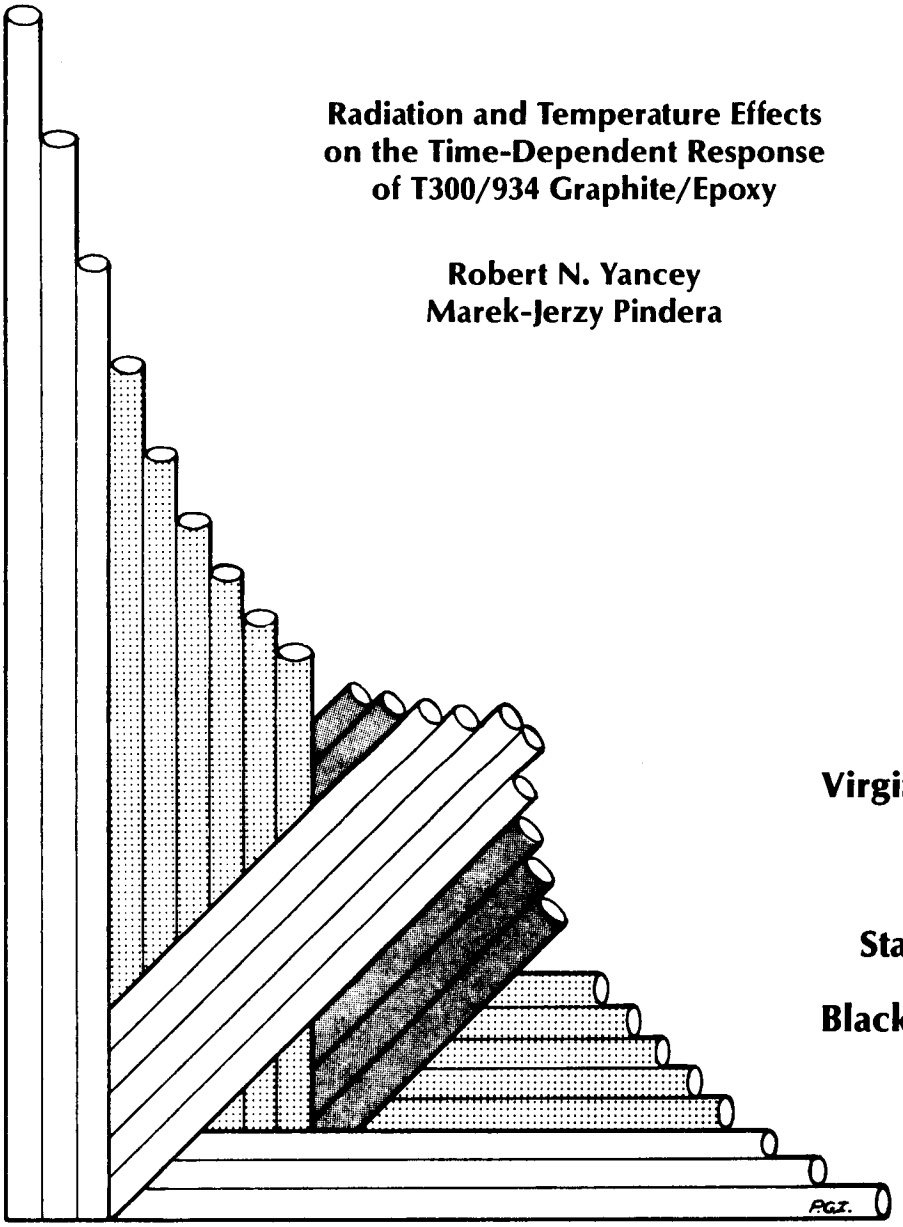

Radiation and Temperature Effects on the Time-Dependent Response of T300/934 Graphite/Epoxy

Robert N. Yancey
Marek-Jerzy Pindera

Virginia Polytechnic Institute and State University

Blacksburg, Virginia 24061

College of Engineering
Virginia Polytechnic Institute and State University
Blacksburg, Virginia 24061

March 1988

CCMS-88-02
VPI-E-88-5

Radiation and Temperature Effects on the Time-Dependent Response of T300/934 Graphite/Epoxy

Robert N. Yancey[1]
Marek-Jerzy Pindera[2]

Department of Engineering Science & Mechanics

Interim Report 69
The NASA-Virginia Tech Composites Program
NASA Grant NAG-1-343

Prepared for:

Applied Materials Branch
National Aeronautics and Space Administration
Langley Research Center
Hampton, Virginia 23665

---

[1] Graduate Student, Department of Engineering Science & Mechanics

[2] Assistant Professor, Department of Engineering Science & Mechanics

Radiation and Temperature Effects on the Time-Dependent Response of T300/934 Graphite/Epoxy

(ABSTRACT)

A time-dependent characterization study was performed on T300/934 graphite/epoxy in a simulated space environment. Creep tests on irradiated and non-irradiated graphite/epoxy and bulk resin specimens were carried out at temperatures of 72 °F and 250 °F. Irradiated specimens were exposed to dosages of penetrating electron radiation equal to 30 years exposure at GEO-synchronous orbit. Radiation was shown to have little effect on the creep response of both the composite and bulk resin specimens at 72 °F while radiation had a significant effect at 250 °F. A healing process was shown to be present in the irradiated specimens where broken bonds in the epoxy due to radiation recombined over time to form cross-links in the 934 resin structure. An analytical, micromechanical model was also developed to predict the viscoelastic response of fiber reinforced composite materials. The model was shown to correlate well with experimental results for linearly viscoelastic materials with relatively small creep strains.

Acknowledgements

This research was supported by the NASA-Virginia Tech Composites Program under Grant NAG-1-343. The present investigation is a direct outgrowth of the work on radiation effects of composites initiated by Professor Carl Herakovich and the late George Sykes of NASA Langley Research Center. Appreciation is expressed to Wayne Slemp and Joan Funk at NASA Langley Research Center for their help in preparing the specimens. Appreciation is also expressed to Professor Hal Brinson for the use of testing equipment located in the Laboratory for Experimental Mechanics and Non-Metallic Materials Characterization at VPI & SU.

Table of Contents

List of Illustrations

List of Tables

1.0 Introduction

1.1 Composites

The use of resin-matrix composites has become quite commonplace in the aerospace field today. Much of the truss structure of the proposed space station will be made of graphite/epoxy [1]. High Technology Communication Satellites and future Space Platforms such as the Space Telescope would be virtually impossible without composites [2-7]. These projects are a result of an increased awareness of the advantages composite materials offer. The most commonly mentioned advantages are superior strength-to-weight and stiffness-to-weight ratios but other advantages are beginning to surface. Some of these additional advantages are low thermal conductivity, low thermal expansion with the ability to eliminate it completely, and the ability to tailor composites to specifically meet certain needs. Engineers now look to composite materials not only to save weight but to design structures that meet requirements that were previously thought unrealistic with more common materials such as metals and plastics. Good dimensional stability and high specific damping characteristics make composites an excellent choice for projects such as the Space Telescope and communication satellites [1]. With the advent of sophisticated computer codes that can deal with the complexities involved in the analysis of composite materials, design engineers see the unlimited

potential they have to design extremely sophisticated and efficient structures [8]. Composite materials are changing the entire approach to structural design.

Although we have come a long way in understanding composite materials, problems and challenges still exist with many of these materials. Resin matrix composites such as graphite/epoxy are presently the most widely used advanced composites. This type of composite is limited in most cases by the resin itself which has a limited operating temperature range and properties that can change noticeably within this range. The resin can also age with time and become embrittled [9-11]. Another characteristic of polymer resins is creep. Epoxy resins are made up of long molecular chains that are cross-linked together to form a complicated molecular structure. The cross-linking is highly irregular throughout the internal structure and this allows chains to bend, slide, twist, and curl around each other. Chemical bonds are constantly broken and reformed and as a result, the structure never remains the same. When a tensile load is applied to a polymer, kinks in the molecular chains are quickly straightened which produces an instantaneous deformation. This is usually referred to as the elastic response. If the load remains, however, these chains slowly begin to slide, twist and uncurl causing more deformation. This time-dependent deformation is known as creep [12,13]. Creep presents unique problems to design engineers since they must not only design a structure to withstand present loads and displacements but must also consider the given loads and displacements over the design lifetime of the structure. The structure is no longer "rigid" but is constantly displacing and dissipating energy. This introduces complexities into the design of dimensionally stable structures. Much work has been done to help designers better quantify the creep characteristics of resins and more importantly resin matrix composites [14]. Some of this work, paying special attention to the effects of the space environment on creep behavior, will be discussed below.

1.2 Space Environment

Structural designers need to pay special attention to the extremes of the space environment when designing space structures. These environmental factors can seriously affect structural integrity of resin matrix composites. The space environment has many conditions not commonly regarded in the design of earth-bound structures. The major environmental factors that need to be considered in space are vacuum, temperature cycling, and radiation. These factors are most pronounced in high earth orbits such as GEO-synchronous orbit. Previous work dealing with the effect of these environmental extremes on resin matrix composites is outlined below.

1.2.1 Vacuum

All space environments are characterized by near vacuum. Although this is often seen as advantageous since it helps eliminate corrosive environments and can decrease structural degradation, it is a major concern with resin matrix composites. Moisture, along with small trapped organic molecules such as carbon monoxide (CO) and carbon dioxide (CO_2) that have been separated from the polymer chains of the epoxy, can "outgas" from the polymer network drying out and embrittling the epoxy [9]. This outgassing can also cause voids to form, thus disrupting the molecular structure of the resin. These voids can be of two types. First, they can be small internal voids left behind by the space occupied by the outgassed molecule. This increases the free volume of the epoxy which can facilitate movement of the molecular chains and thereby increase the amount that the material will creep over time [14,15]. Secondly, if outgassing occurs within the composite, larger voids can develop in the composite network. Gas pockets can form within the structure causing delaminations and matrix cracking both of which can significantly affect the composite strength and stiffness [16,17].

1.2.2 Temperature

The space environment is also characterized by large temperature fluctuations. Since the environment is a near vacuum, there are few particles that can hold heat. For this reason, the temperature in space is almost entirely dependent on whether the region is in the sun's path or blocked from its rays. Orbiting structures can experience temperatures as high as + 250 °F when in the light and heat of the sun and as low as -250 °F when blocked from the sun's rays.

The temperature extremes and temperature cycling experienced by orbiting spacecraft can seriously affect resin matrix composites due to the dissimilar thermal properties of the composite constituents. The coefficient of thermal expansion of a resin is quite different than that of a stiff fiber such as graphite. With a temperature change, the resin in bulk form will expand or contract differently than a graphite fiber under the same conditions. Since the composite is a rigid structure composed of fibers and resin, an expansion or contraction compromise is reached by the two components. As a result, each component compensates for the expansion or contraction deficiency with a mechanical load. For example, a graphite/epoxy composite when cooled will experience, in the direction of the fibers, a mechanical tensile load in the matrix and a mechanical compressive load in the fibers. In a free and unconstrained state, the matrix upon cooling contracts significantly and the graphite fiber expands slightly [18]. Being constrained by each other in the composite, the fiber and matrix are restricted in their respective expansion or contraction. The result is tension in the matrix and compression in the fiber. With this behavior, thermal cycling actually results in mechanical load cycling of the resin and fibers. This load cycling can fatigue the structure at the fiber-resin level which often results in microcracking of the resin matrix [19].

Temperature can also have an effect on the epoxy network itself. Temperature increases the motion of molecular chains in the epoxy allowing for a less rigid molecular structure which facilitates creep [20]. The increased motion coupled with the increased free volume created by outgassing can significantly increase the ability of the molecules to slide, twist, and uncurl.

1.2.3 Radiation

Another significant factor in the space environment is radiation. There are many types of radiation in space and the types change depending on the location in orbit. Several types of radiation experienced in high-earth orbits are not significant at low-earth orbits. At high-earth orbits, low energy radiation such as visible and ultraviolet light is present along with charged particles such as electrons and protons, and high energy radiation such as cosmic, gamma and x-rays [21,22]. Low energy forms of radiation are believed to have little if any effect on resin matrix composites. High energy forms of radiation can affect surface properties of materials but are unable to penetrate significantly into the material. Charged particles, if accelerated to high speeds, can penetrate the structure and cause damage. These charged particles seem to damage the polymer resin structure more adversely than they do stiff fibers such as graphite. Graphite fibers have been shown to be essentially inert to all forms of radiation [23].

Most scientists conclude that the main effect of radiation is chain scission and separation of low molecular weight products such as radicals and ionic centers from the epoxy network. Chain scission increases the mobility of molecular chains and also enhances disentanglement of the low molecular weight chains formed [26]. The increased chain mobility and disentanglement can cause chain slippage which manifests itself as creep behavior [26,27]. Along with molecular chain movement, unstable radicals present in the irradiated epoxy will eventually recombine. Recombination of radicals is highly dependent on chain mobility. At low temperatures, the radicals produced by radiation are quite immobile and remain trapped in the structure. As temperature increases, the radicals move more freely which allows them to recombine. Based on thermal cycling and Dynamic Mechanical Analysis (DMA) data, Tenney, Sykes, and Bowles [21] proposed that all the radicals will recombine eventually and that temperature accelerates this activity. Recombination of radicals results in increased cross-linking creating a more rigid structure but one more brittle as well [21,22,26].

1.3 Background

Much work has been done at Virginia Tech to quantify the effects of the space environment on T300/934 graphite/epoxy. The work was initiated by Herakovich and Sykes and they conducted separate studies with Milkovich, Reed, and Fox. A brief summary of their work is given below, emphasizing the results leading to the present study.

1.3.1 Tensile Results

Milkovich, Herakovich, and Sykes [16] studied the effects of radiation and temperature on the tensile response of T300/934 graphite/epoxy. Quasi-static monotonic tensile tests were performed on unidirectional coupons with fiber orientations of 0°, 10°, 45°, and 90°. Three temperatures were used, namely cryogenic (-250 °F), room (+ 72 °F), and elevated (+ 250 °F). Half of the specimens were subjected to electron radiation representative of 30 years in GEO-synchronous orbit. For the 0° coupons, radiation had little effect on stiffness. Radiation combined with elevated temperature, however, significantly reduced the strength. For the 90° coupons, radiation lowered the strength for all three test temperatures and lowered the stiffness at elevated temperature. For the 10° and 45° off-axis coupons, radiation had a significant effect on strength at the elevated temperature but little effect on stiffness. For the 10°, 45°, and 90° coupons, radiation at elevated temperature greatly increased the onset of nonlinear behavior in the stress-strain response.

Milkovich, et al. [16] also performed a Dynamic Mechanical Analysis (DMA) and Thermo Mechanical Analysis (TMA) on irradiated and non-irradiated specimens. The DMA test is a way to determine the glass transition temperature (T_g) by monitoring damping of the polymer as a function of temperature. Determination of how the glass transition temperature changes indicates the state of the epoxy molecular chain network. As shown in Figure 1, reduction in the glass transition

temperature indicates reduction in the cross-link density. An increase in the magnitude of the damping peek indicates reduction in the average molecular weight of the molecular chains which represents the average size of the molecules in the network. Widening of the peek curve indicates greater distribution of molecular weights. Tests of the baseline and irradiated specimens indicated that radiation resulted in the reduction of cross-link density and average molecular weight. Radiation also increased the distribution of molecular weights. Figure 2 illustrates these results.

The TMA test evaluates the relative softness of a material with respect to temperature. A probe is lightly spring-loaded onto the specimen and its penetration is monitored as a function of temperature. The results of the TMA tests performed by Milkovich, et al. [16] show that irradiation softened the material at lower temperatures indicating both a lowering of the T_g and in increase in the creep behavior. This is shown in Figure 3. The anomaly at the end of the TMA curve is due to the probe being pushed away from the irradiated specimen at elevated temperature due to delaminations caused by low molecular weight products boiling off.

Milkovich, et al. [16] concluded that irradiation affected only the epoxy resin and had little effect on the graphite fibers. He also concluded that radiation resulted in chain scission of the epoxy network which serves to weaken the epoxy resin. The mechanism described by Milkovich, et al. [16] is one in which small molecular groups are broken off from the main chains due to radiation. These small molecules tend to "freeze" the structure at low temperatures creating a stiffer structure. At high temperatures, these molecules boil off and "plasticize" the material. Milkovich, et al. [16] concluded that this mechanism explains the nonlinear behavior seen at elevated temperatures in the irradiated condition.

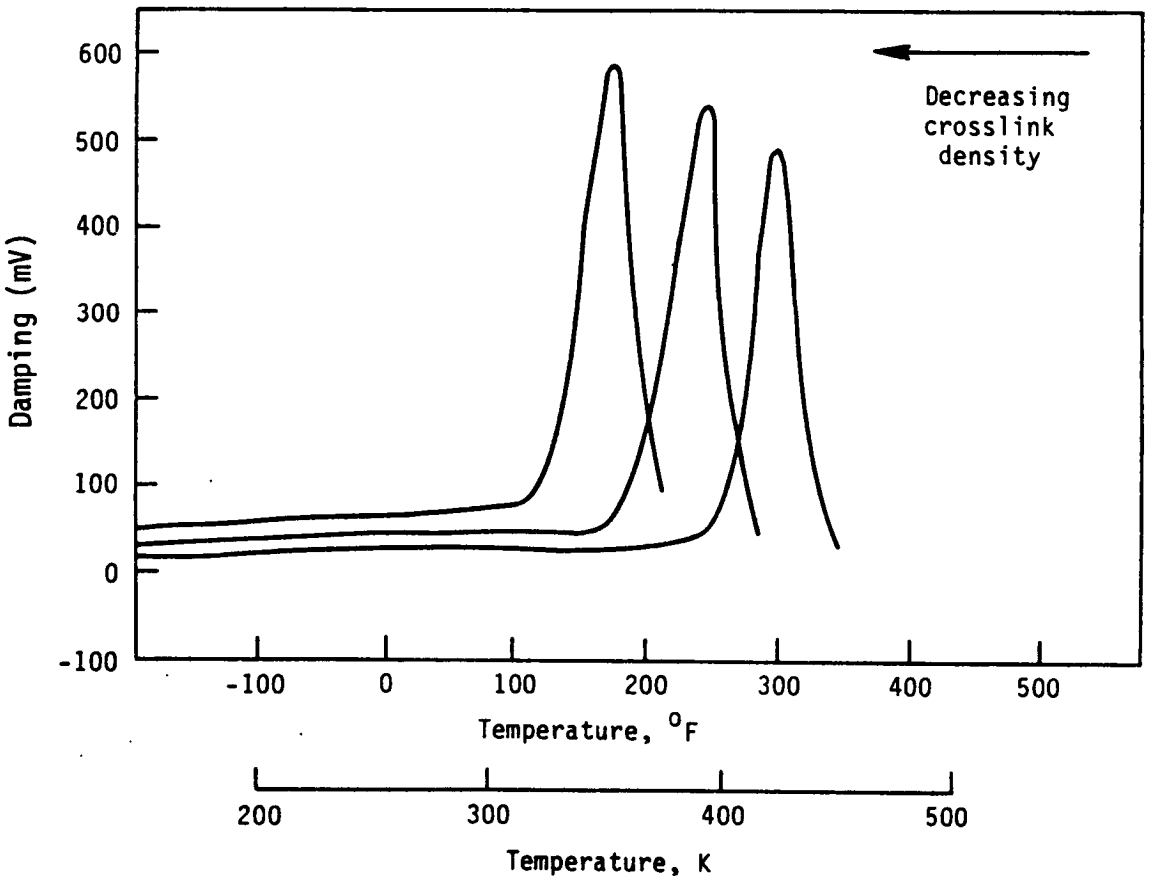

Figure 1. Shifting of DMA Curves: [27]

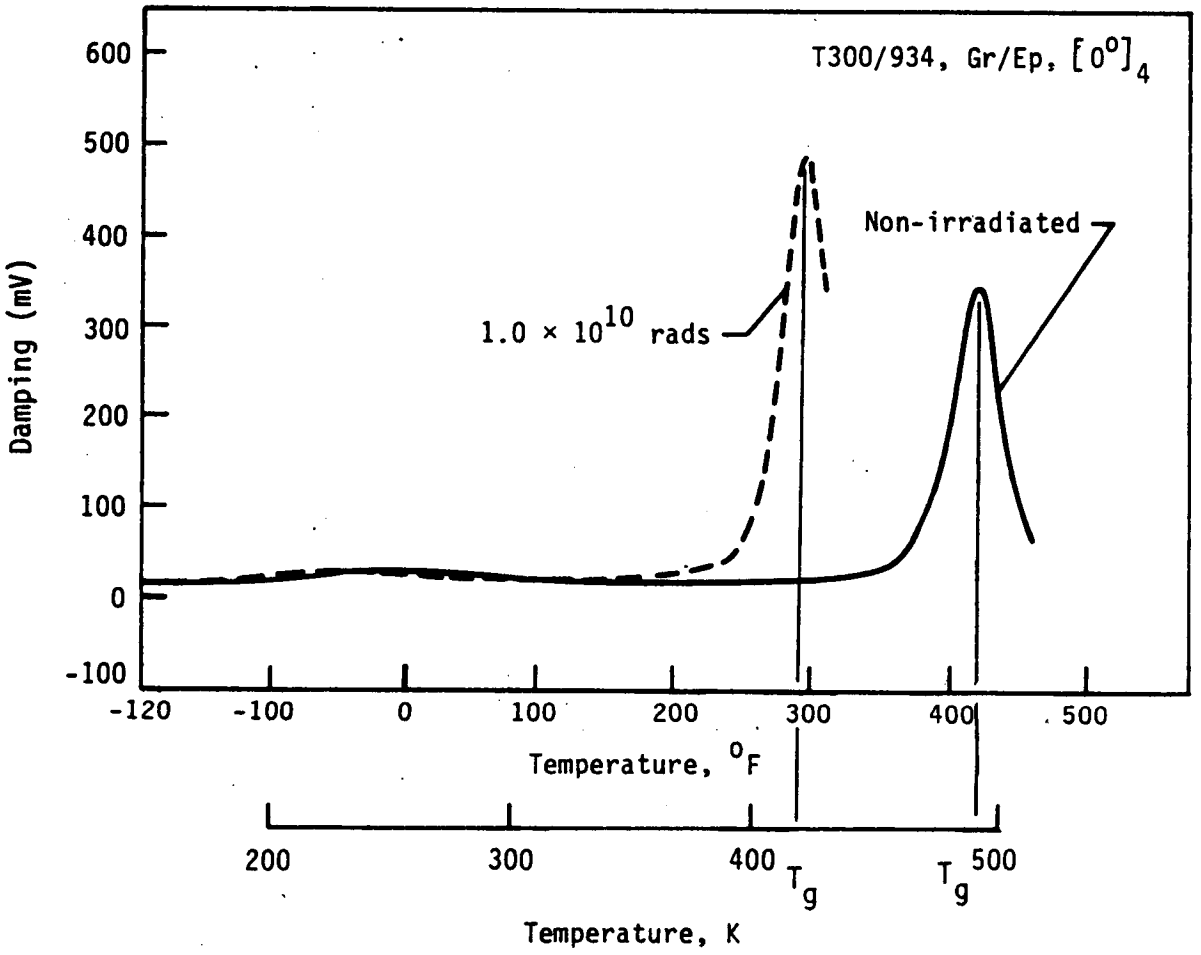

Figure 2. Results of DMA Test on T300/934: [27]

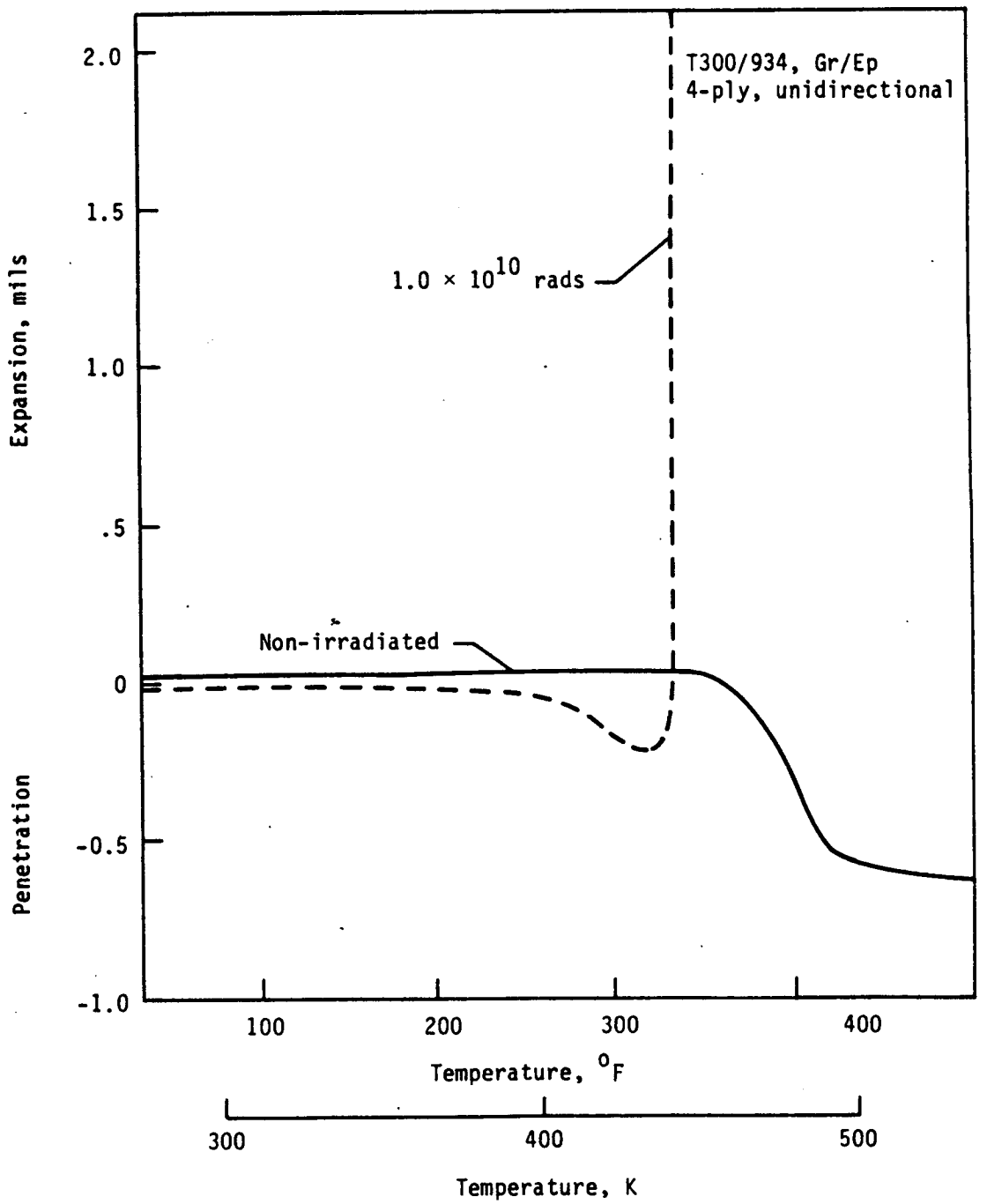

Figure 3. TMA Results for T300/934: [27]

1.3.2 Modified Epoxy and Cyclic Results

Reed, Herakovich, and Sykes [23] continued the investigation of Milkovich, et al. [16] and attempted to verify one conclusion of that investigation. Milkovich, et al. [16] concluded that small molecules broken off during irradiation were a result of additives used in the processing of the epoxy resin and not an inherent property of the epoxy resin itself. Milkovich, et al. [16] proposed to eliminate the additive and thus solve the problem. In order to verify Milkovich's hypothesis, Reed, et al. [23] performed the same tests with a modified T300/934 graphite/epoxy where the processing additives had been left out during the manufacturing process. Little difference was seen with the results of Reed, et al. [23] in comparison with Milkovich, et al. [16]. It was concluded that the radiation was affecting the epoxy network itself.

Reed, et al. [23] also performed cyclic tension tests on the original (unmodified) epoxy composite investigated by Milkovich, et al. [16]. Each specimen was subjected to quasi-static loading beyond the linear range, subsequent unloading to zero, and finally immediate re-loading to failure. These tests were conducted to evaluate better the nature of the nonlinear behavior observed by Milkovich, et al. [16]. Figure 4 and Figure 5 show sample results of the longitudinal cyclic response of the 10° off-axis specimen under various conditions of temperature and radiation. As seen, hysteresis is present in the response for all conditions and the second and final loading does not proceed through the reversal point of the loading/unloading cycle. If the nonlinear behavior observed by Milkovich, et al. [16] were purely plastic, the re-loading response should pass through the reversal point of the preceding cycle. The fact that in this case the reloading proceeds as it does suggests that viscoelastic behavior is present. The irradiated coupons at elevated temperature have a much larger hysteresis indicating a greater contribution of viscoelastic behavior. Figure 6 and Figure 7 show the shear response in the material principal coordinate system of the 10° off-axis specimen. For shear, the hysteresis is larger in all cases indicating that the viscoelastic response is dominant in shear.

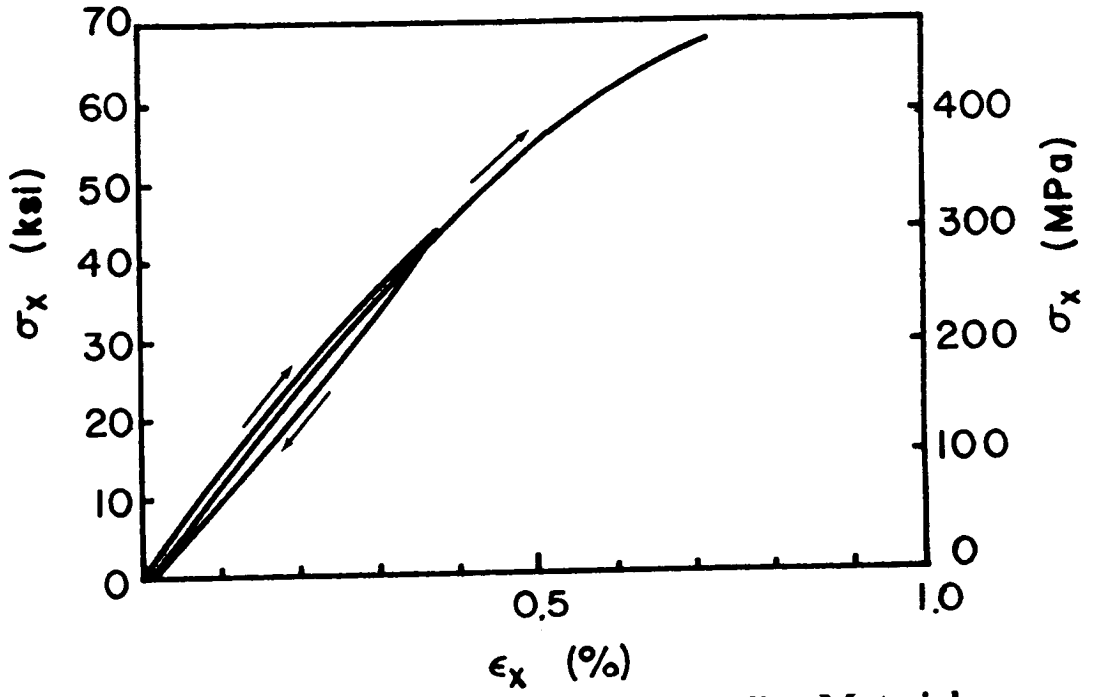

a) Room Temperature Tested - Baseline Material

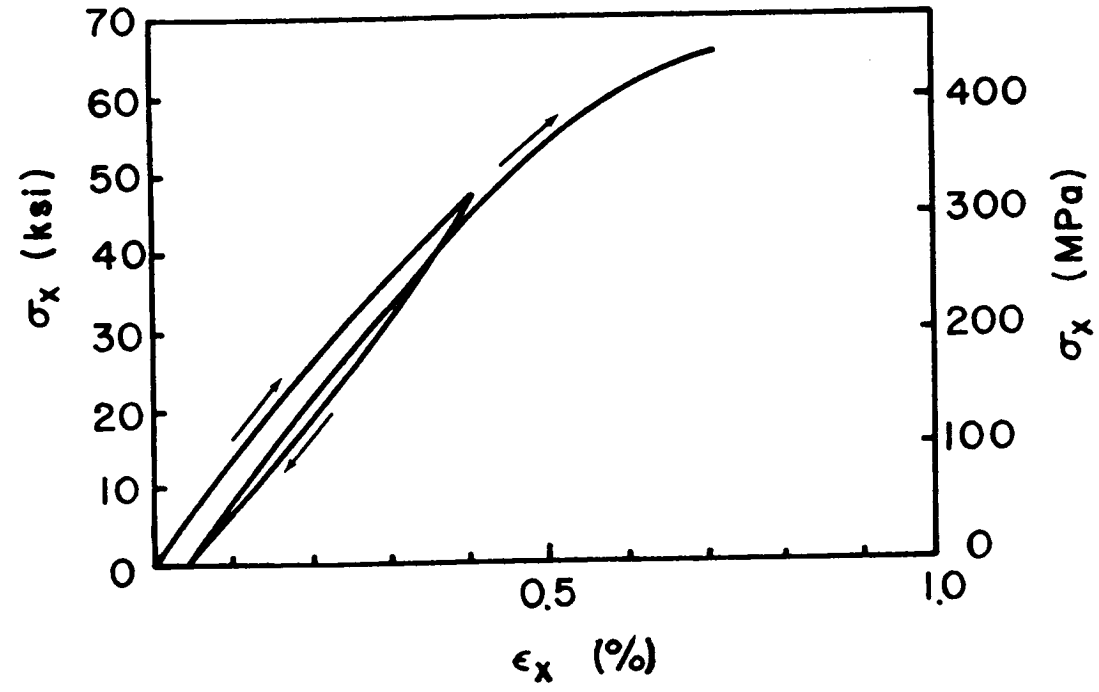

c) Room Temperature Tested - Irradiated Material

Figure 4. 10° Cyclic Room Temperature Axial Results: [28]

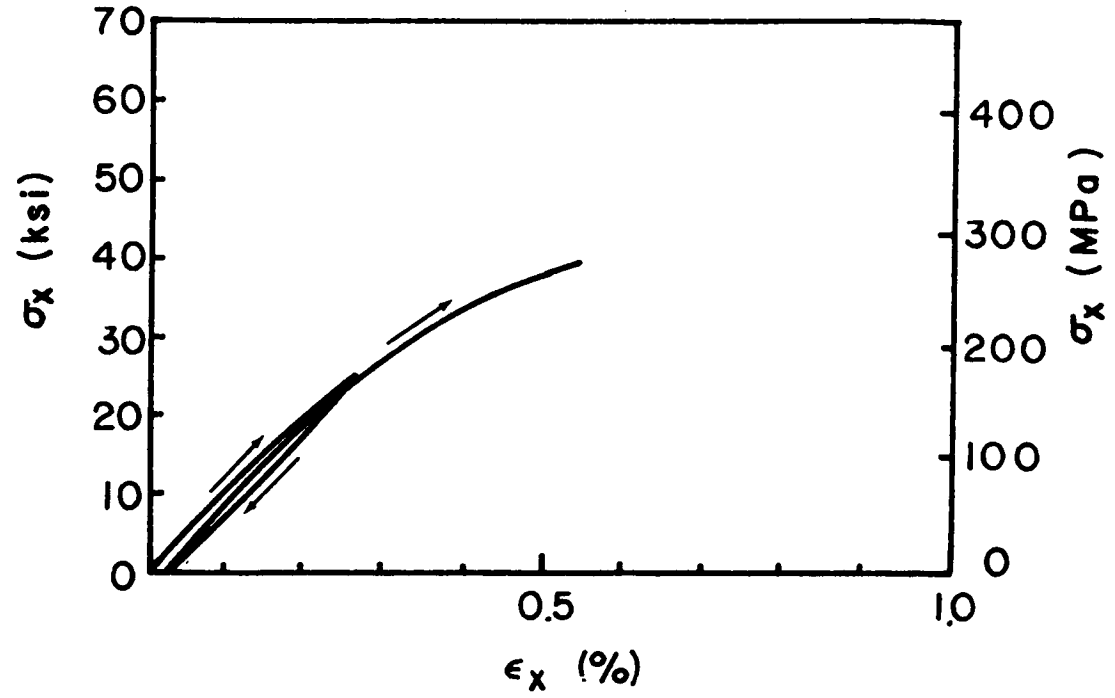

b) Elevated Temperature Tested - Baseline Material

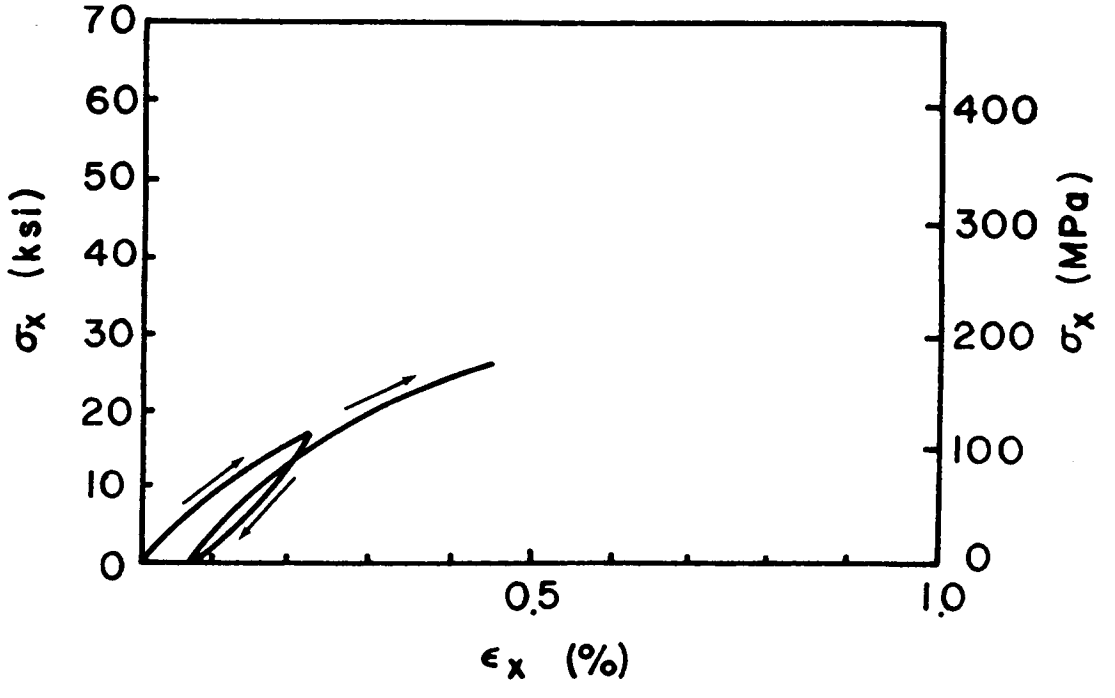

d) Elevated Temperature Tested - Irradiated Material

Figure 5. 10° Cyclic Elevated Temperature Axial Results: [28]

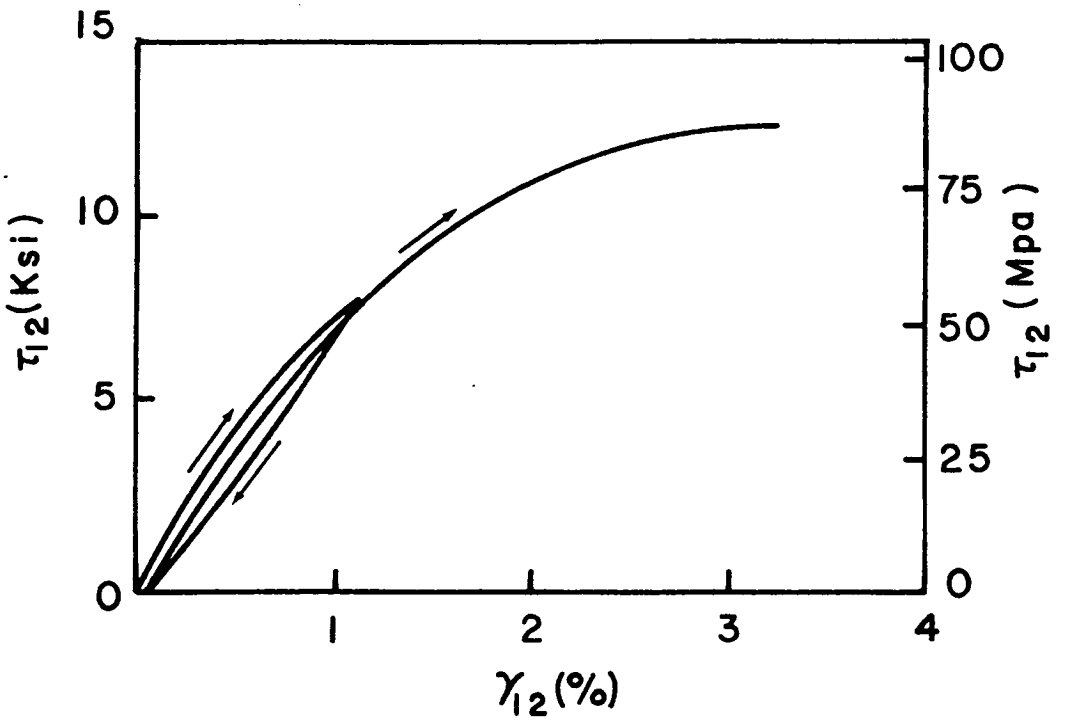

a) Room Temperature Tested - Baseline Material

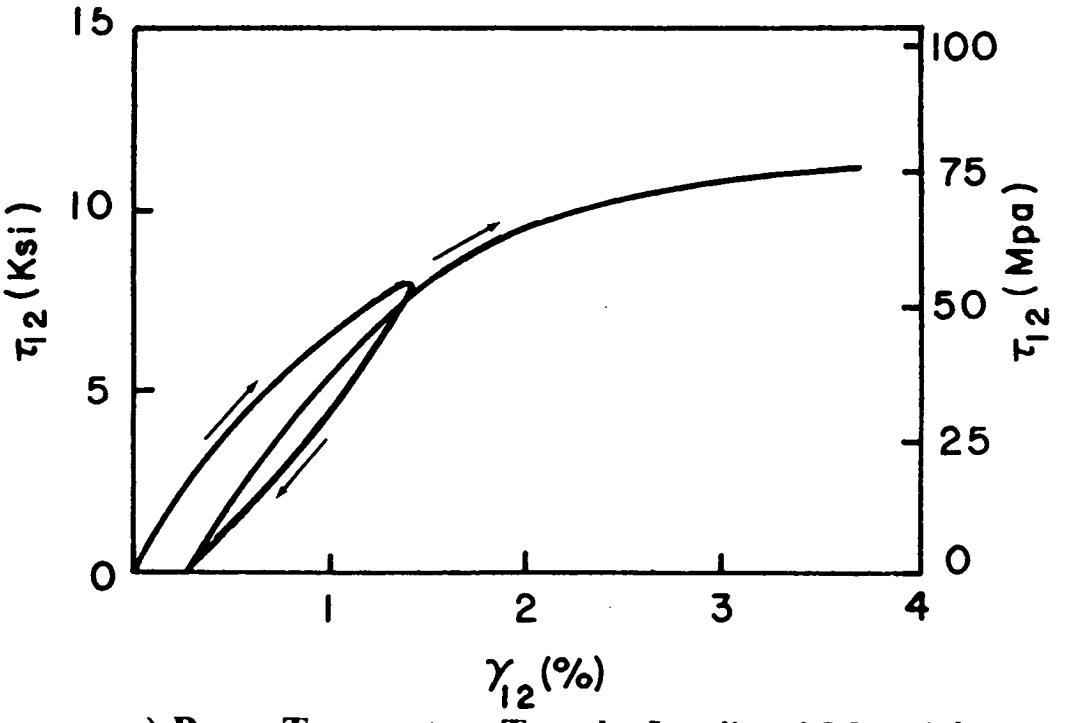

c) Room Temperature Tested - Irradiated Material

Figure 6. 10° Cyclic Room Temperature Shear Results: [28]

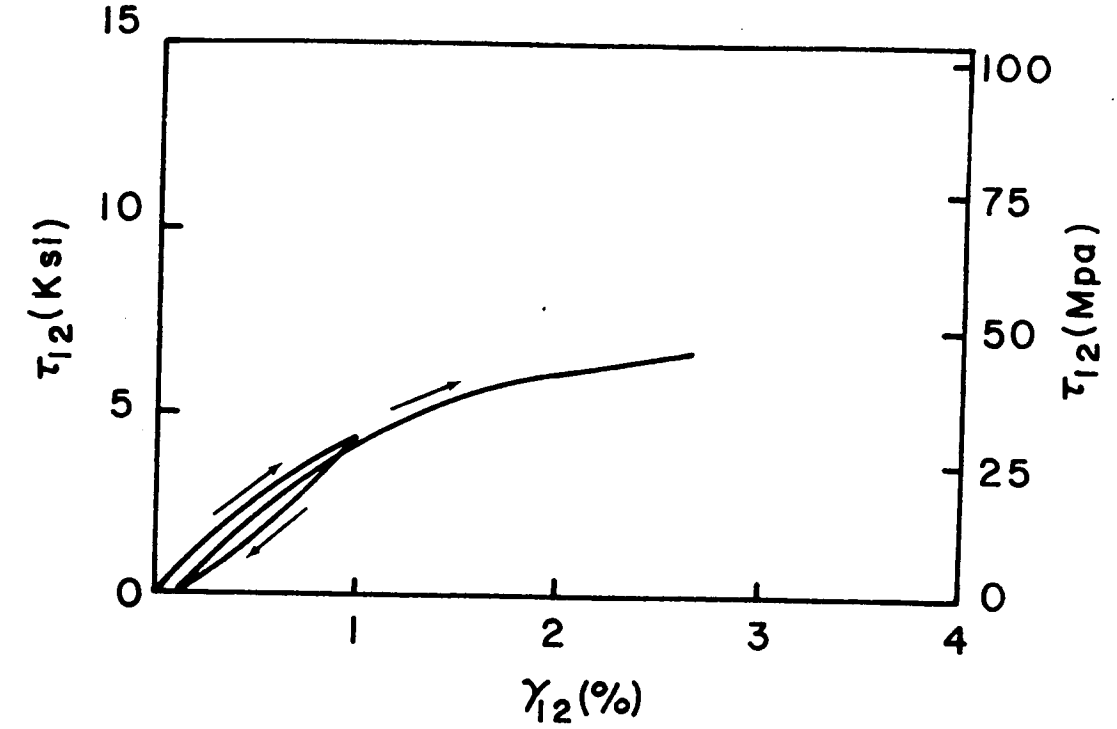

b) Elevated Temperature Tested - Baseline Material

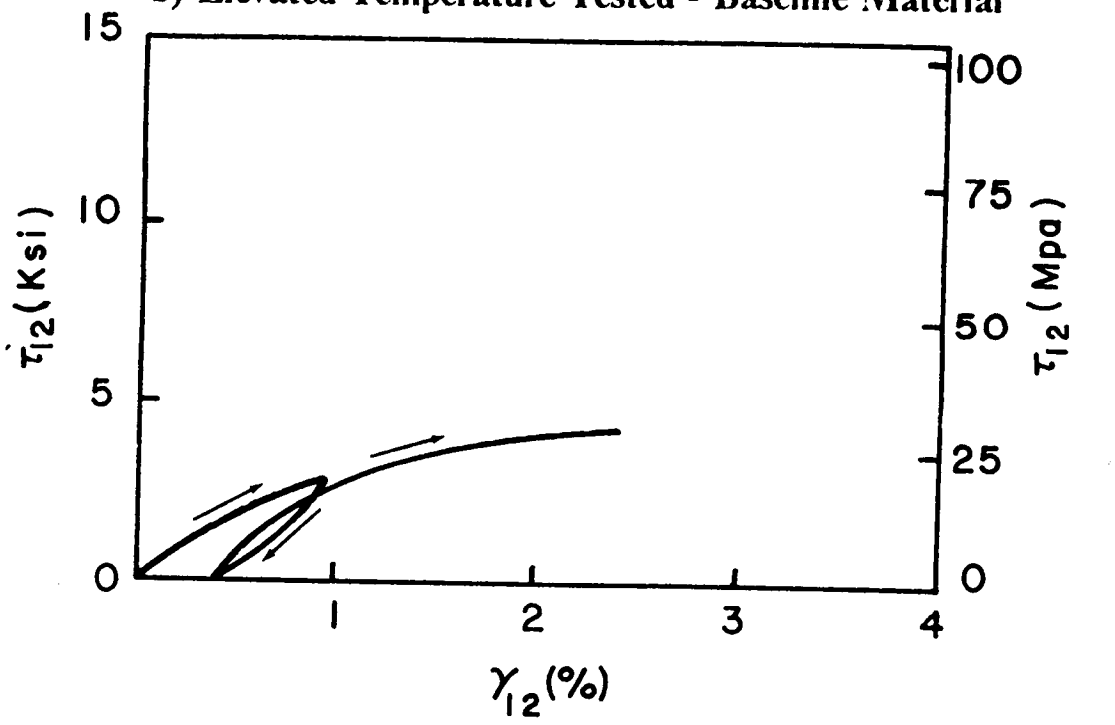

d) Elevated Temperature Tested - Irradiated Material

Figure 7. 10° Cyclic Elevated Temperature Shear Results: [28]

Reed, et al. [23] performed additional tests on the graphite fibers alone. Radiation was shown to have little if any effect on the strength or stiffness of the fibers.

1.3.3 Compression and Bulk Resin Results

Fox, Herakovich, and Sykes [26] continued the investigation into radiation and temperature effects on the T300/934 composite system by examining the compressive properties under the same conditions as those employed by Milkovich, et al. [16] and Reed, et al. [23]. The results show similar reductions in stiffness and strength observed by Milkovich, et al. [16]. Bulk resin tests were also conducted. The trends of these results agree favorably with the composite tensile results. These results are shown in Figure 8. At elevated temperature in the irradiated condition, reduction in strength coupled with nonlinear behavior is observed. This further supports the conclusion that the radiation significantly affects the epoxy resin which contributes to the response of the composite. Fox,et al. [26], Reed, et al. [23], and Milkovich [16], et al. all concluded that chain scission due to radiation is the principal degradation mechanism in the epoxy resin. These conclusions are drawn mainly from the DMA and TMA data and appear to explain many of their results.

1.3.4 Conclusions

The effects of radiation on the 934 resin system seem to correlate well with previous work done on radiation effects of polymers. Chain scission and the formation of radicals is consistent with the DMA and TMA results obtained by Milkovich, et al. [16]. This effect would indeed decrease the cross-link density and average molecular weight of the epoxy network, thus initially increasing the viscoelastic behavior observed by Reed, et al. [23]. Chain scission and low molecular weight products will increase chain mobility and thus facilitate creep behavior. At temperatures near the T_g, the chains are very mobile and substantial viscoelastic behavior is present. In the irradiated condi-

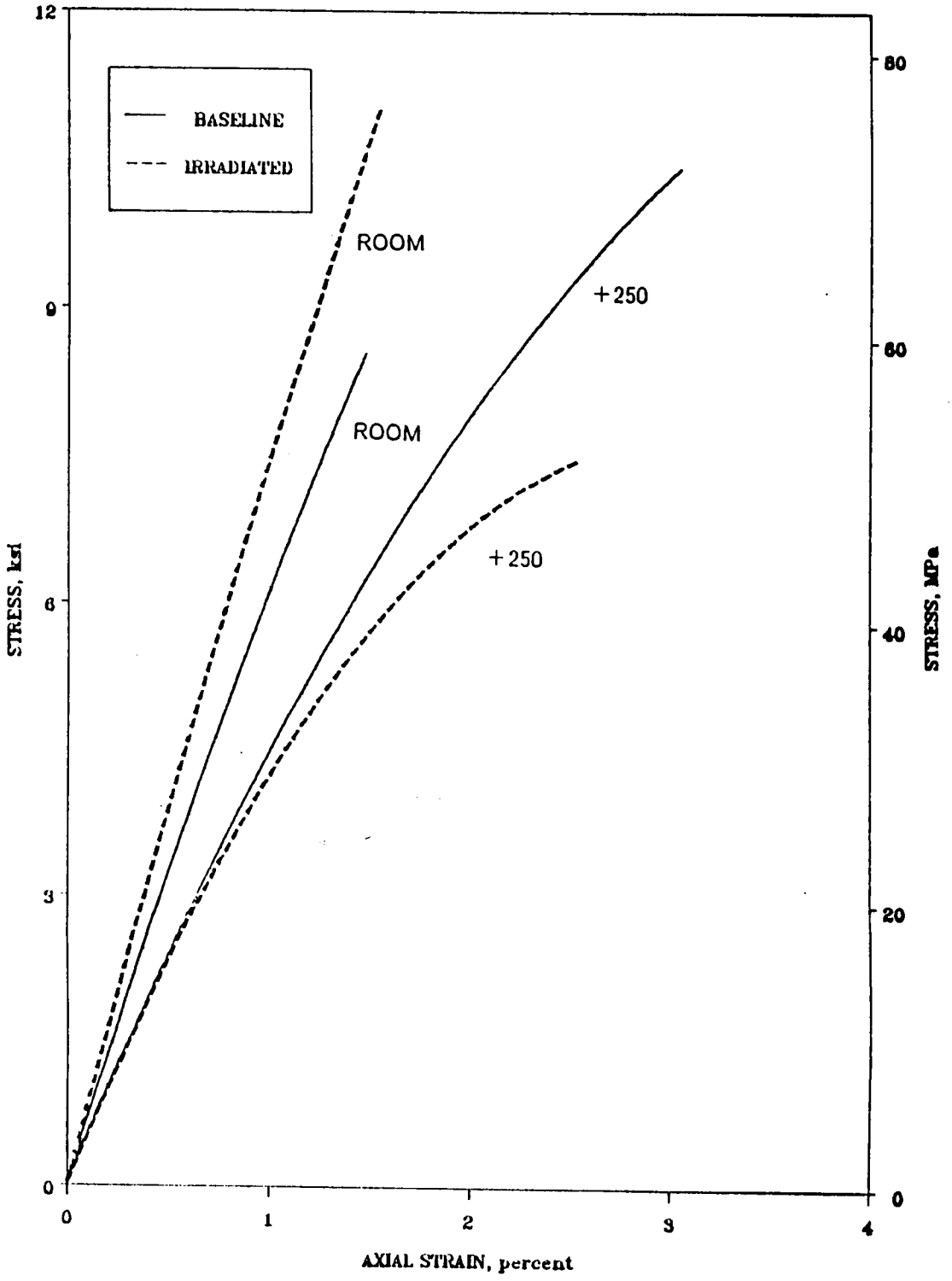

Figure 8. Tensile Results of 934 Resin: [29]

tion, + 250 °F is very close to the T_g. The increase in viscoelastic behavior would increase the apparent onset of nonlinear behavior seen by Milkovich, et al. [16] and Fox, et al. [26].

The tests carried out by Milkovich, et al. [16], Reed, et al. [23], and Fox, et al. [26] were all quasi-static in nature. Their results do correlate with the literature on radiation effects of polymers. The literature also suggests, however, that these radicals will recombine over time to form cross-links. Due to their short-term duration, quasi-static tests of the type performed by Milkovich, et al. [16], Reed, et al. [23], and Fox, et al. [26] give very little information on this phenomena. Time-dependent tests of a longer duration will clarify this occurrence by monitoring the deformation as a function of time, temperature, and radiation. They will also help to quantify the viscoelastic behavior of T300/934 graphite/epoxy.

1.4 Objectives

The objectives of this study are two-fold. The first objective is to quantify the effects of radiation and temperature on the time-dependent behavior of T300/934 graphite/epoxy. In order to meet this objective, creep tests on irradiated and non-irradiated graphite/epoxy specimens were carried out at two test temperatures, namely + 250 °F and + 72 °F. Penetrating electron radiation was chosen since it seems to have the most significant effect on resin matrix composites [16,23,26]. Creep tests were conducted on different fiber orientations of the graphite/epoxy under these varying conditions. Creep tests were also carried out on the bulk 934 resin. The goal was to better understand how radiation and temperature affected the matrix dominated creep response of this composite system.

The second objective of this study is to develop a time-dependent predictive tool for fiber reinforced composite materials with the aid of the micromechanics approach. In this approach, the composite is viewed at the level of a single fiber. Micromechanical models, as now formulated, are able to

predict composite elastic properties from the constituent elastic properties. To accomplish the objective of this study, existing micromechanical models were modified by use of the Correspondence Principle to predict composite viscoelastic properties from constituent viscoelastic properties. This allows designers to combine computationally many different materials to find the one that has the viscoelastic properties he or she desires.

2.0 Experimental Investigation

This chapter discusses the techniques and procedures employed in the experimental portion of this investigation. The discussion will begin with a presentation of the test matrix and a description of the specimen preparation techniques. The specimen preparation techniques used in this study are identical to those used by Milkovich, et al. [27], Reed, et al. [28], and Fox, et al. [29] and more detailed descriptions of these procedures can be found in the above references. A detailed discussion of the various testing machines and testing equipment will then be presented. This chapter will conclude with a discussion of the data acquisition systems used to gather the necessary information.

2.1 Test Matrix

Table 1 shows the test matrix used for this study. Tensile creep tests were conducted on unidirectional coupons with fiber orientations of 0°, 10°, 45°, and 90°. These are the same fiber orientations used by Milkovich, et al. [27], and Reed, et al. [28]. Bulk resin creep tests were also performed.

Table 1. Test Matrix

	T300/934			
	BASELINE		IRRADIATED	
Coupon	RT	ET	RT	ET
0°	3	3	3	3
10°	3	3	3	3
45°	3	3	3	3
90°	3	3	3	3
Bulk Resin	3	3	3	3

Creep tests are a common method to characterize the time-dependent response of a material. A creep test consists of an instantaneous loading of a specimen to a given load level, maintaining that load level for a given time, and monitoring the deformation as a function of time. A perfectly elastic material in a creep test will exhibit an instantaneous strain which then remains constant with time. A time-dependent material in a creep test will also exhibit an instantaneous strain but then the strain will increase with time. The manner in which the strain increases characterizes the time-dependent response of the material.

2.2 *Material*

The material used in this study was T300/934 graphite/epoxy. T300 is a graphite fiber made by Thornel (Union Carbide) and 934 is a thermoset epoxy resin. An eight-ply panel and a four-ply panel were manufactured according to standard procedures [27-29].

2.3 *Specimen Preparation*

Both panels were C-scanned to check for large voids or flaws and none were detected. The specimens were cut from the panels to the dimensions of 6″ x 0.5″ (152.4 mm x 12.7 mm). This dimension was chosen to optimize the number of specimens that could be placed in the irradiation facility without overly compromising the specimen aspect ratio. The specimen dimensions are shown in Figure 9. The 0° and 45° specimens were cut from a single eight-ply panel at VPI & SU. The 10° and 90° specimens were cut from a single four-ply panel at NASA Langley Research Center. The edges were all visually inspected for smoothness and parallel alignment.

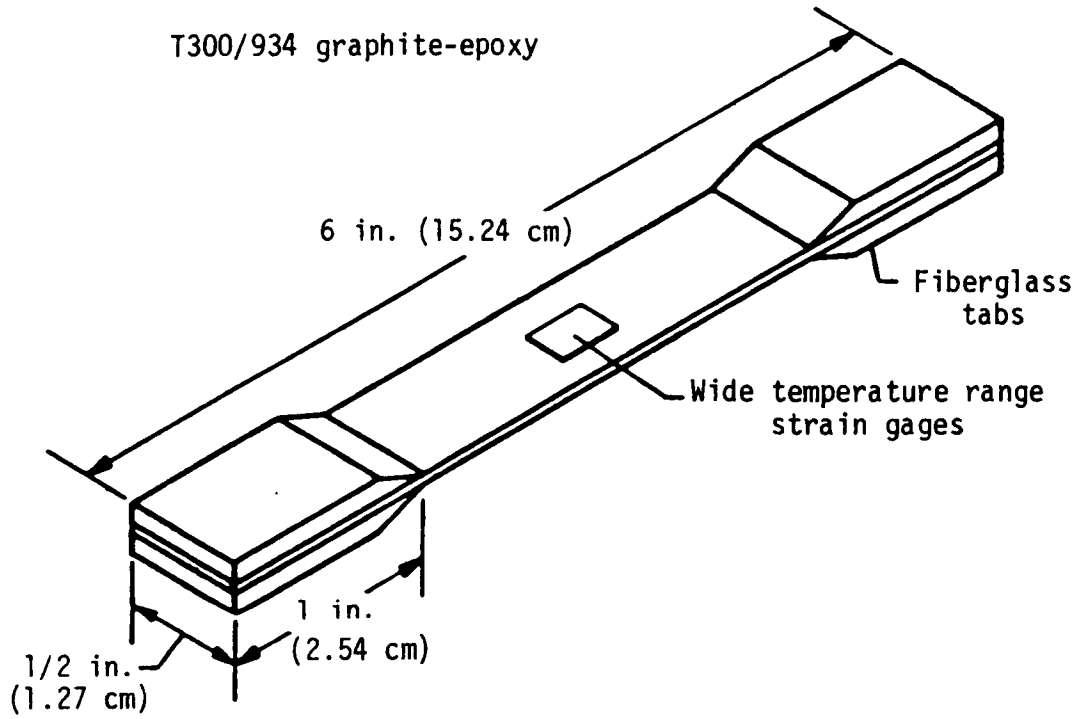

Figure 9. Composite Tensile Specimen Dimensions: [27]

After machining, half of the specimens were subjected to electron radiation in the radiation facility at NASA Langley Research Center. The specimens were irradiated with 1 MeV electrons at a dose rate of 50 Mrads/hr for 200 hours. This yielded a total dose rate of 10,000 Mrads which is equivalent to 30 years exposure in GEO-synchronous orbit. The 10° and 90° degree coupons were irradiated together in the same batch and the 0° and 45° coupons were irradiated in a separate batch.

The specimens were tabbed with 1.25″ x 0.5″ (31.8mm x 12.7mm) fiberglass at each end. The tabs were beveled at 30 degrees and applied at NASA Langley Research Center using standard tabbing procedures [28].

The bulk resin specimens were manufactured according to procedures outlined by Fox [29]. The specimen shape was the small "dog-bone" specimen (type V) from ASTM Standard D638-82a [30]. A photograph of the gripped composite and bulk resin specimens is shown in Figure 10.

All the specimens were instrumented with strain gages. The strain gages were applied with AE-15 adhesive which was cured at 120 °F for 6 hours under 15 psi pressure. Due to the fact that temperature accelerates the recombination of radicals in the epoxy network, 120 °F was chosen as the adhesive cure temperature so as to not expose the specimens to relatively high temperatures for long periods of time while still allowing the adhesive to cure properly. A temperature of 120 °F is the lowest adhesive cure temperature recommended by the adhesive manufacturer [31]. This also follows the strain gaging procedure used by Milkovich, et al. [27], Reed, et al. [28], and Fox, et al. [29]. Table 2 shows the gages used for each specimen group. After curing the adhesive, all gages were measured for misalignment using a microscope available at VPI & SU.

All specimens were held under vacuum for at least five days prior to testing. Specimens were removed from the vacuum chamber immediately before testing. It should be noted that the specimen preparation techniques used by Milkovich, et al. [27], Reed, et al. [28], and Fox, et al. [29] were all followed for this study. More detailed descriptions of specimen preparation can be found in those references.

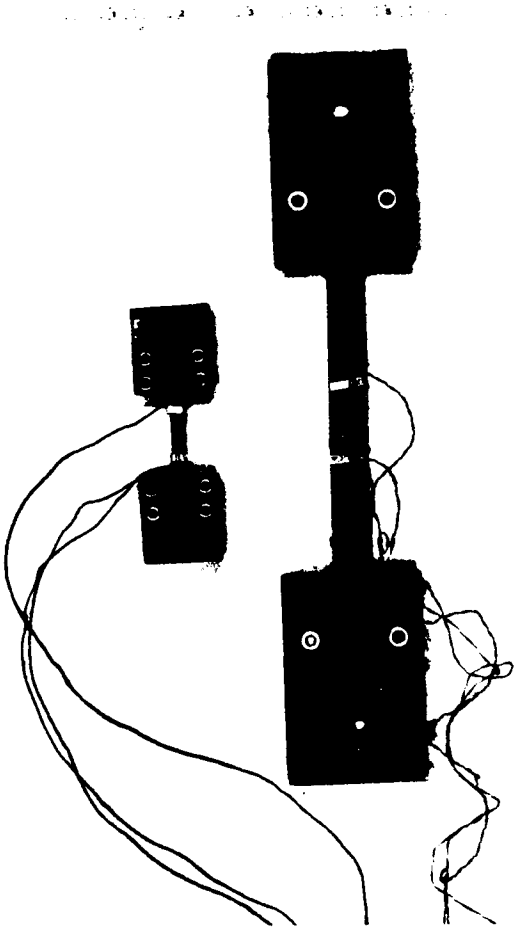

Figure 10. Photographs of Gripped Composite and Bulk Resin Specimens

Table 2. Strain Gages Used For Instrumentation

	Strain Gage Usage	
Laminate	Strain Gage	Adhesive
0°	WK-06-120WR-350	AE-15
10°	WK-06-120WR-350	AE-15
45°	WK-06-120WR-350	AE-15
90°	SK-06-125AD-350	AE-15
Bulk Resin (Long)	EA-06-062AQ-350	AE-15
Bulk Resin (Trans)	EA-06-045AL-350	AE-15

- Long = Longitudinal Gage
- Trans = Transverse Gage

2.4 *Testing*

2.4.1 Composite Creep

The 10°, 45°, and 90° tensile creep tests were performed on either a three-to-one or ten-to-one lever arm creep frame, both of which are located at VPI & SU. The three-to-one creep frame had a motor which gently released the weight to apply the load. The ten-to-one creep frame had a manual crankshaft which lowered the weight to apply the load. Photographs of these two creep frames are shown in Figure 11 and Figure 12. The specimens were gripped with steel grips that were tightened with socket-head cap screws. The alignment in the grips was checked with a square rule and marks on the grips were used for centering. Load was applied with steel pins going through the grips and the load frame. A schematic of this is shown in Figure 13. The 0° tensile creep tests were conducted on a United Testing Systems (UTS) screw-driven, load controlled testing machine located at VPI & SU.

2.4.2 Bulk Resin Creep

The bulk resin creep tests were performed using a dead weight fixture designed by Signor [32] and modified by the author. The grips designed by Fox, et al. [29] were also used in the present investigation. The load train consisted of the grips with pins, the specimen, 20 lb. test nylon line, a two foot steel rod, and a load pan.

The nylon line was used to shorten the distance between the eye bolt and the base in case the specimen broke while loading. The steel loading rods were aligned at the base of the frame with cardboard inserts. The cardboard satisfactorily aligned the rods without significantly increasing the

Figure 11. Photograph of Three-to-One Creep Frame

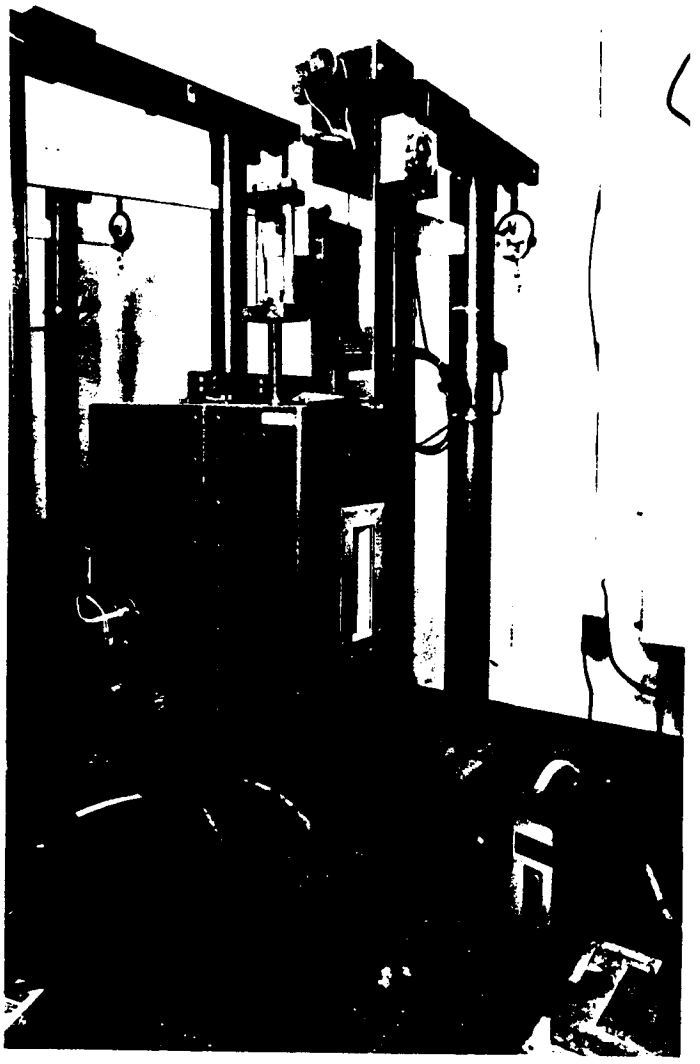

Figure 12. Photograph of Ten-to-One Creep Frame

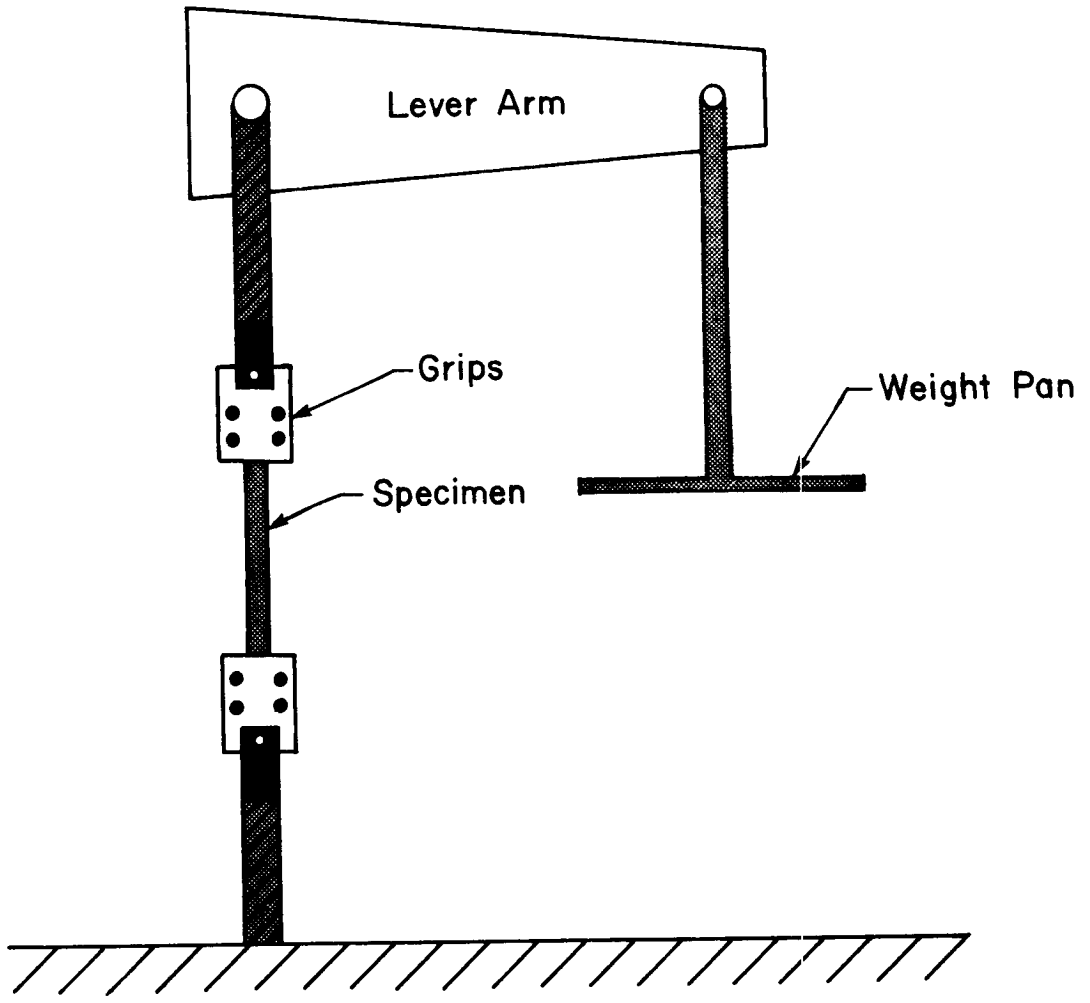

Figure 13. Load Train for Composite Creep Frame

friction hindering vertical movement of the rod. Weights were stacked on a steel disk which was threaded onto the end of the rod.

The entire assembly was placed on a wooden platform. An oven was placed on the platform and the load frame was then placed inside the oven. The rod hung down through a hole in the oven and between slats in the platform. A hole was drilled in the steel rod and the load could by removed from the specimen by simply lifting up the rod and putting a bolt through the rod and two brackets attached to the underside of the wooden platform. The lifting of the rod introduced slack in the nylon line which in turn took the load off the specimen without applying any compressive load. For loading, the bolt was removed and the rod gently let down until the weight was supported by the specimen. The assembly, including the wooden platform, the oven, and the load frame was leveled before testing. A schematic of the entire assembly is shown in Figure 14. A photograph of the entire assembly is shown in Figure 15.

2.5 Loading Sequence

The creep behavior of the specimens was determined at four different load levels, approximately 20%, 40%, 60%, and 80% of the ultimate load for the given configuration. Each specimen was held at each load level for two hours. After each loading, the load was removed and the specimen was allowed to recover for two hours. This process was repeated four times, each time at a new load level. The entire load sequence is shown in Figure 16. A listing of the load levels used for each specimen is given in Table 3. These load levels are approximately equal to the above percentages of the ultimate loads although they are also dependent on the availability of weights in the laboratory.

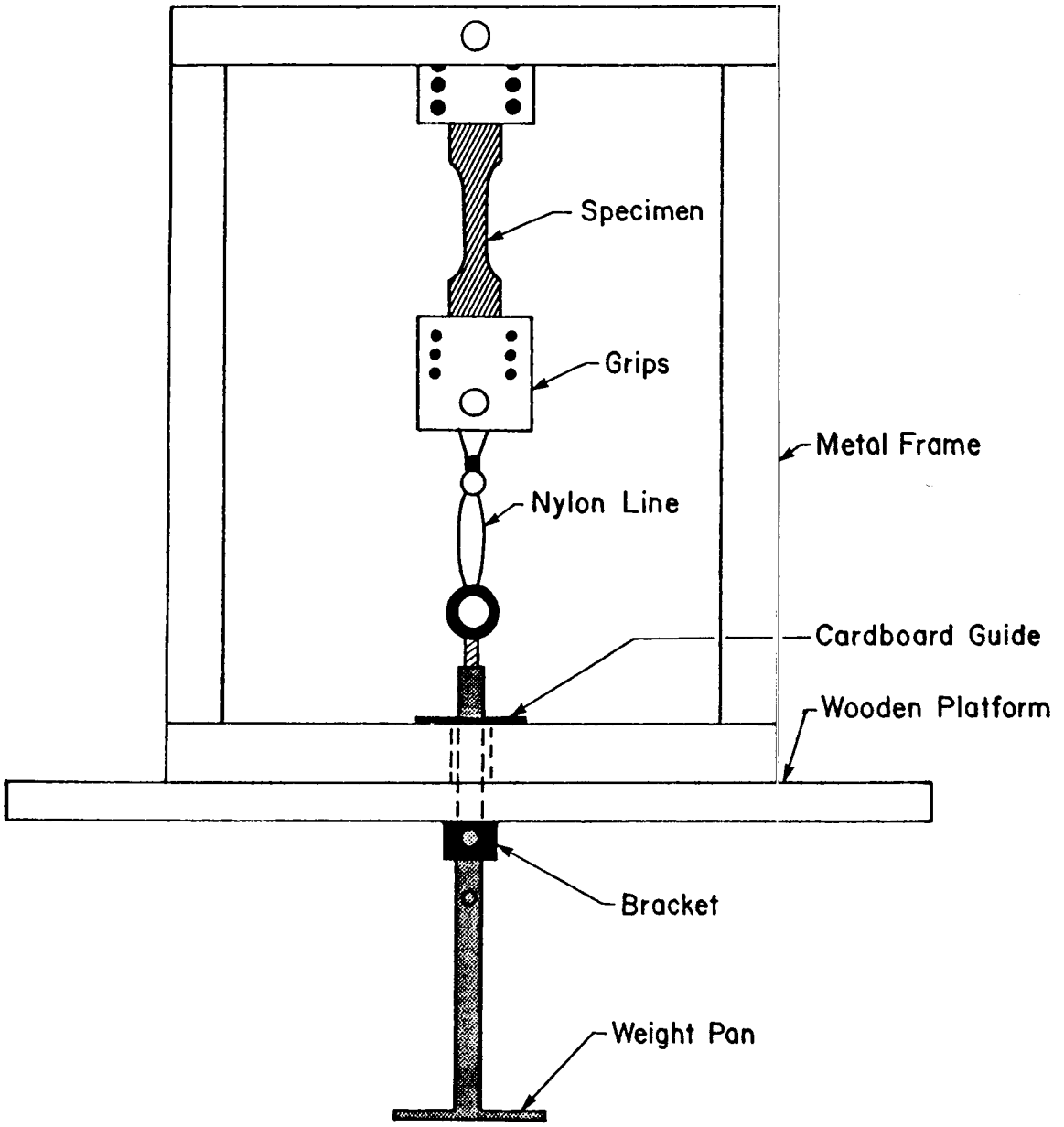

Figure 14. Bulk Resin Loading Assembly

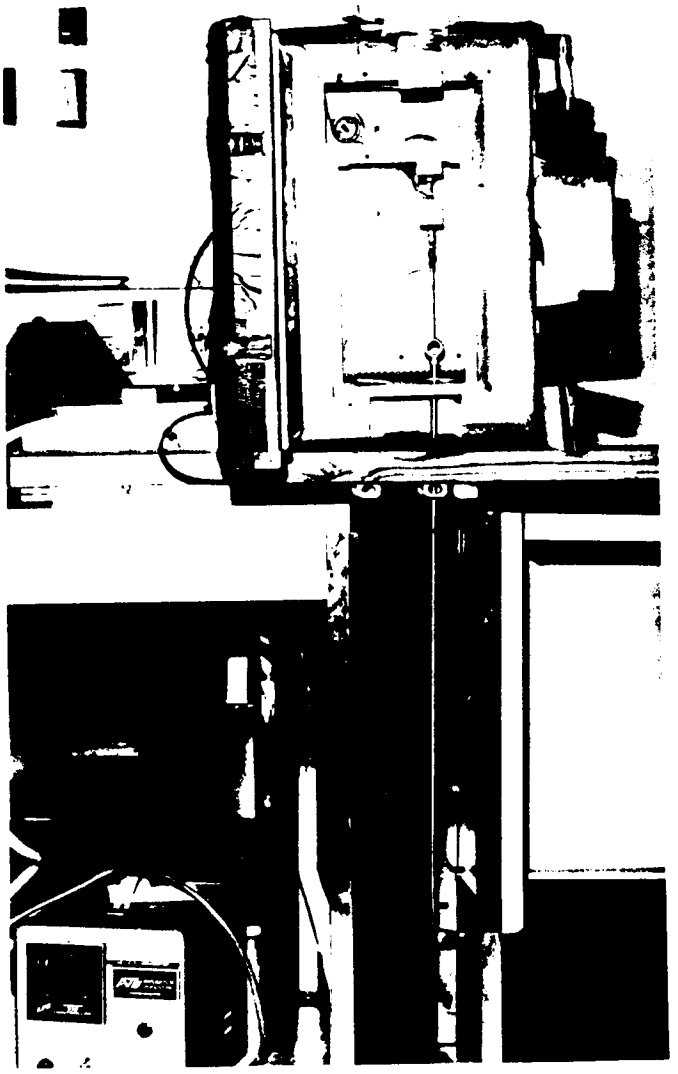

Figure 15. Photograph of Bulk Resin Loading Assembly

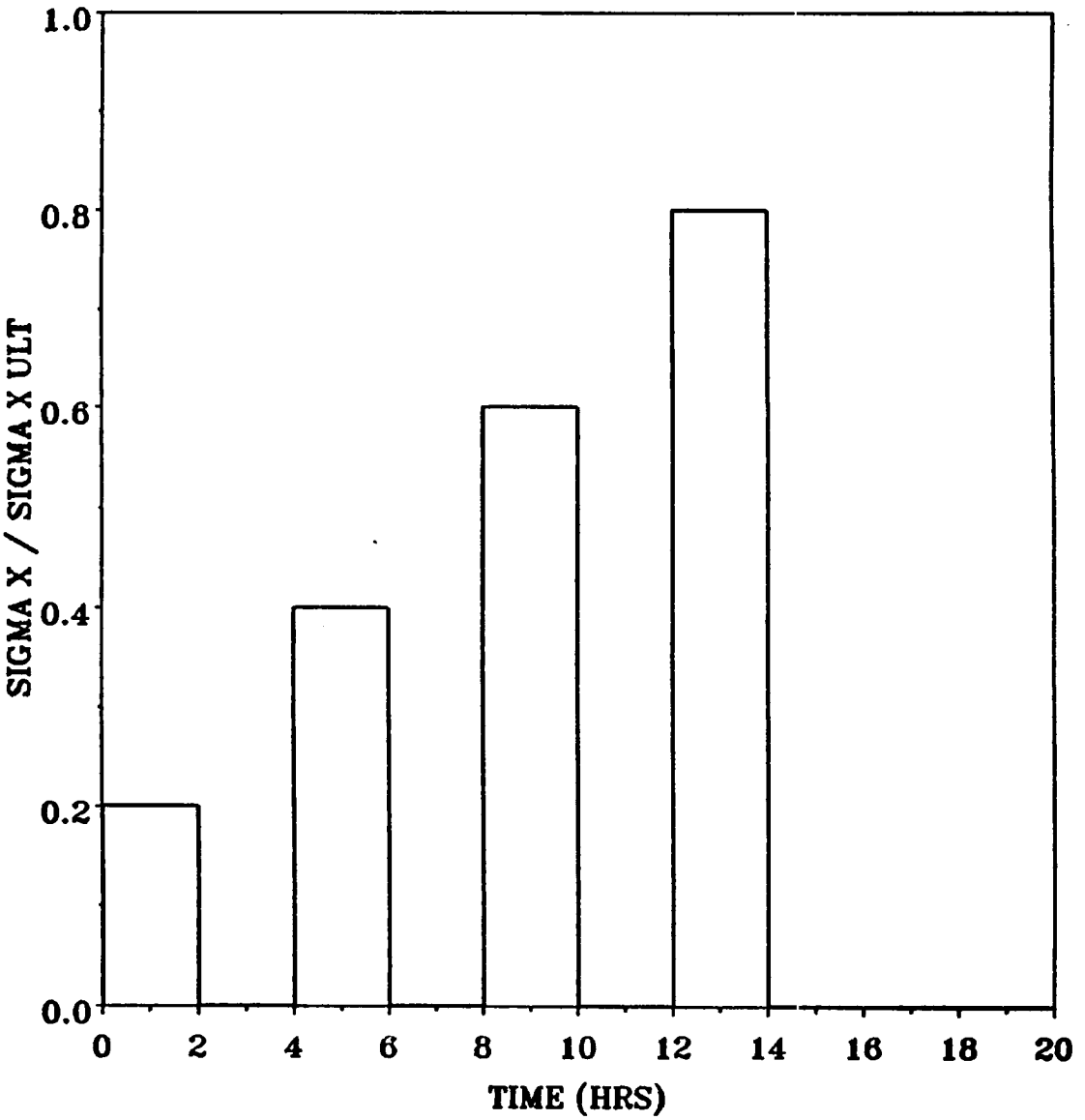

Figure 16. Loading Sequence for All Tests

Table 3. Load Levels Used For Each Specimen Group

	Testing Load Levels			
	Load Level			
Coupon	1 (KSI)	2 (KSI)	3 (KSI)	4 (KSI)
NR-BR	1.60	3.20	4.80	6.40
IR-BR	1.60	3.20	4.80	6.40
NE-BR	1.60	3.20	4.80	6.40
IE-BR	1.60	3.20	-	-
NR-10	7.26	14.53	21.79	29.06
IR-10	7.26	14.53	21.79	29.06
NE-10	7.26	10.82	14.85	18.89
IE-10	7.26	10.82	11.14	14.85
NR-45	4.75	7.25	9.75	12.25
IR-45	4.75	7.25	9.75	12.25
NE-45	4.75	7.25	9.75	12.25
IE-45	1.50	2.25	3.00	3.75
NR-90	1.21	2.42	3.64	4.85
IR-90	1.21	2.42	3.64	4.85
NE-90	1.21	2.42	3.64	4.08
IE-90	1.21	1.66	2.42	2.87

2.6 *Data Acquisition*

Data for the 10°, 45°, 90°, and bulk resin tests was acquired with an Orion Data Acquisition System interfaced with an IBM-AT personal computer. The data acquisition system was driven by a software package entitled MATPACO. This is very similar to the software package MATPAC2 developed by Hidde [33]. MATPACO has the capability to vary the intervals at which data is taken while the test is running. This capability was used to increase the data acquisition intervals as the test progressed so that sufficient data was obtained without creating data files so large as to be unmanageable. After loading and recovery, the data acquisition was halted and the system, including the strain gages, was reinitialized. This was done to permit each loading and recovery to be saved in a separate file. After the data was recorded it was corrected for transverse sensitivity and gage misalignment. Data for the 0° tensile creep tests was taken in a similar fashion with an IBM-XT personal computer interfaced with a Data Translation DT2805/5716 A/D, D/A board and a Vishay 2100 system signal conditioner/amplifier.

Temperature for the elevated temperature tests was monitored with a thermocouple attached to the grips holding the test specimen. Generally, the temperature was kept between 245 °F and 255 °F yet the temperature rarely fluctuated more then 1-2 °F for each test. Temperature was not monitored for the room temperature tests but all tests were run in temperature controlled rooms that were kept at between 72 °F and 75 °F. Although humidity varied from day to day, all tests were conducted on specimens freshly removed from the vacuum chamber.

3.0 Experimental Results

The presentation of the experimental results will begin with a discussion of the nomenclature used for the descriptions of the data presented in this chapter. A brief discussion on the outcome of the 0° tests will be followed by a presentation of entire history plots for the 10° and 90° results at room temperature and elevated temperature. These results show general trends of the composite under the loading sequence described in Section 2.5. Following a discussion of the general behavior of these results, individual plots will be presented for all four conditions at a given load level. This further illustrates the effect of temperature and radiation on the creep response of the composite and bulk resin specimens. Since the results were consistent, a representative test is presented for each condition. No smoothing or averaging of the test data was performed and all plots represent actual test data. A discussion on linearity of the results will also be presented. Linearity will be an important assumption in Chapter 4.0 and will be discussed in more detail in Section 3.5. This chapter will end with a discussion of the healing process of the epoxy resin and its effect on the results. This phenomena is able to give acceptable explanations to the results that will now follow.

3.1 Nomenclature

The nomenclature used to identify the tests will be discussed below. The testing conditions will be hereafter identified by a two letter code. The first letter refers to the specimen condition. N stands for non-irradiated and I for irradiated. The next letter refers to the test temperature. R stands for room temperature and E stands for elevated temperature. The four conditions will therefore be referred to as NR (non-irradiated room temperature), IR (irradiated room temperature), NE (non-irradiated elevated temperature), and IE (irradiated elevated temperature).

When referring to stresses and strains, standard notation will be used to differentiate between global coordinates and material principal coordinates. Global coordinates will be referred to as the x-y-z coordinates while material principal coordinates will be referred to as the 1-2-3 coordinates. Global coordinates refer to the coordinate system of the test coupon where the coordinate axes are parallel to the coupon edges. The material principal coordinates refer to the coordinate system of the unidirectional composite where the coordinate axes are parallel and transverse to the fibers. This is illustrated in Figure 17.

3.2 0° Results

In order to obtain a complete time-dependent material characterization of the T300/934 system, tensile creep tests were carried out on 0° coupons. These specimens exhibited no observable creep in the time frame tested. Accurate elastic properties of the 0° coupons were obtained, however, and these properties will be used in Section 5.2.1.

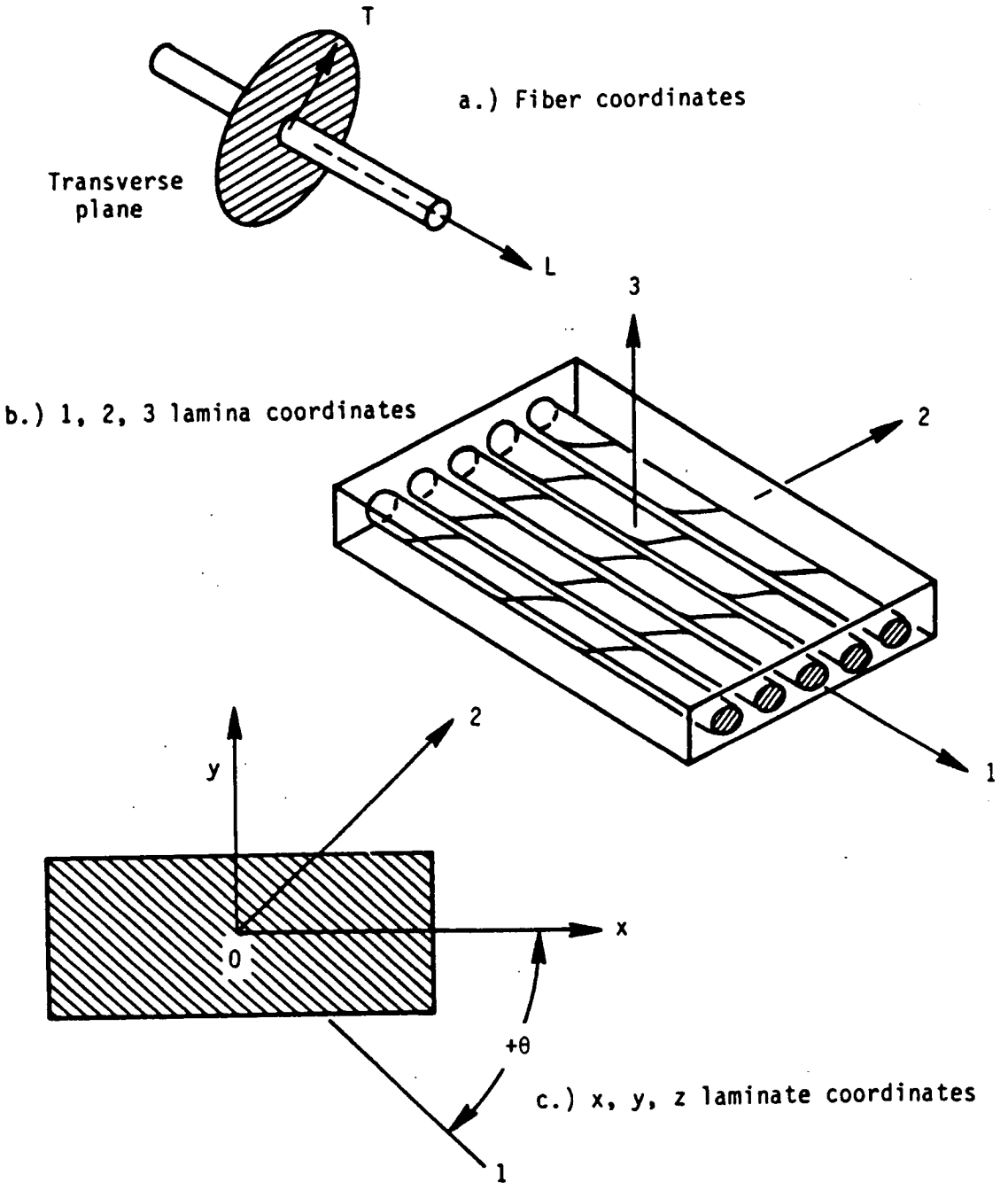

Figure 17. Local and Global Coordinate Systems

3.3 *Entire History Results*

3.3.1 10° Results

Figure 18 shows the longitudinal response for the entire loading history of the 10° off-axis tensile coupon at room temperature. The load levels for both specimens are identical. The creep response for the irradiated and non-irradiated specimens is nearly the same except for a slight difference in the elastic response. Differences in the elastic response may be due to actual changes in the material but may also be due to slight variations in the cross-sectional area of individual specimens. It is seen that a slight permanent strain remains after the loading/recovery cycle at each load level for both conditions.

Figure 19 shows the longitudinal creep response for the entire loading history of the 10° off-axis tensile coupon at elevated temperature. The load levels in this case are not the same for both conditions due to the much lower ultimate stress of the IE specimens. It can be seen, however, that the creep response for the irradiated condition is unlike the response for the non-irradiated condition. The creep response for the non-irradiated condition looks similar to the room temperature results. The creep response for the irradiated condition is quite different. The initial creep response is significant and its corresponding recovery exhibits a large permanent strain. As the test progresses, the magnitude of the creep behavior for the IE condition appears to diminish with subsequent loading. The recovery after each loading seems to exhibit less permanent strain than the recoveries of previous loadings. The final recovery strain of the IE condition, however, shows a large permanent strain. As shown, the final recovery strain value upon completion of the test is much different than the initial strain value of zero strain.

Figure 20 and Figure 21 show the 1-2 shear response for the entire loading history of the 10° off-axis tensile coupon. Figure 20 shows the room temperature results and Figure 21 shows the ele-

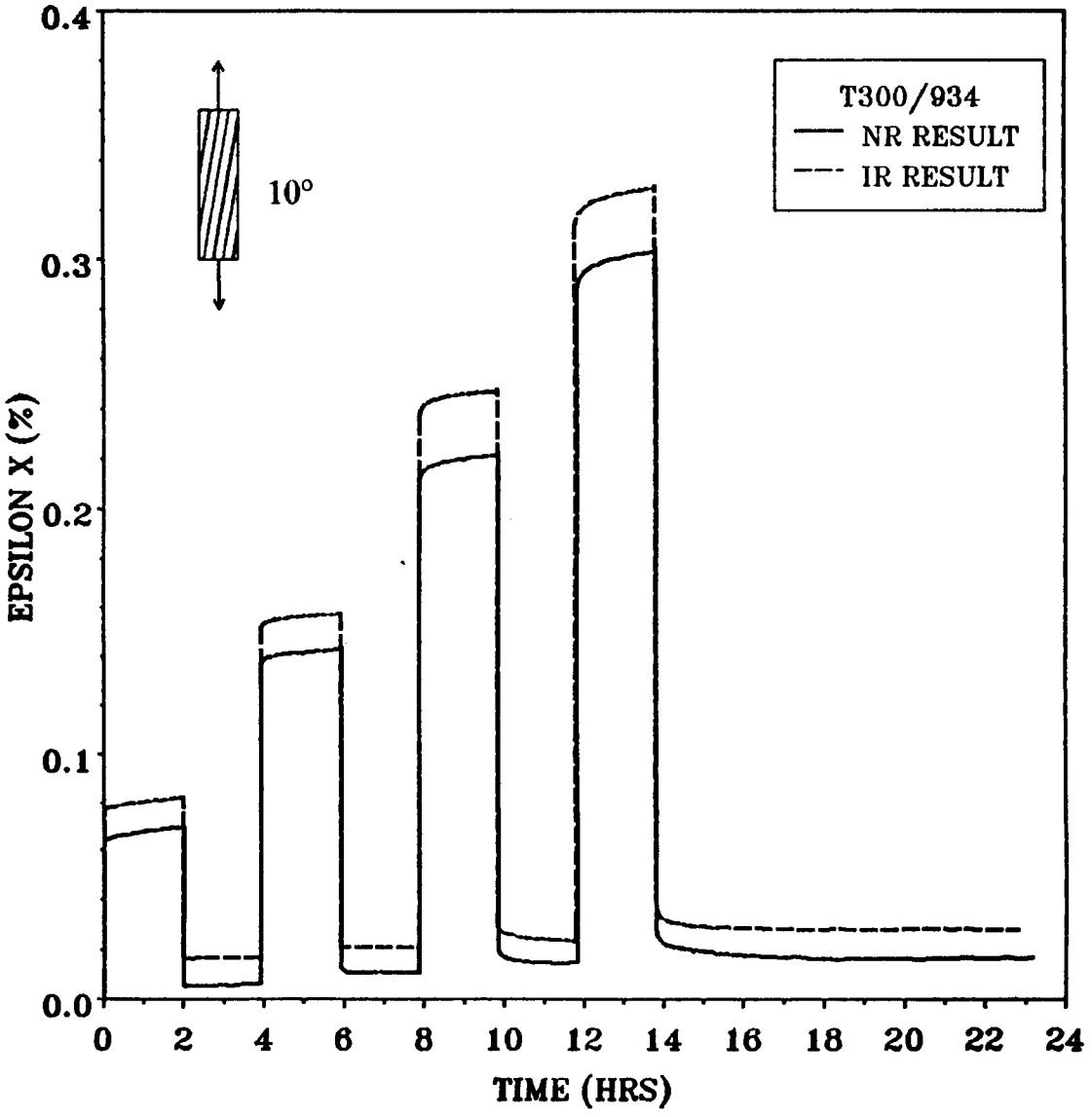

Figure 18. 10° Entire History Longitudinal Result Test at Room Temperature

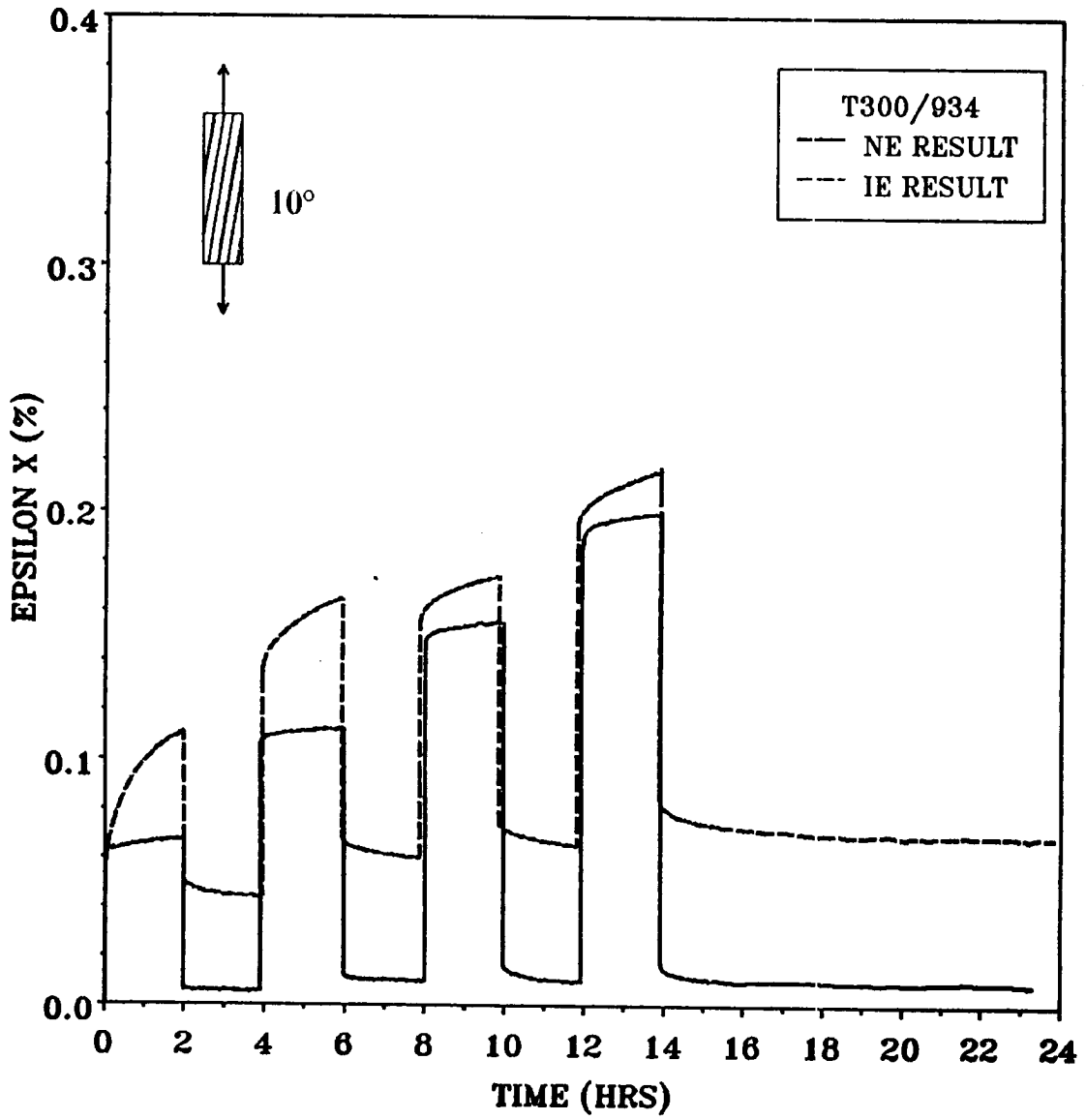

Figure 19. 10° Entire History Longitudinal Result at Elevated Temperature

vated temperature results. The same trends can be seen here, but in a much more pronounced fashion. The room temperature results show similar behavior for both the irradiated and non-irradiated conditions except for the elastic response. The recovery in both cases exhibits a small permanent strain. The elevated temperature results show a dramatic difference in the two responses. The non-irradiated condition shows similar behavior to the room temperature results while the irradiated condition shows a very large creep deformation. Upon recovery, the IE condition shows a significant permanent strain. As in Figure 19, the permanent strain diminishes with subsequent loadings yet the final permanent strain upon completion of the test is almost as great as the strain attained by the NE coupon at the highest load level. It should be noted that the final load level for the IE test is less than the final load level for the NE test. These results suggest that the creep behavior of the epoxy resin is most critical in shear. This is supported by the 90° creep test data discussed in the subsequent section.

3.3.2 90° Results

Figure 22 and Figure 23 show the longitudinal creep response for the entire loading history of the 90° tensile coupons. Figure 22 shows the room temperature results and Figure 23 shows the elevated temperature results. As with the 10° tests, the room temperature results are nearly identical for the two conditions. The load levels for both conditions are the same. Both specimens show creep behavior at all load levels. The recovery, however, seems to proceed in a different manner than observed with previous results. The recovery after the initial two loadings appears to be representative of creep rather than recovery. This behavior will be discussed in Section 3.6.3.

The elevated temperature results show a difference but one not nearly as dramatic as for the 10° results. The load levels for these two tests are not the same due to the much lower ultimate stress of the IE specimen. The non-irradiated result is similar to the room temperature results. The irradiated condition does exhibit significant creep but the difference between the IE and NE results

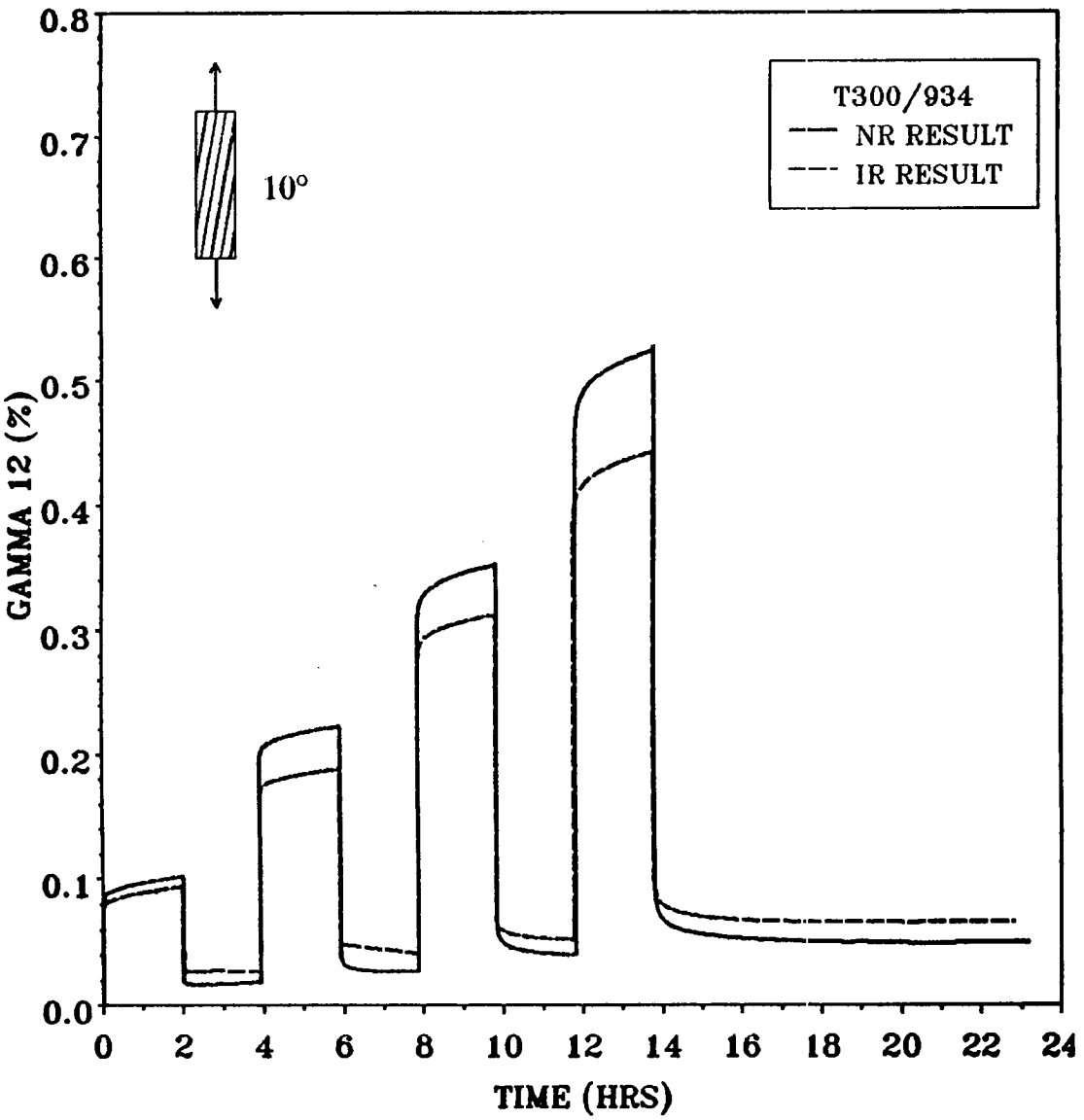

Figure 20. 10° Entire History Shear Results at Room Temperature

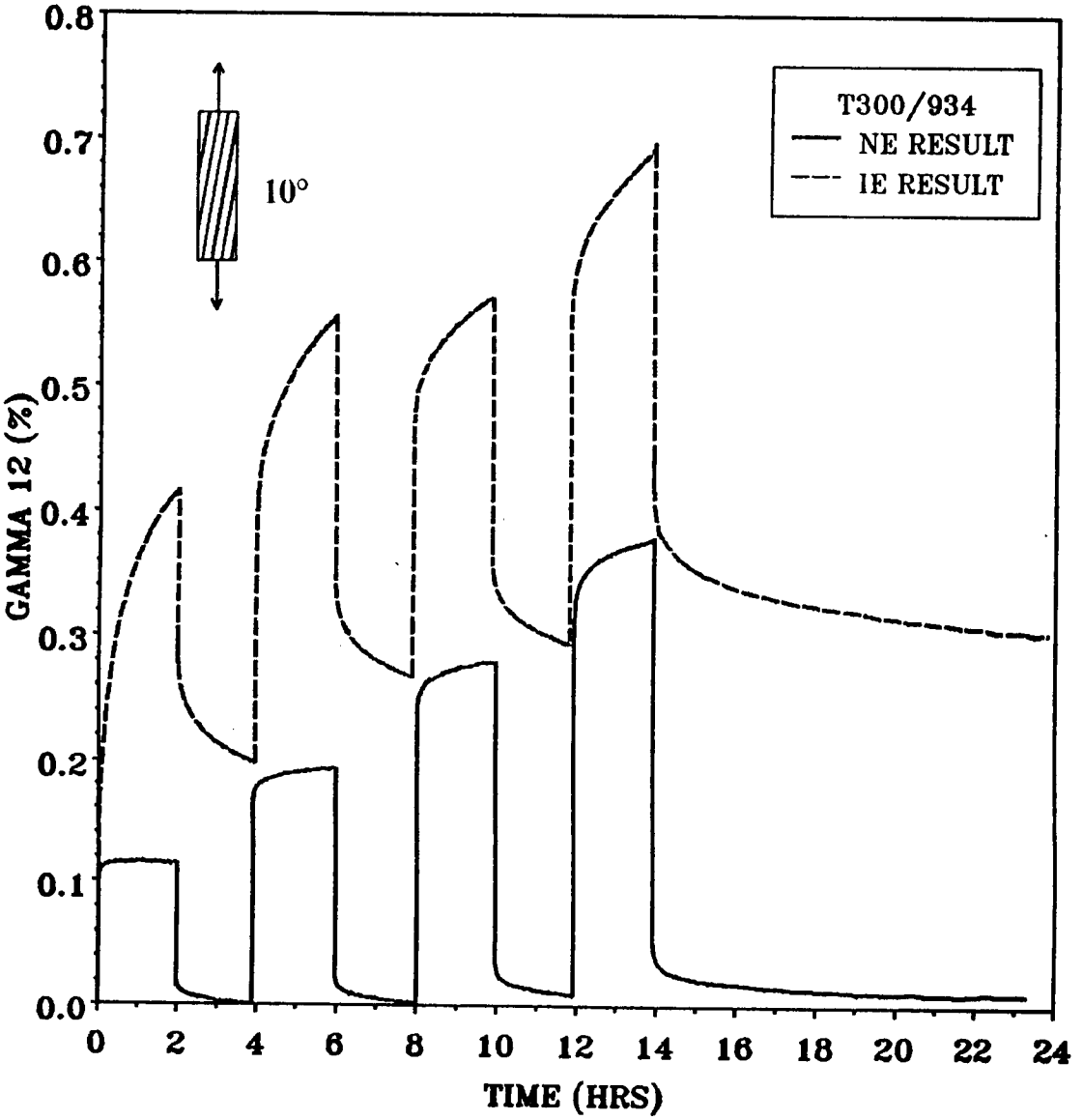

Figure 21. 10° Entire History Shear Results at Elevated Temperature

isn't nearly as great as the difference seen with the 10° tests. The recovery for both cases appears to approach strain values *lower* than the initial strain. This will be discussed in Section 3.6.3.

The state of stress in a 90° coupon subjected to uniaxial tension is composed of principal normal stresses with little if any shear stress present. As seen in the 10° off-axis results, shear stresses in the matrix appear to have a significant effect on the creep response of the specimen. The fact that the creep response is diminished significantly when the shear stress is eliminated, such as with the 90° tests, leads to the assumption that creep is most apparent in shear. While normal stresses do have a significant effect on the creep response, this effect is not as great as seen when shear stresses in the matrix are present.

3.4 Individual Results

To better see the effect of radiation and temperature on the creep response of both the T300/934 graphite/epoxy composite and the bulk 934 resin, individual results at a given load level for all conditions will be presented. The results from all four conditions (NR,IR,NE,IE) are presented for each test. Longitudinal (ε_x) and shear (γ_{12}) results are presented for the 10° and 45° off-axis tests and longitudinal results alone are presented for the 90° and bulk resin tests. The creep and recovery results are presented for a single loading and recovery at a given load level. As mentioned in Section 2.5, each test consisted of four loadings at approximately 20%, 40%, 60%, and 80% of the ultimate load. Since the ultimate loads vary widely between differing conditions, each condition is not loaded to the same load levels [16]. For this reason, only two load levels are compared for each test. For these results, the initial strain readings for each loading have been set to zero so that the creep responses can be accurately compared. As shown in Section 3.3, permanent strains are often present upon recovery. In the following plots, the permanent strain values have been subtracted

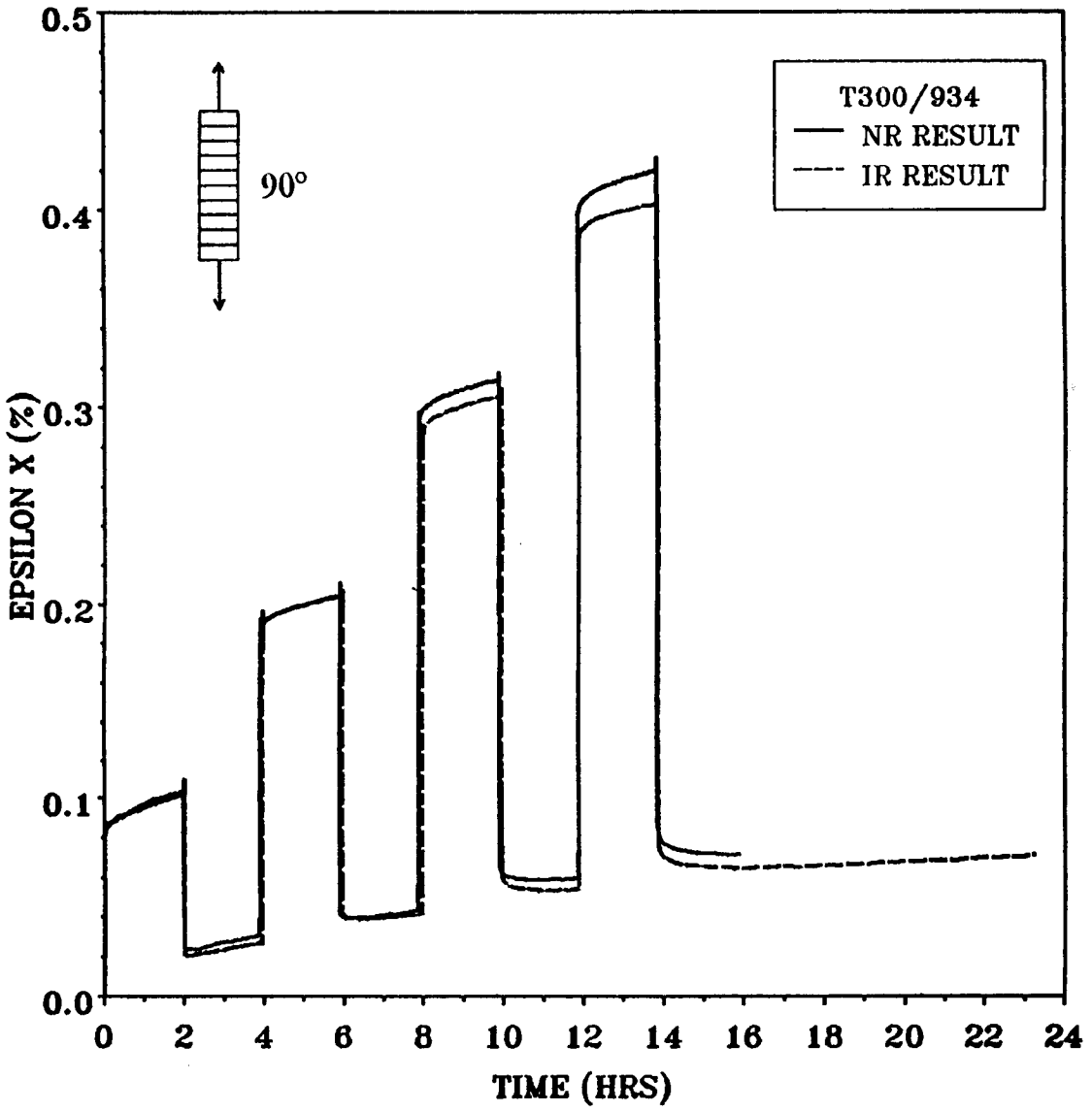

Figure 22. 90° Entire History Longitudinal Results at Room Temperature

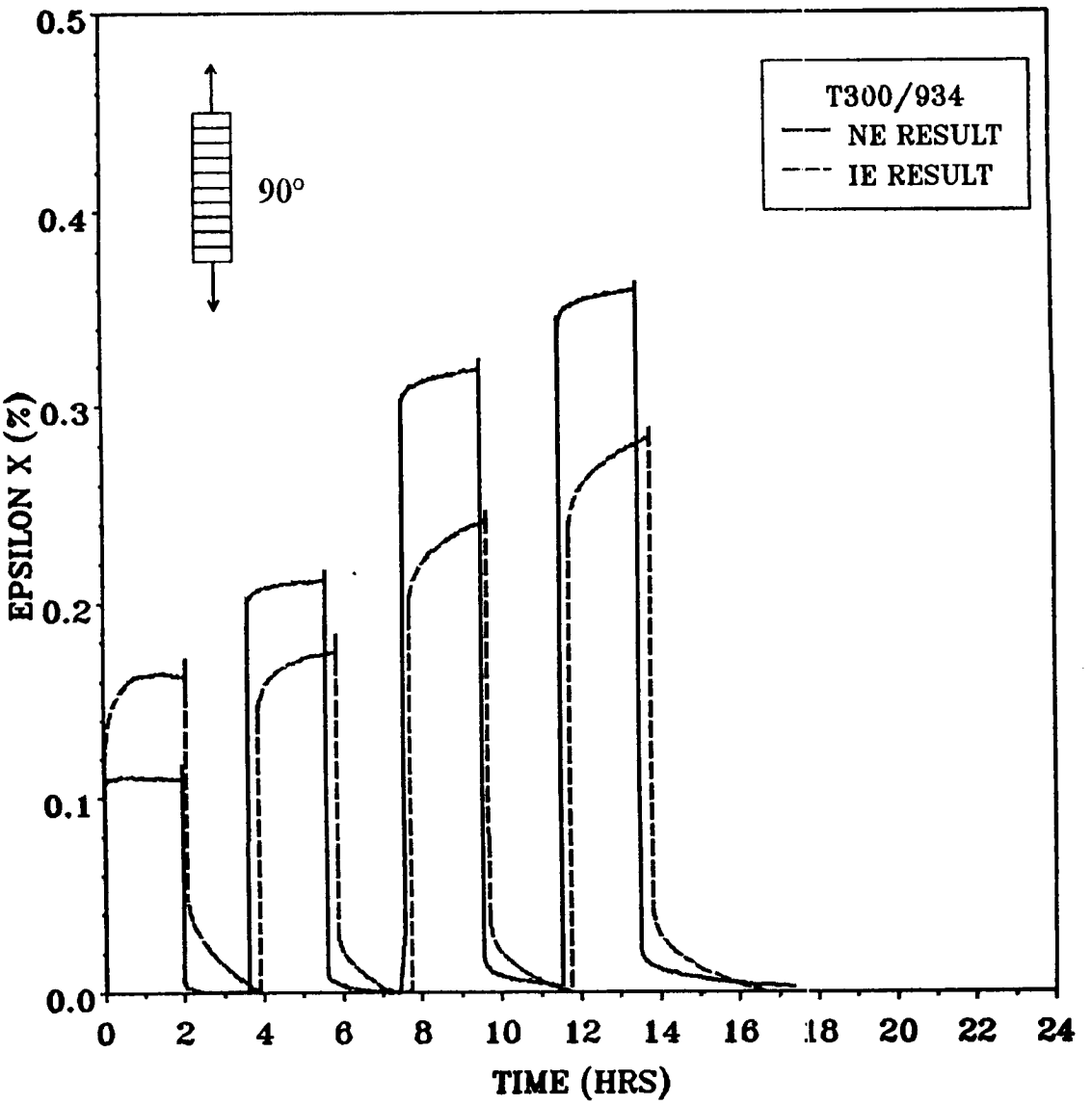

Figure 23. 90° Entire History Longitudinal Results at Elevated Temperature

from the actual strain values so that each test is presented from the same initial strain value, namely zero strain. This should be kept in mind when reviewing the following plots.

3.4.1 Bulk Resin Results

Figure 24 shows the creep response for the bulk resin results under a constant load of 1.60 KSI. This is the initial loading for all conditions. The NR and IR results are nearly identical except for the elastic response. The NE test does show a slight increase in the creep behavior while the IE test shows a dramatic increase in the creep response. The recovery for the IE result shows a large permanent strain. The differences in the elastic response of these specimens correlates well with the elastic moduli evaluated by Fox, et. al. [29]. A comparison of the elastic moduli is given in Appendix C.

A second figure for the second load level is not shown since the strain on the initial loading for the IE test nearly approached 2% and the gages only functioned properly up to this level. The gages began to peel off soon after the second load level. Figure 25 shows the entire strain history of the IE bulk resin test which only goes slightly beyond the second loading. As observed in the figure, the creep after 30 minutes at the second loading is less than the creep after 30 minutes at the initial loading. This agrees with the decrease in creep behavior on subsequent loadings seen with the graphite/epoxy composite results.

3.4.2 10° Results

Figure 26 shows the longitudinal creep response of the 10° off-axis tensile coupon under a constant load of 7.26 KSI. This is the initial loading for all conditions. The NR and IR conditions are nearly identical in the creep response. The NE creep response is slightly greater. The NR, IR, and

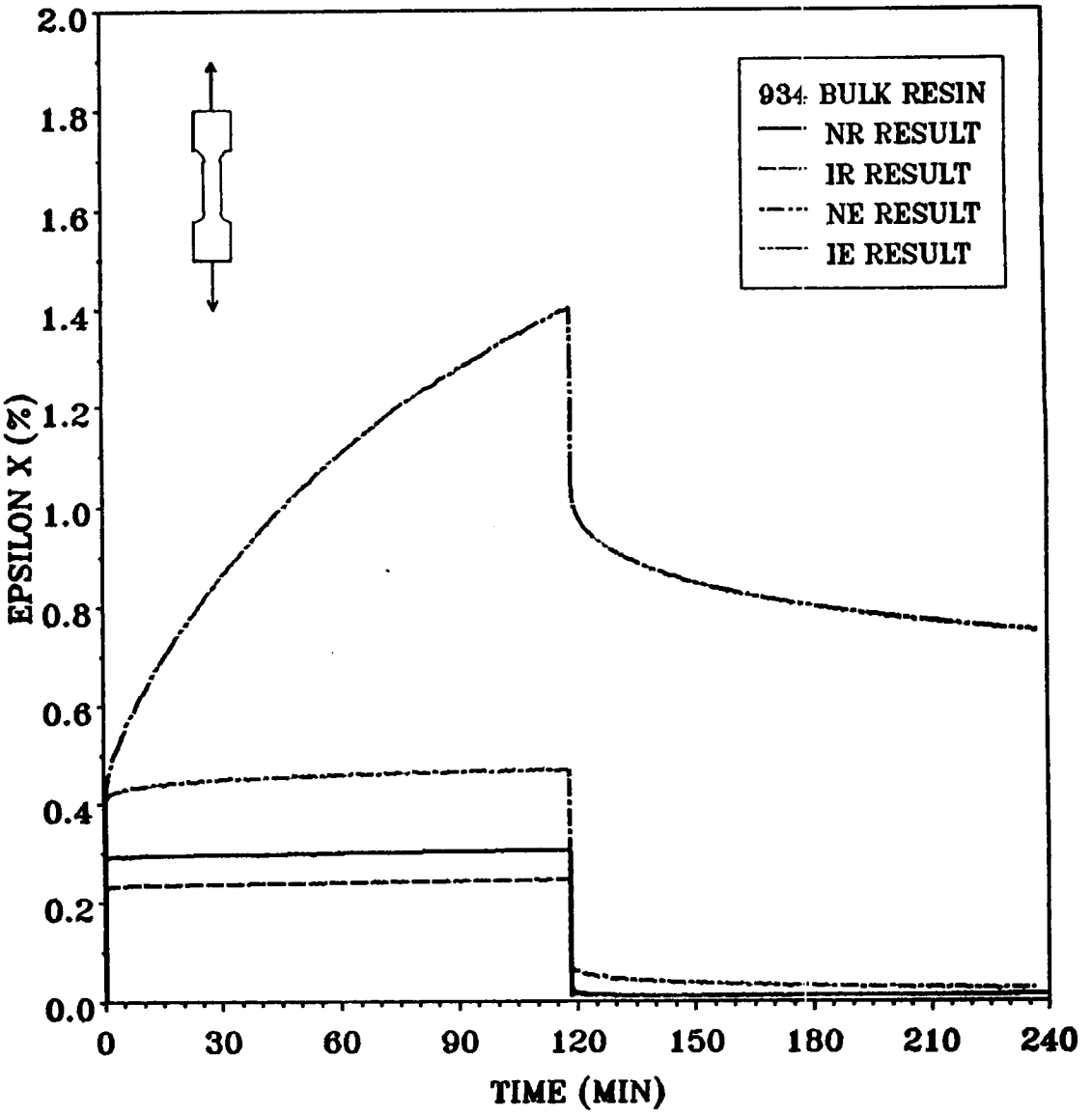

Figure 24. Bulk Resin Results at 1.60 KSI

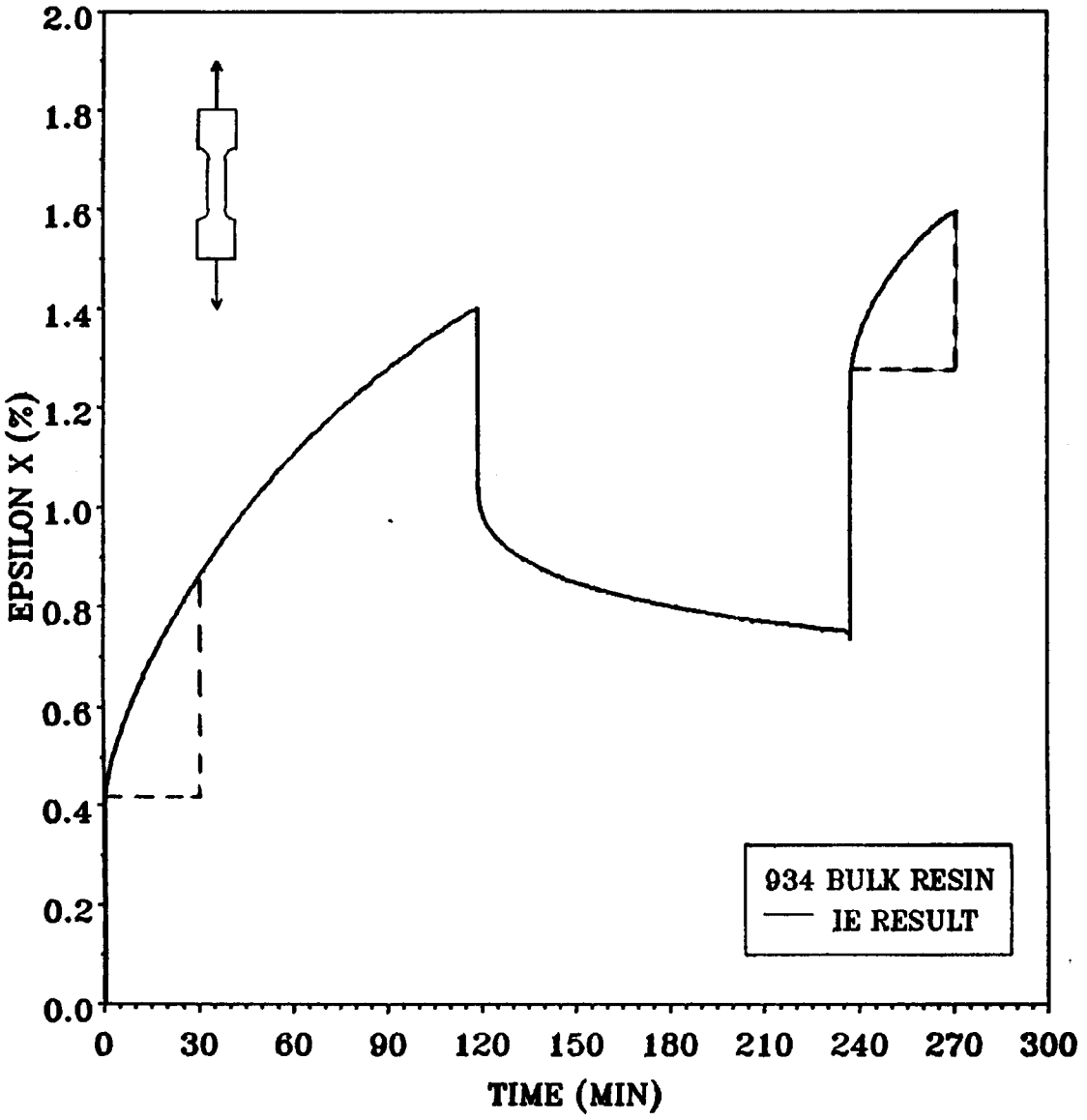

Figure 25. Bulk Resin Results for Entire Loading History

NE results are all fairly similar and differ only in the magnitude of the elastic response. The IE result is quite different from the other conditions. Significant creep is present in this condition and the recovery exhibits a large permanent strain.

Figure 27 shows the longitudinal creep response for the 10° off-axis test under a constant load of 14.85 KSI. This is the second loading for the NR, IR, and NE results and the third loading for the IE result. The creep response for the NR, IR, and NE results is similar to the results shown in Figure 26 for 7.26 KSI while the IE result is quite different from the IE response at 7.26 KSI. The creep response is still greater for the IE condition as compared with the other conditions but it isn't nearly as significant as seen on the initial loading. The recovery at 14.85 KSI exhibits less permanent strain than observed at 7.26 KSI. It should be noted that this is the third loading for the IE test and the creep response seems to diminish with each successive loading.

Figure 28 and Figure 29 show the 1-2 shear creep response in the material principal coordinate system for the 10° off-axis tensile coupon under a constant load of 7.26 KSI and 14.85 KSI respectively. Similar trends can be seen here as compared with the longitudinal creep response. The magnitudes in shear, however, are much greater than the longitudinal strain magnitudes. For the IE results at 7.26 KSI, the creep in shear is very significant and the recovery exhibits a large permanent strain. At 14.85 KSI, the creep response for the IE condition diminishes somewhat and the recovery shows less permanent strain. The important point to note here is the overall magnitude of the creep response in shear.

3.4.3 45° Results

Figure 30 shows the longitudinal creep response for the 45° off-axis tensile coupon at the initial load level. Because of failure of many of the specimens at loads well below the ultimate loads observed by Milkovich, et al. [16], the initial load level for the NR, IR, and NE specimens was at 4.20

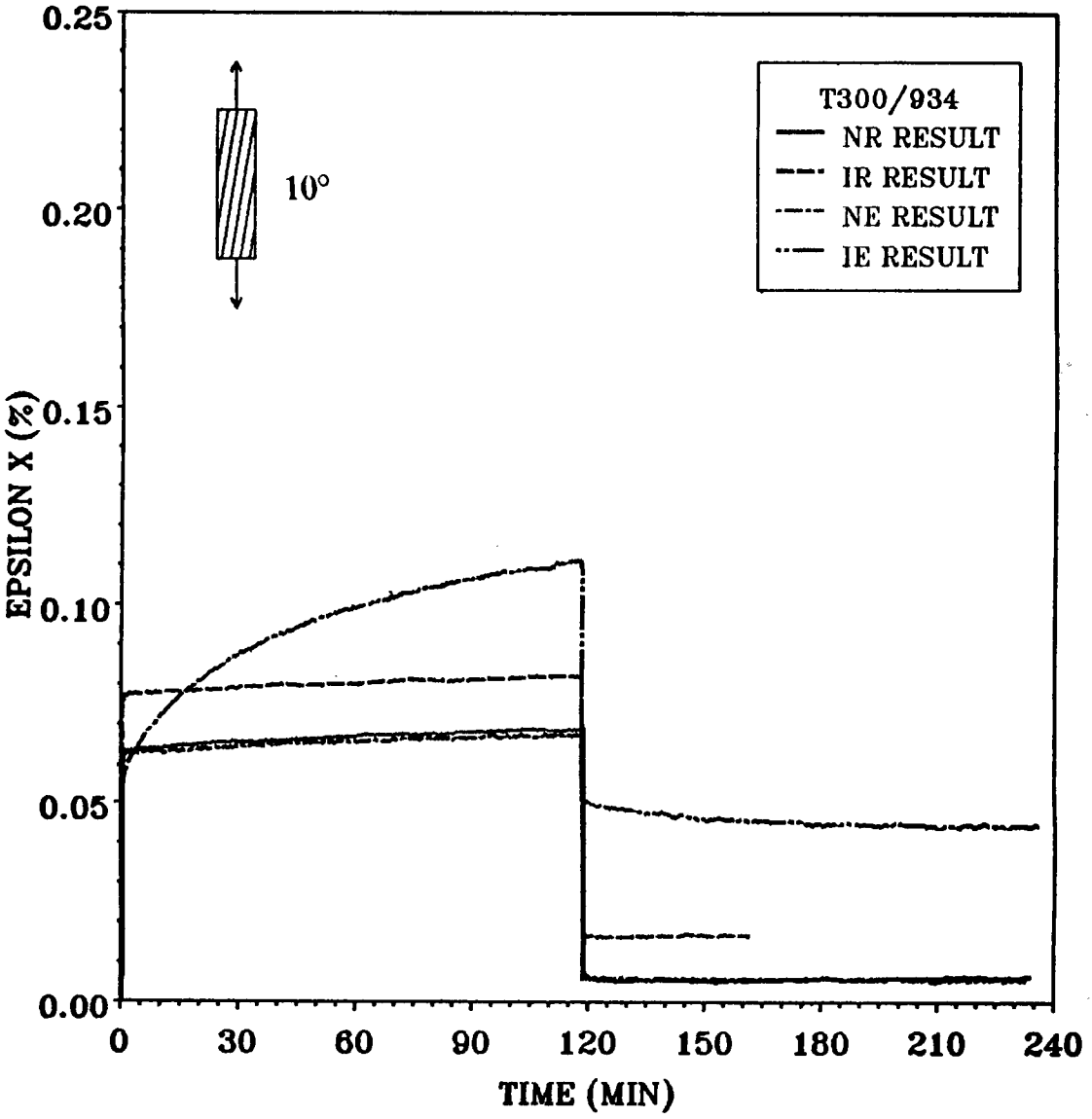

Figure 26. 10° Off-Axis Longitudinal Results at 7.26 KSI

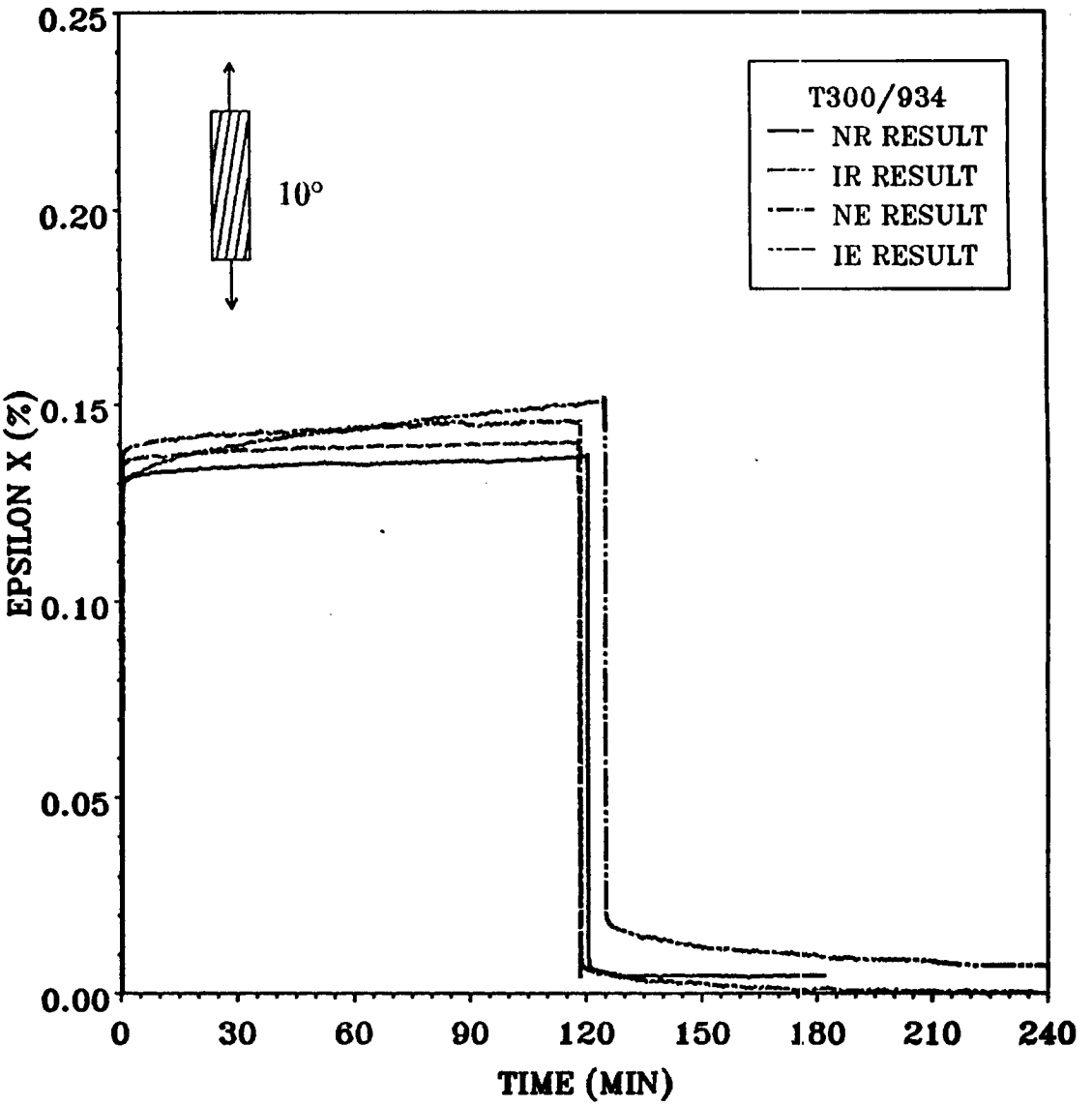

Figure 27. 10° Off-Axis Longitudinal Results at 14.85 KSI

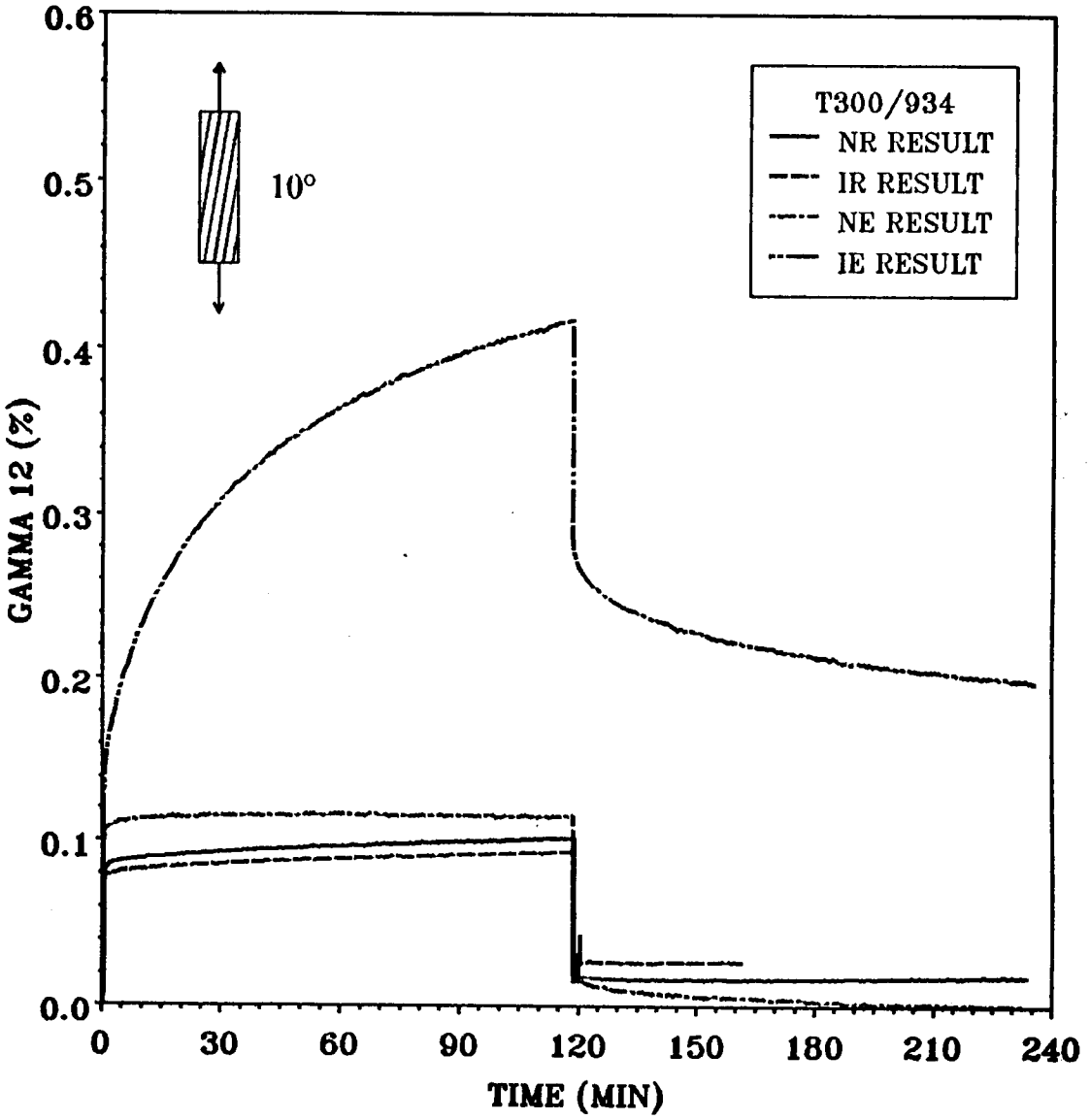

Figure 28. 10° Off-Axis Shear Results at 7.26 KSI

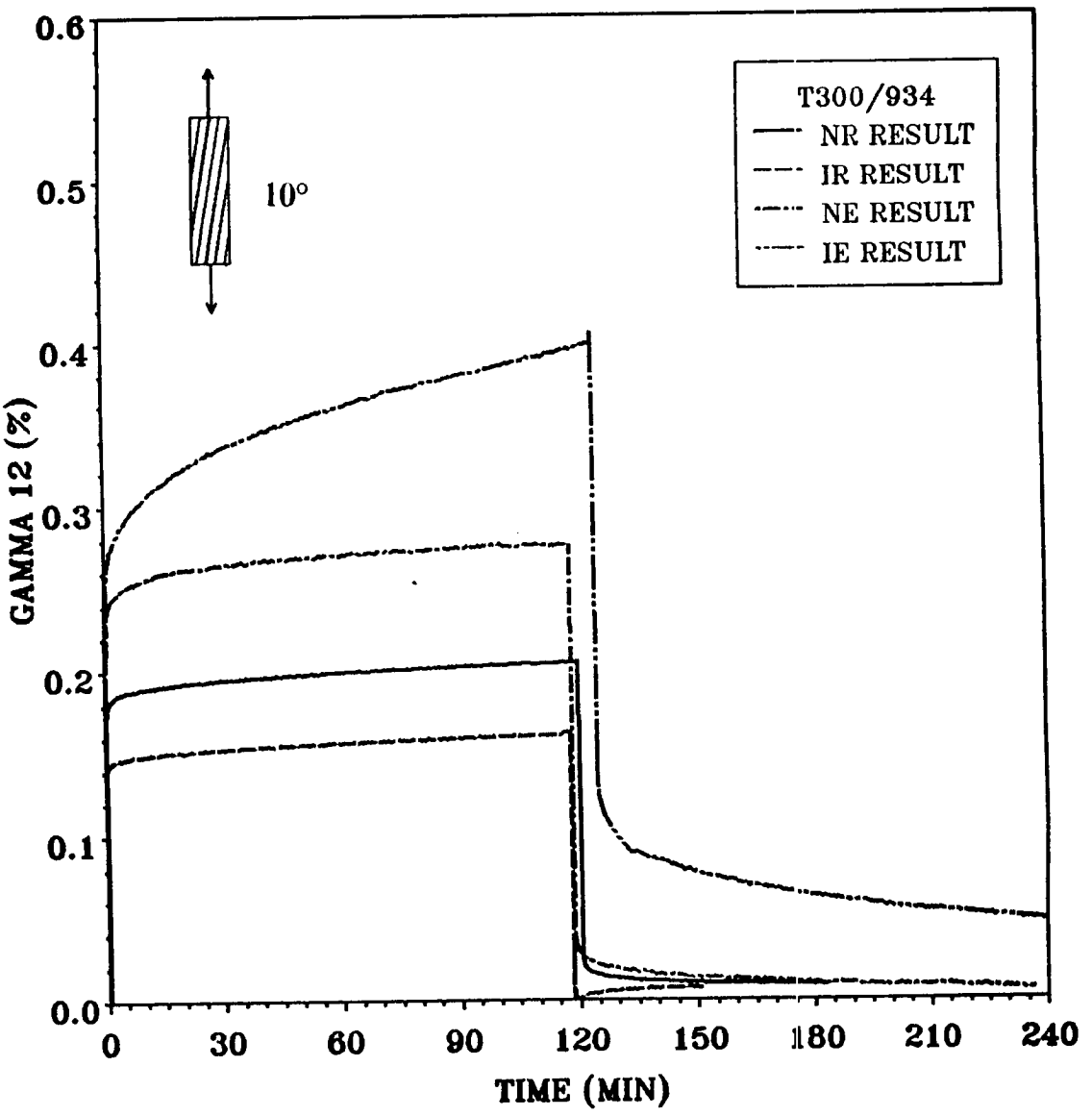

Figure 29. 10° Off-Axis Shear Results at 14.85 KSI

KSI and the initial load level for the IE condition was at 1.50 KSI. The plot is similar to the one shown in Figure 26. The NR, IR results are fairly similar and the NE condition shows slightly more creep than the room temperature results. The IE condition shows significantly more creep and the recovery exhibits a large permanent strain. It should also be noted that the creep for the IE condition does seem to level off quickly although the initial response is fairly steep.

Figure 31 shows the longitudinal creep response for the 45° tensile coupon at the initial load level of 4.20 KSI for the NR, IR, and NE tests and the final load level of 3.75 KSI for the IE test. The NR, IR, and NE results are the same as in Figure 30 but the IE results are again quite different compared to the IE response at 1.50 KSI shown in Figure 30. The creep response of the IE specimen is very close to the response of the other conditions. It is slightly greater than the NR, IR, and NE conditions but it is still much less than the IE creep response seen in Figure 30. The recovery in this case exhibits little permanent strain.

Figure 32 and Figure 33 show the shear creep response in the material principal coordinate system for the 45° off-axis tensile coupon at the same loads as in Figure 30 and Figure 31. These plots show similar trends. The NR, IR, and NE results are nearly identical except for the elastic response. The IE creep response is significant on the first loading and is much less on the final loading. The recovery exhibits a large permanent strain after the initial loading and little permanent strain after the final loading. Again it should be noted that the magnitude of the creep response in shear is significant when compared to the creep response in the longitudinal direction.

3.4.4 90° Results

Figure 34 shows the longitudinal creep response for the 90° tensile coupon at a constant load of 1.21 KSI. This is the initial load level for all conditions. The NR, IR, and NE results are similar except for the elastic response. The NE result does show slightly more creep. The IE results shows

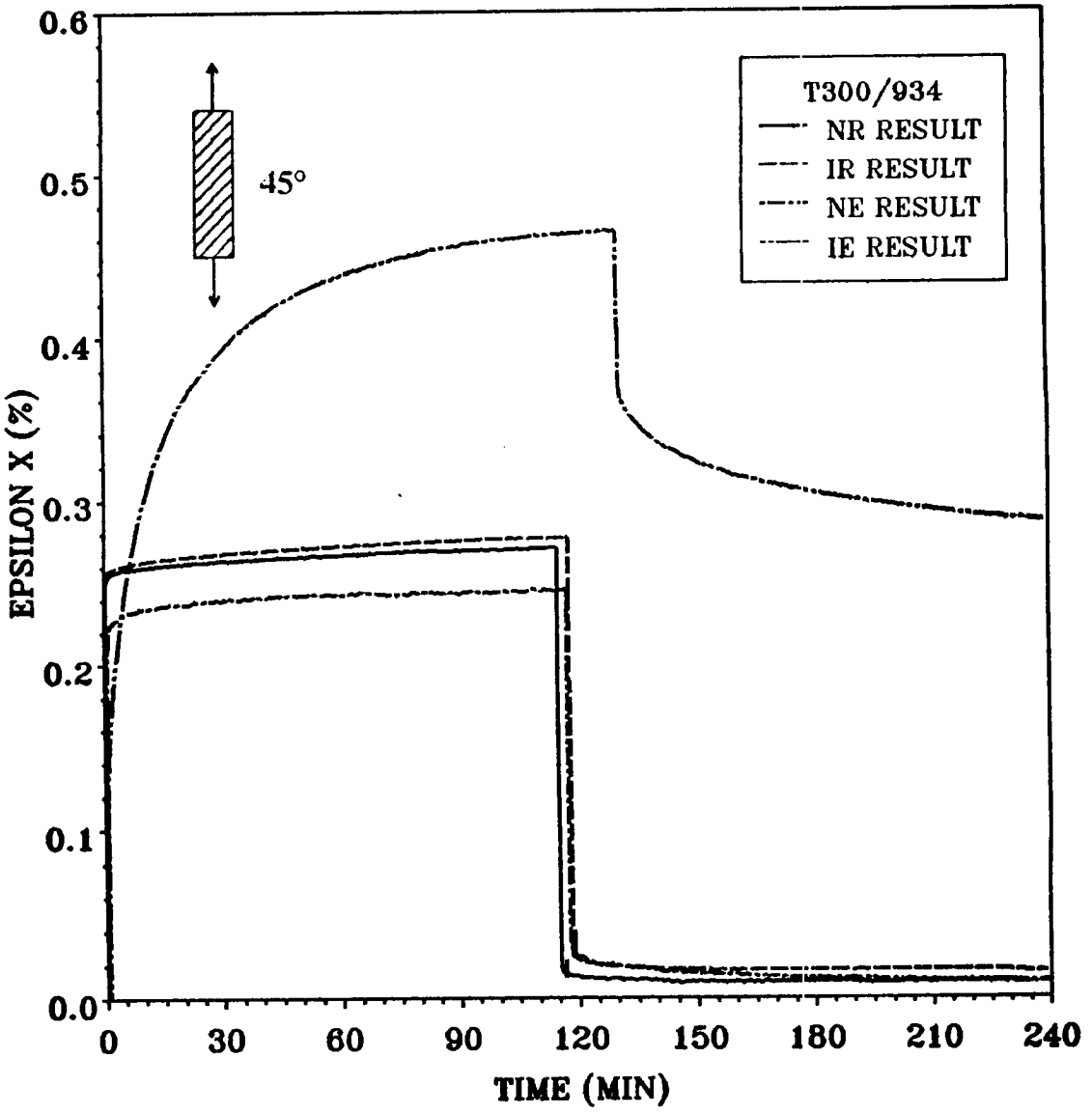

Figure 30. 45° Off-Axis Longitudinal Results at Initial Loading

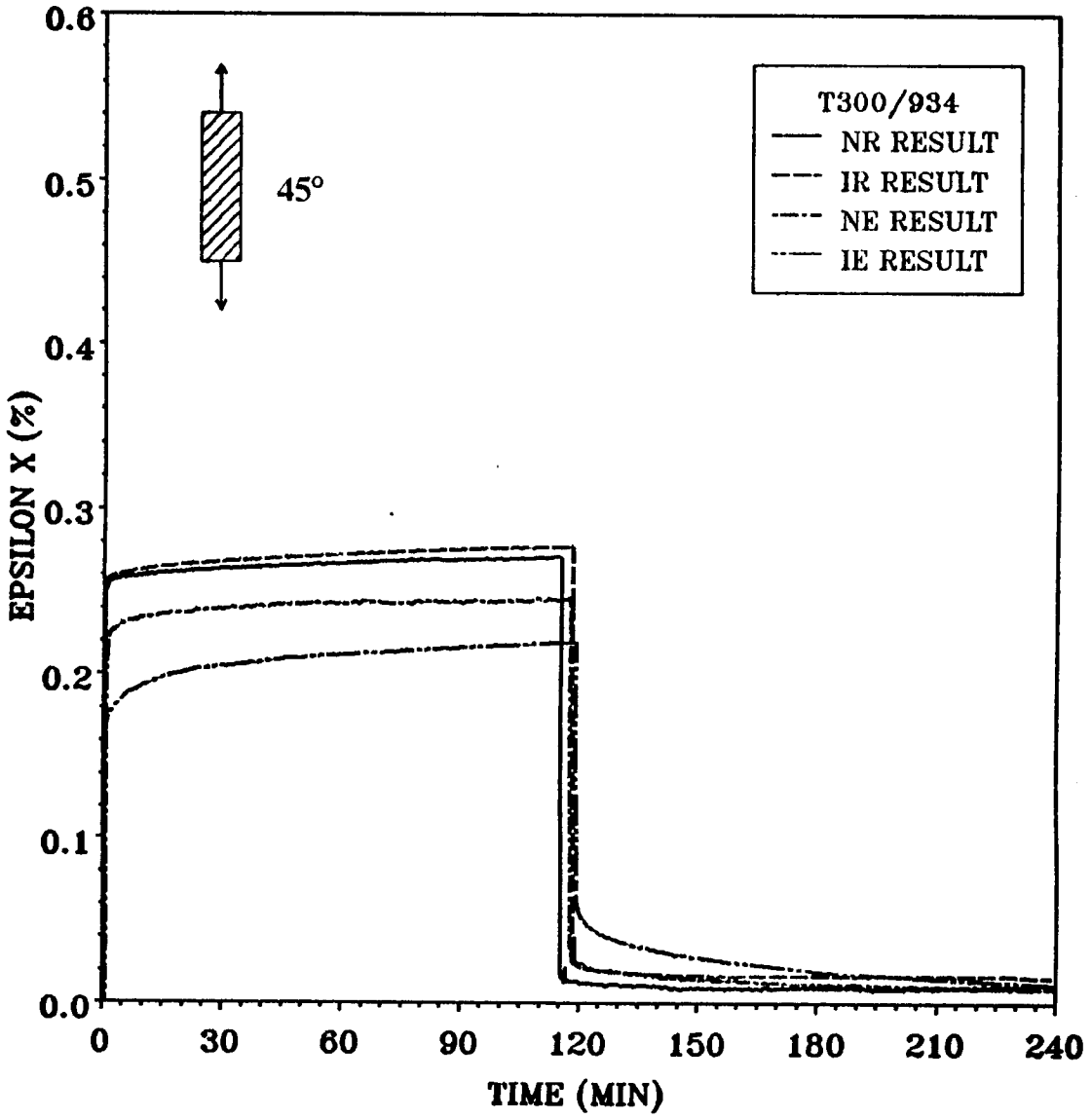

Figure 31. 45° Off-Axis Longitudinal Results at Final Loading

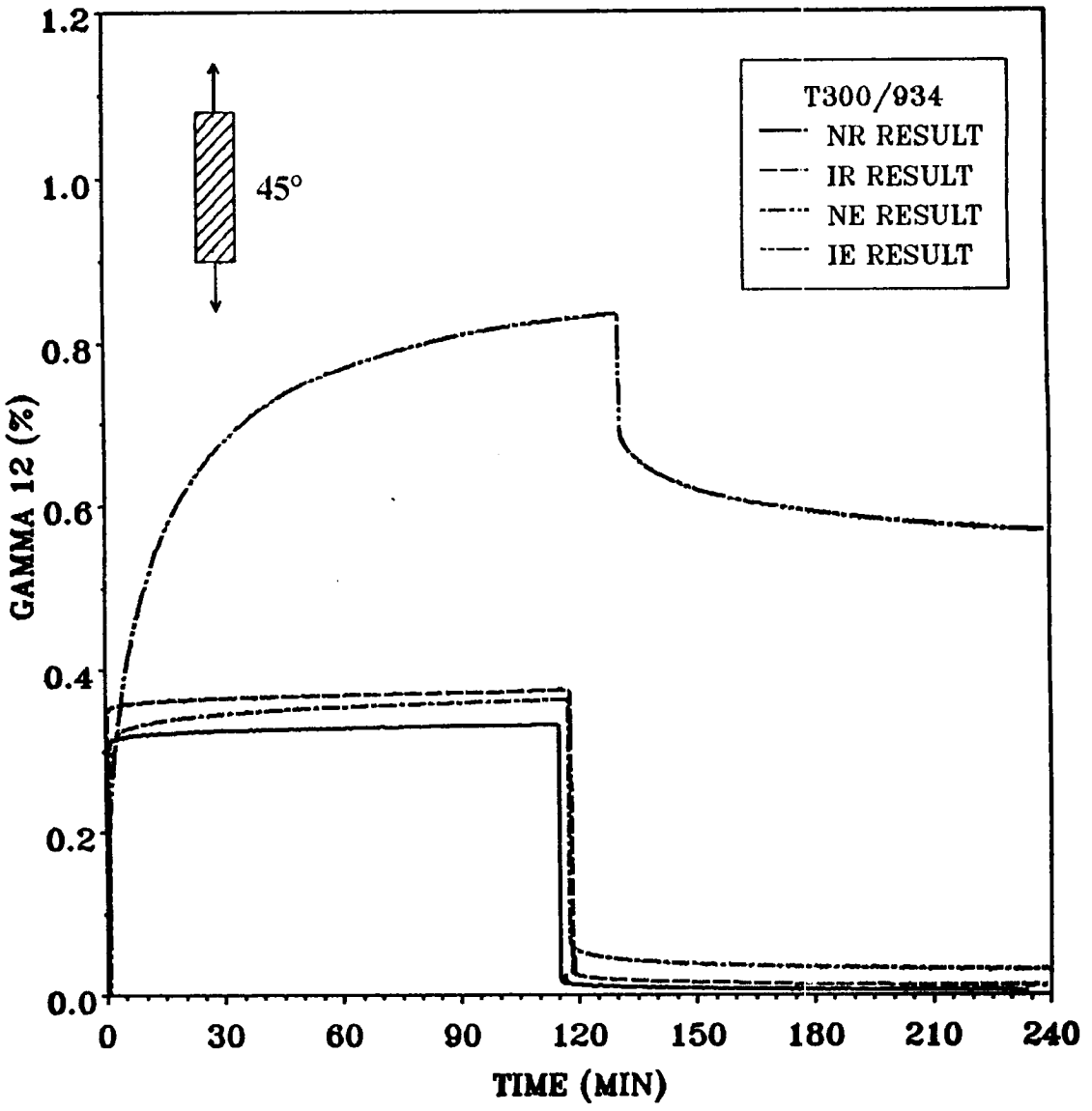

Figure 32. 45° Off-Axis Shear Results at Initial Loading

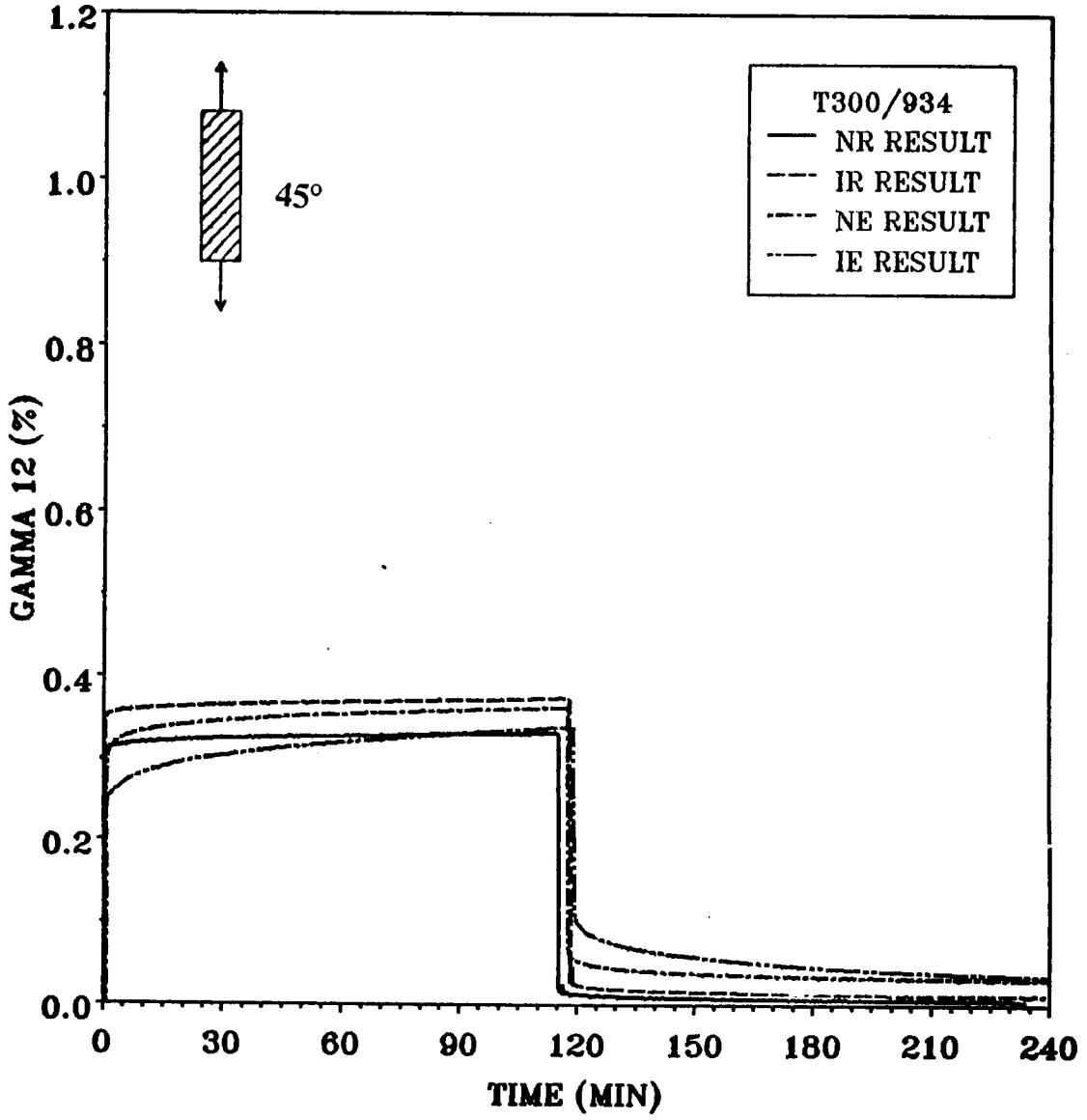

Figure 33. 45° Off-Axis Shear Results at Final Loading

more creep than the other conditions but not to the extent seen in the off-axis tests. The recovery for the IE and NE results appears to be approaching a final state below zero strain. It actually does proceed below zero before the test is completed. This will be discussed in Section 3.6.3. The NR and IR recovery results appear to be in error since the strain is increasing rather than decreasing. This will also be discussed in Section 3.6.3.

Figure 35 shows the longitudinal creep response for the 90° tensile coupon at a constant load level of 2.42 KSI. This is the second loading for the NR, IR, and NE tests and the third loading for the IE test. The creep response for the NR, IR, and NE results is again similar and here the IE creep response more nearly approaches the response of the other conditions. The IE response is still greater at 2.42 KSI but not as much as seen at 1.21 KSI. The recovery again seems to be headed below zero for the elevated temperature results and in fact does go below zero before the test is completed.

3.5 Linearity

In Chapter 4.0, it is assumed that the material used in this study behaves as a linearly viscoelastic material. The conditions and importance of linearity will be discussed in that chapter. An experimental method to check for linearity will be employed in this section for both the bulk resin and composite results.

3.5.1 Linearity Verification

A commonly used method to determine linearity of a material is to construct isochronous stress-strain curves where stress and strain values are plotted for a constant time value. As an example,

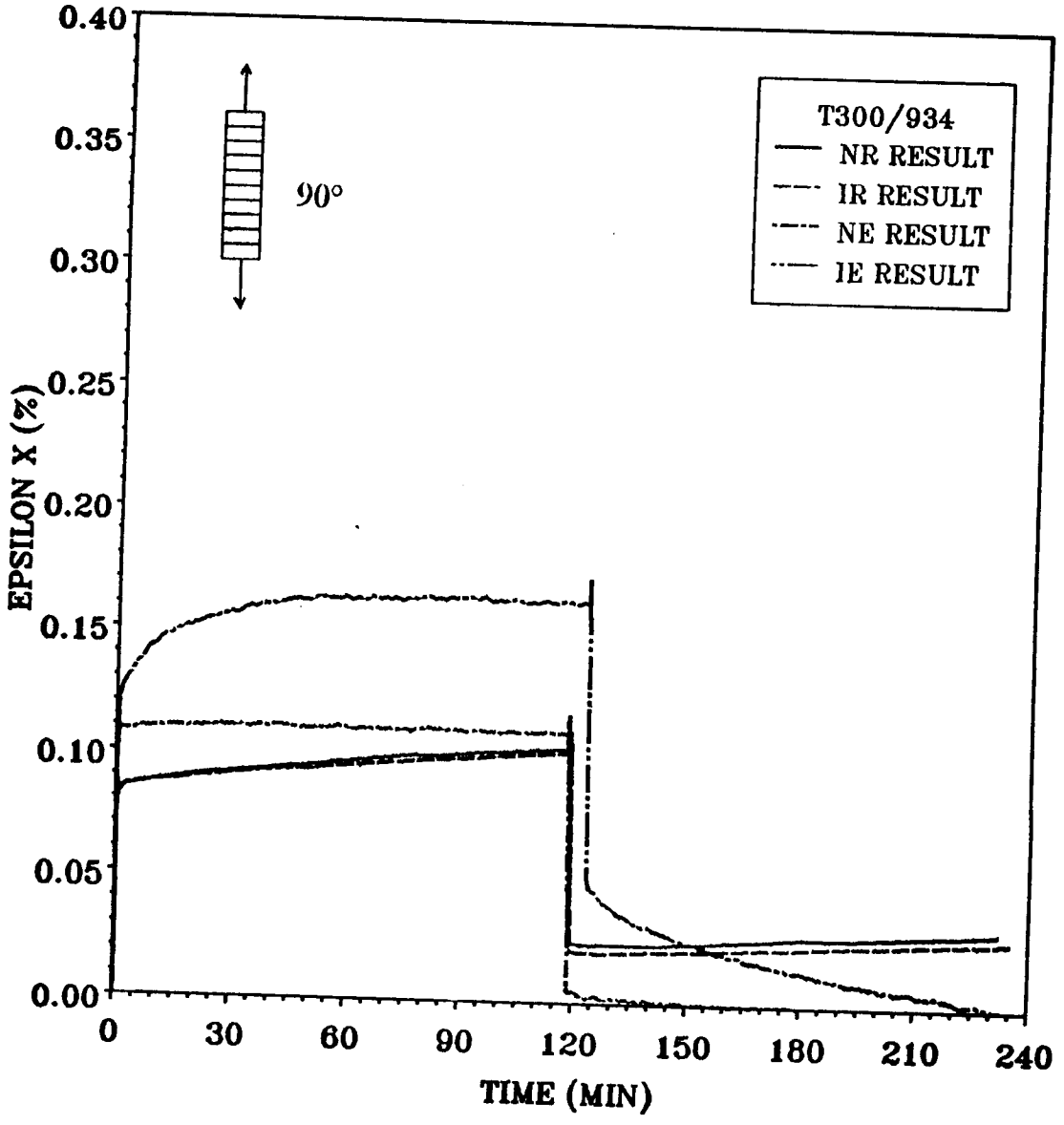

Figure 34. 90° Longitudinal Results at 1.21 KSI

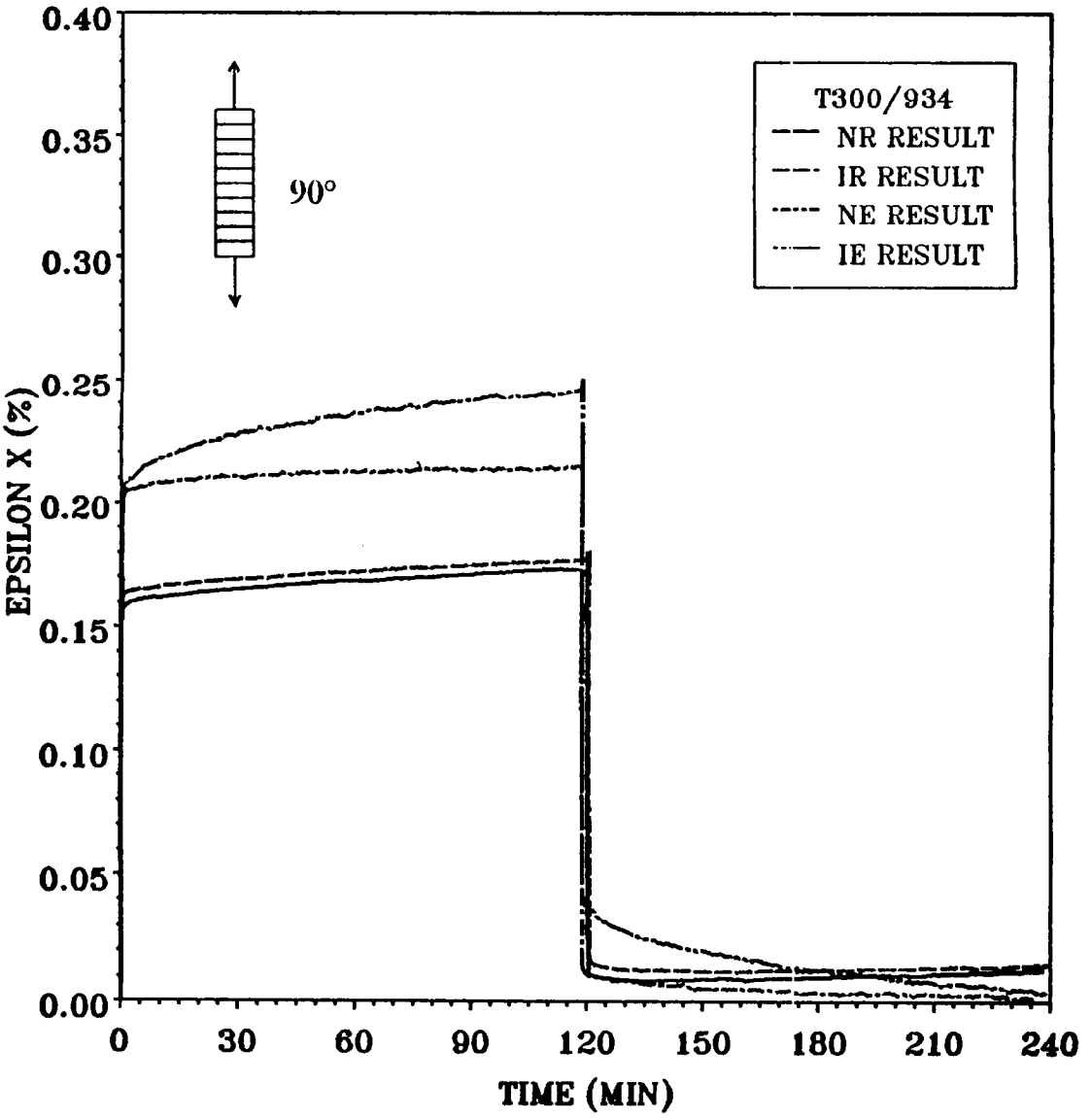

Figure 35. 90° Longitudinal Results at 2.42 KSI

a virgin specimen tested at different load levels will exhibit a response similar to the one in Figure 36. Each curve corresponds to a separate specimen tested at the corresponding load level. The stress and strain data at a given time value, when plotted on a stress-strain grid, should approximate a straight line. By taking different time values, a set of isochronous stress-strain curves is obtained. The material is assumed linearly viscoelastic if the isochronous curves are linear. This is illustrated in Figure 37.

In this study, a single specimen was tested at different load levels while allowing the coupon to recover at the conclusion of each loading. For the NR, IR, and NE results, the recovery exhibited relatively small permanent strains and it was assumed for the linearity verification of these results that each loading was as if on a virgin specimen.

3.5.2 Bulk Resin Linearity

The isochronous linearity curves for the bulk resin results are shown in Figure 38 through Figure 40. The NR, IR, and NE results show linear behavior for all times. Isochronous curves are drawn for 5 minutes, 30 minutes, 60 minutes, and 110 minutes. The linearity of the bulk resin is essential in the analysis of Chapter 4.0. A discussion on the linearity of the IE results will be presented in Section 3.6.2.

3.5.3 Composite Off-Axis Linearity

Isochronous linearity curves for the 10° off-axis results are shown in Figure 41 through Figure 43. The NR, IR, and NE results show linear behavior for all times. Graphite fibers behave as perfectly elastic and therefore linearity of the composite is totally dependent on the linearity of the resin matrix [28]. The linearity of the 10° off-axis tests verifies this assumption.

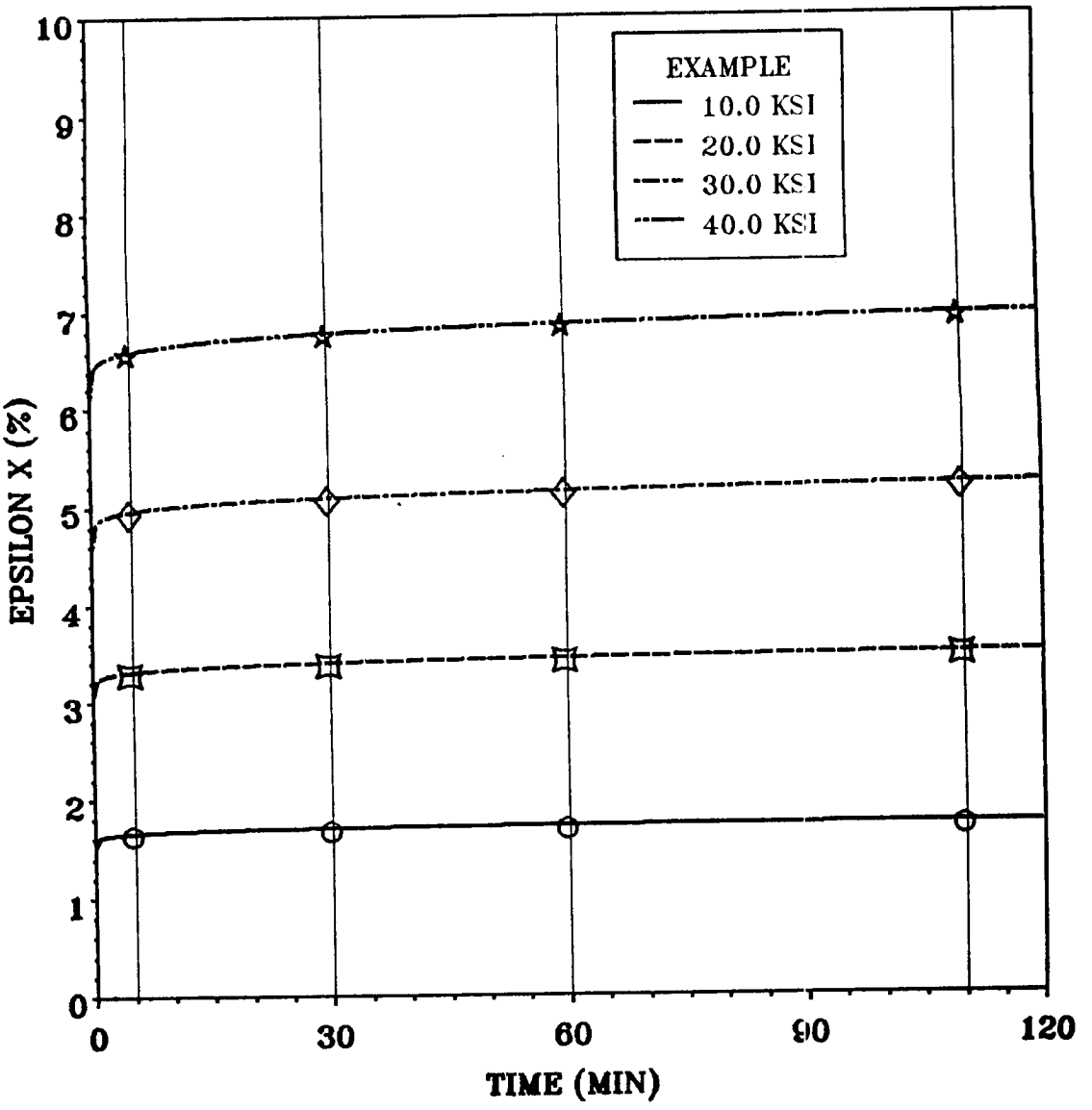

Figure 36. Example Creep Response for Linearity Verification Procedure

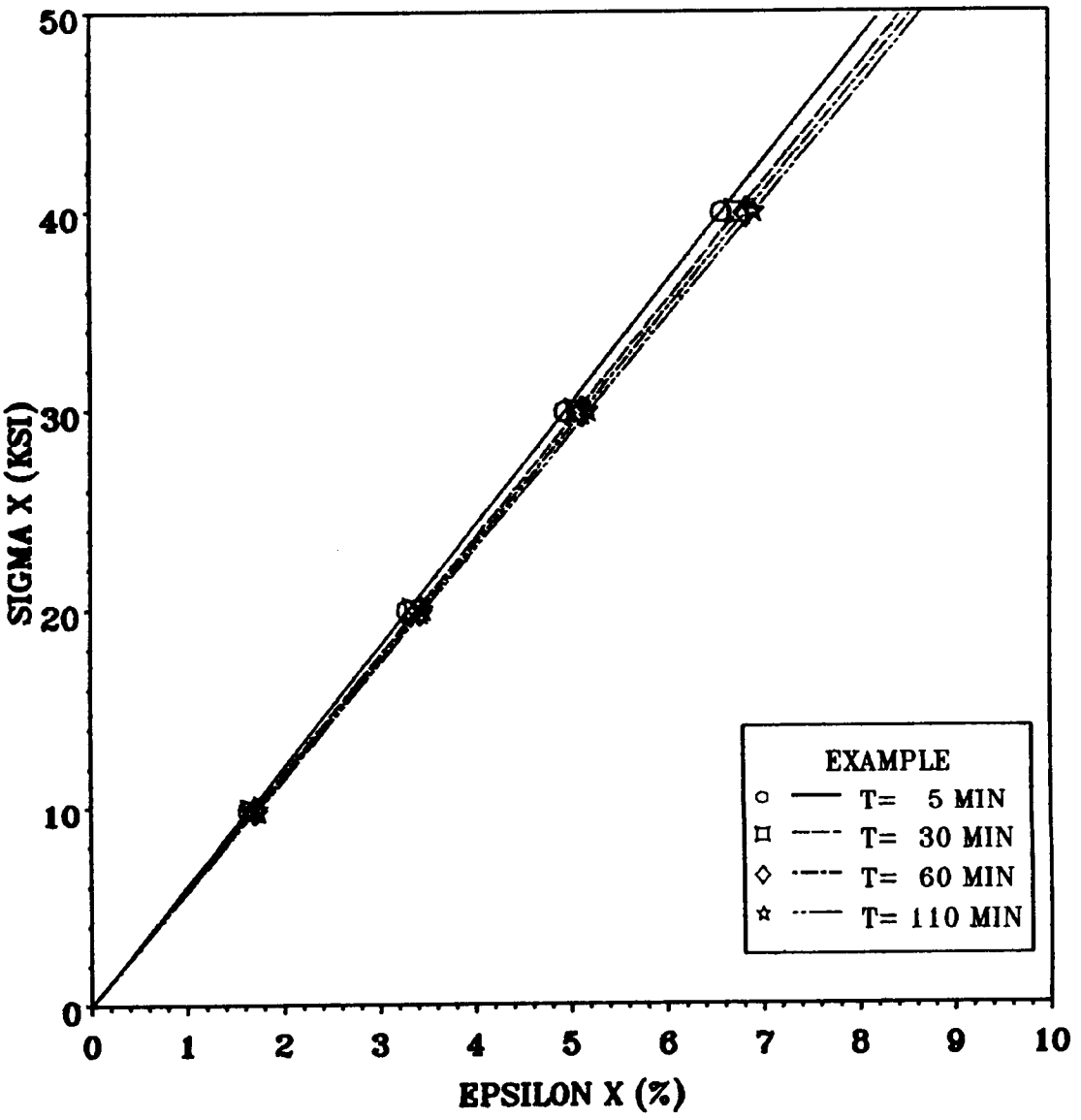

Figure 37. Example Isochronous Lines for Linearity Verification Procedure

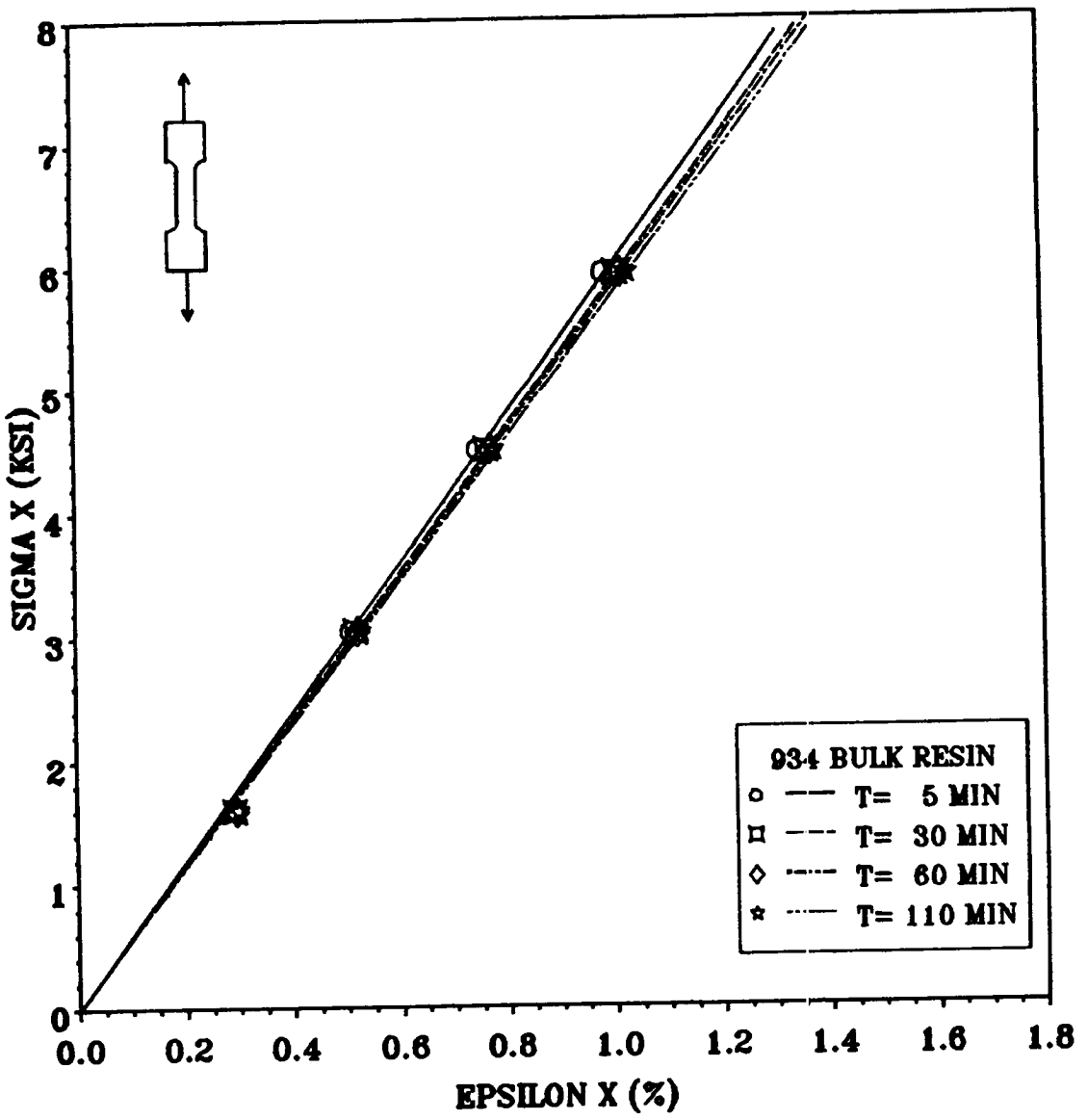

Figure 38. NR Bulk Resin Linearity Verification

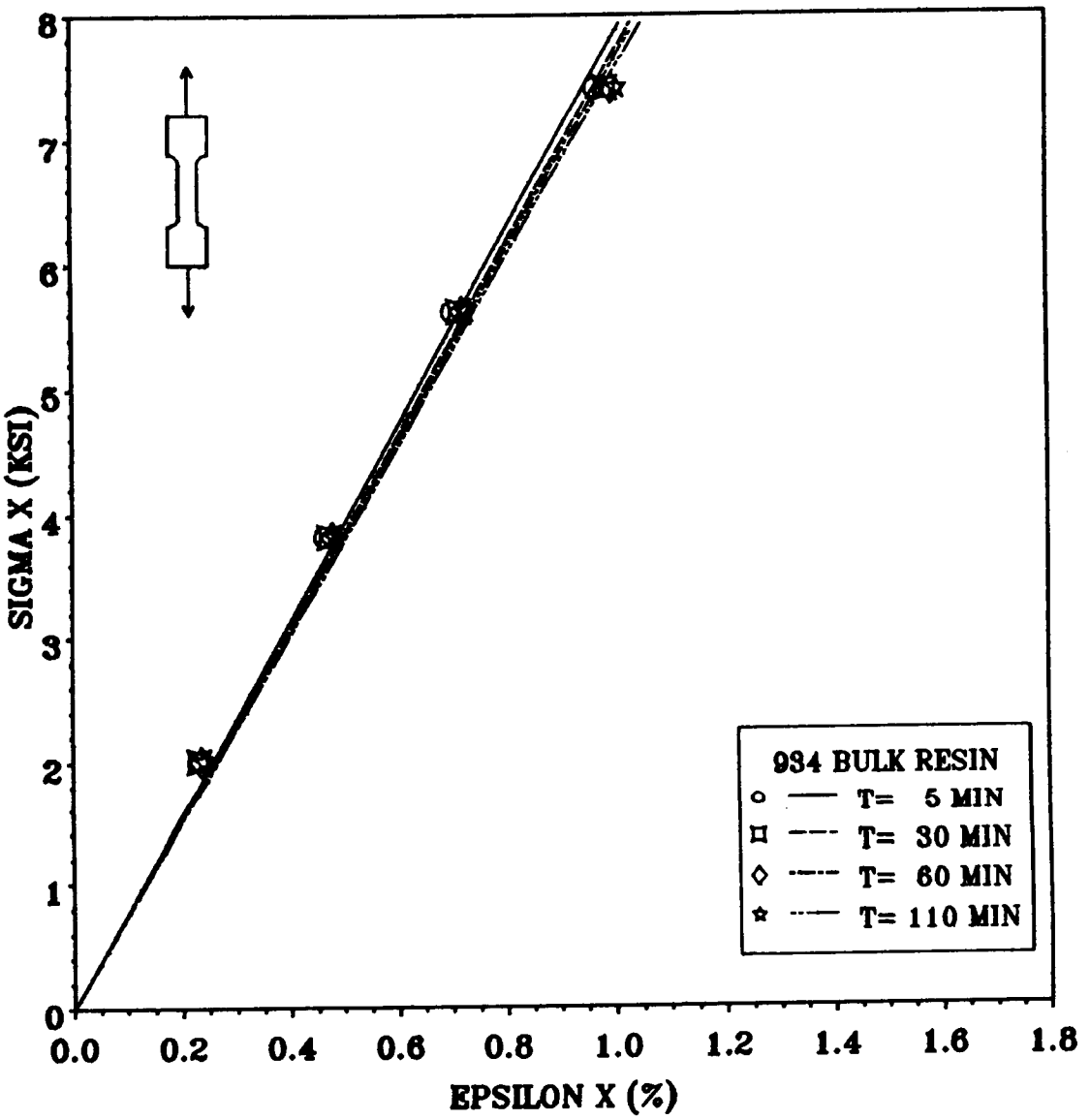

Figure 39. IR Bulk Resin Linearity Verification

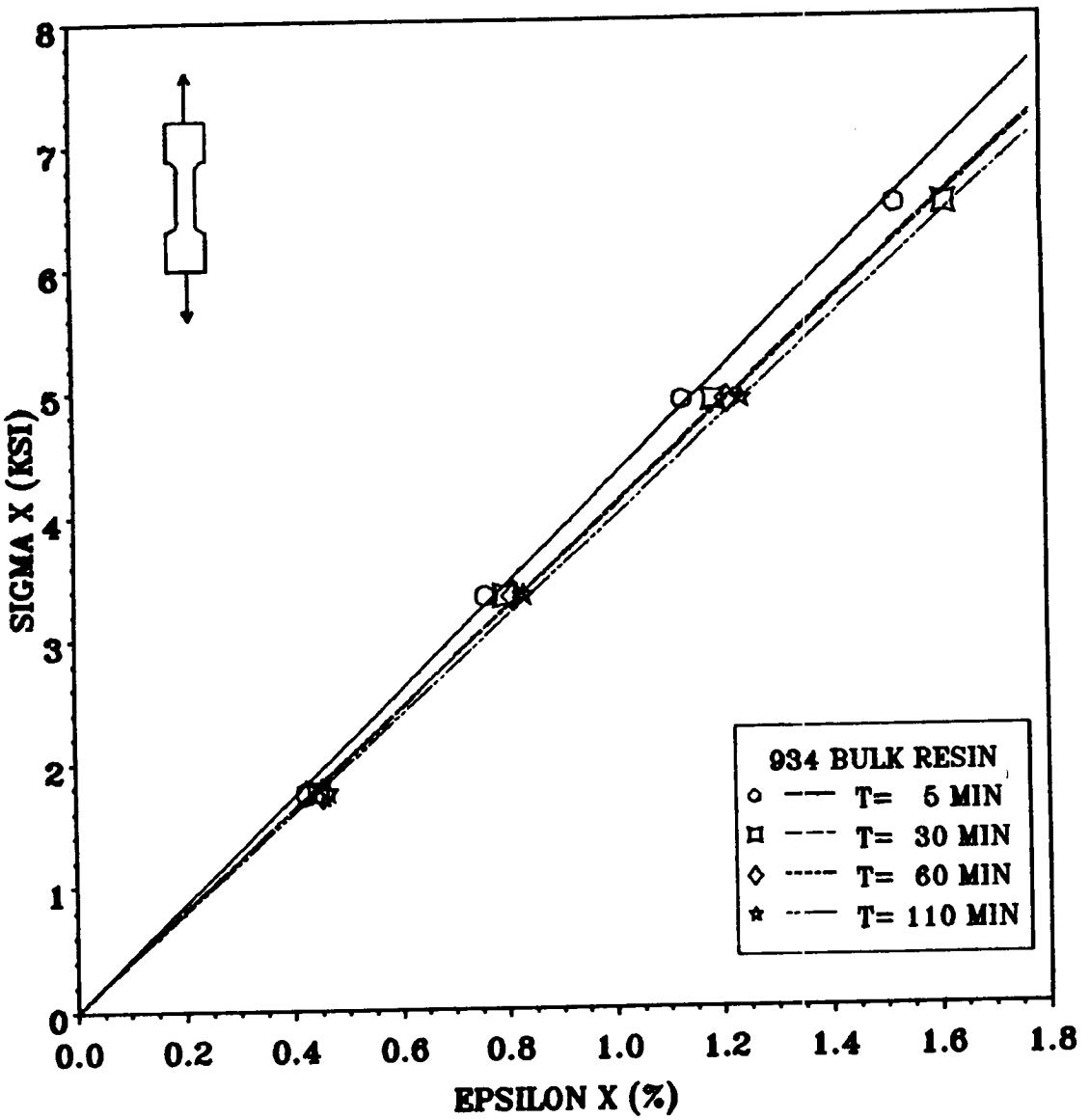

Figure 40. NE Bulk Resin Linearity Verification

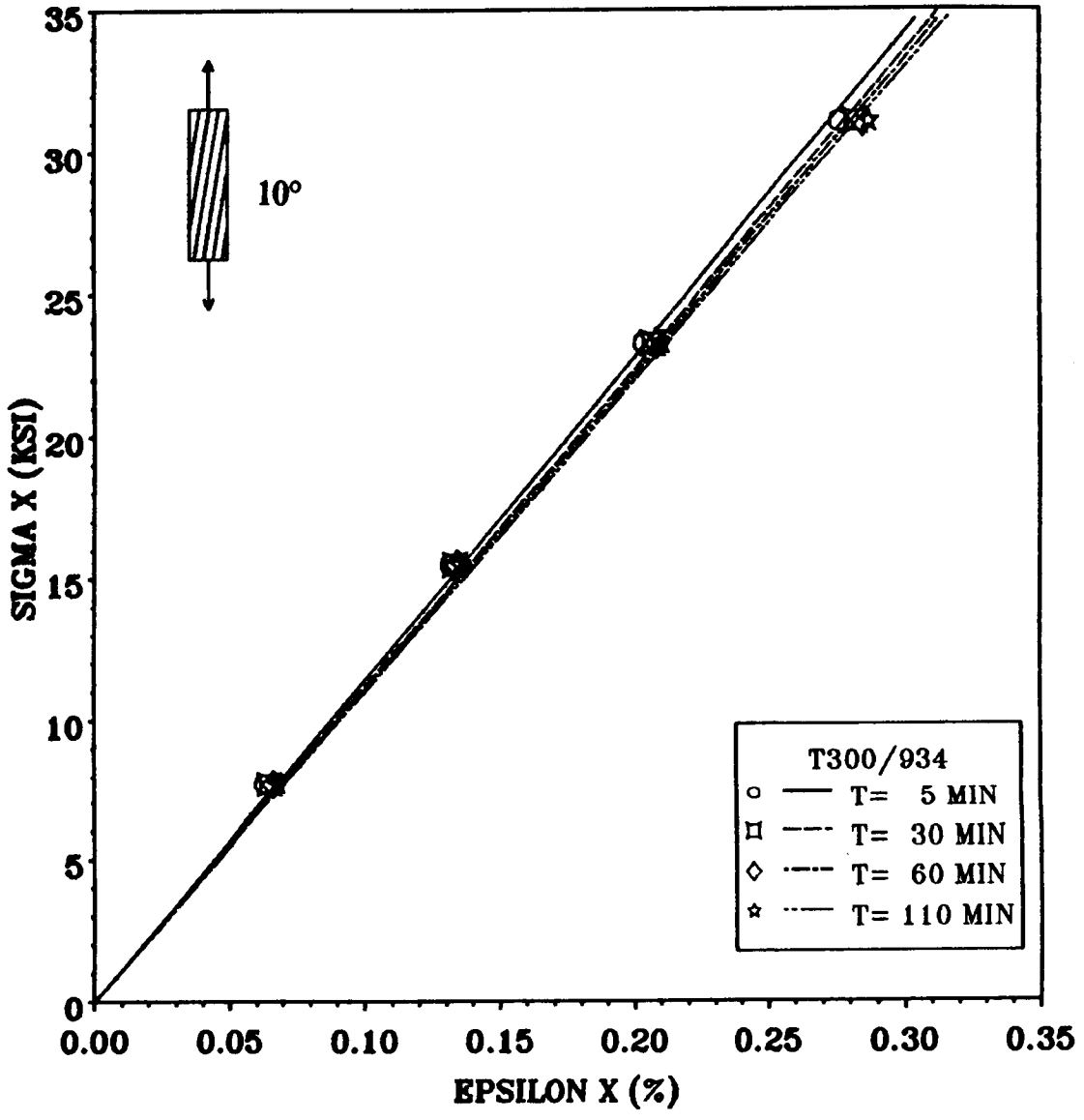

Figure 41. NR 10° Off-Axis Linearity Verification

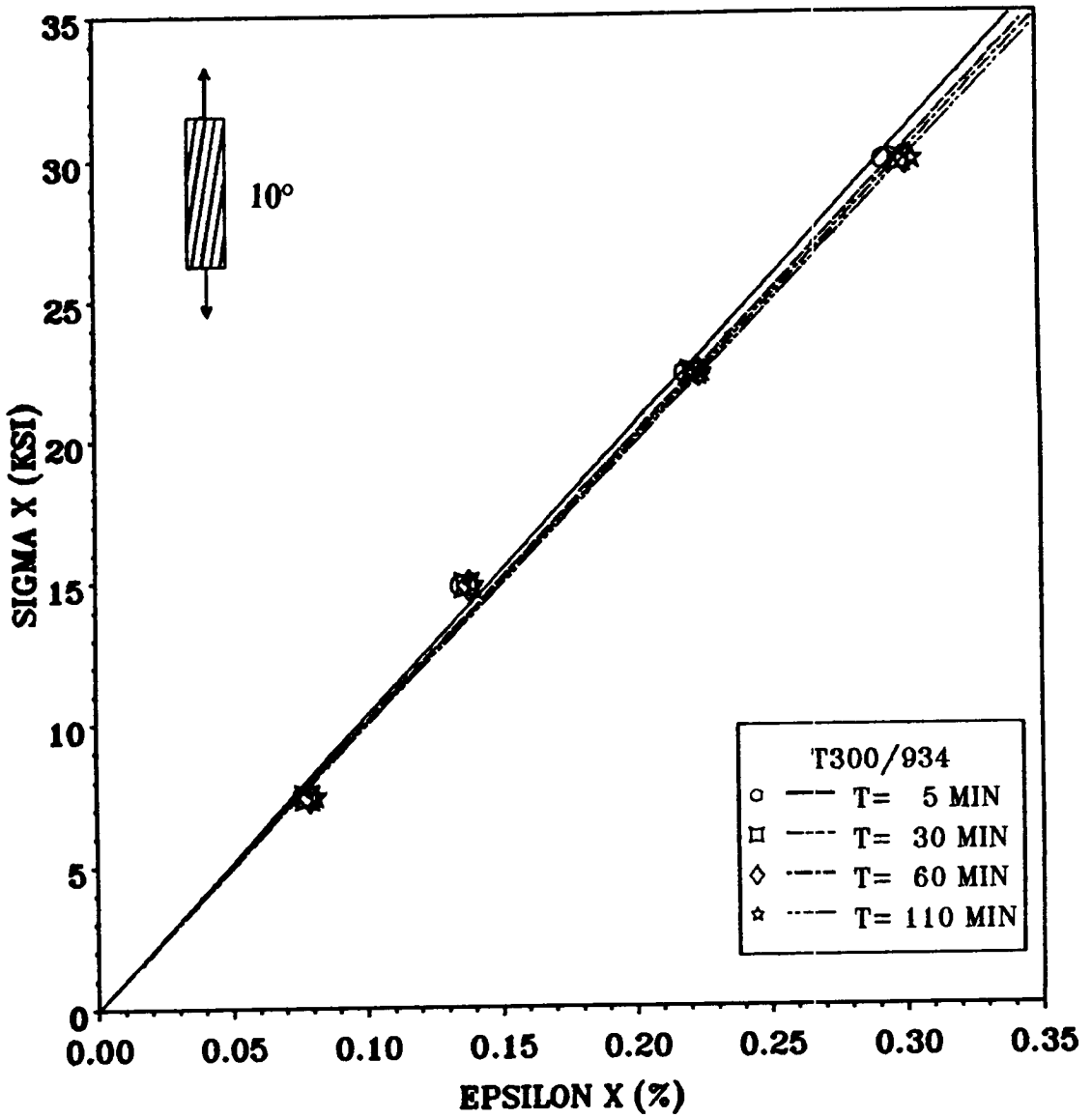

Figure 42. IR 10° Off-Axis Linearity Verification

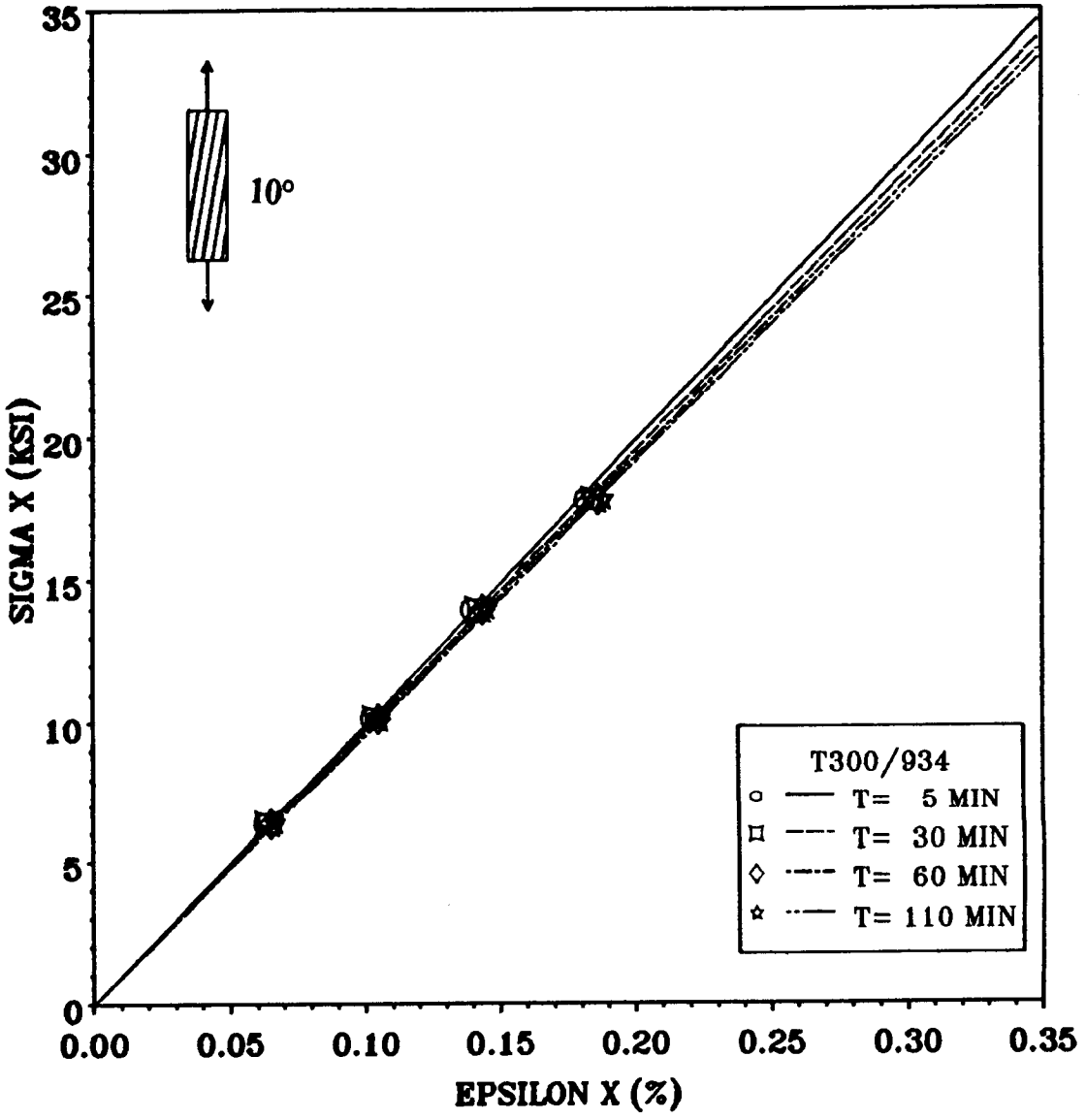

Figure 43. NE 10° Off-Axis Linearity Verification

3.5.4 Elastic Response

An additional verification of linearity is to evaluate the elastic response upon loading and unloading of the specimen. If the elastic response upon loading is identical to the elastic response upon recovery, then linearity of the elastic response is confirmed. Table 4 through Table 7 show the elastic response for the bulk resin, 10°, 45°, and 90° tests respectively. The elastic response for all four load levels is given as the initial instantaneous elastic strain upon loading and the instantaneous elastic strain upon recovery. The percent difference between these two values is given in the last column. Dash marks in the tables indicate data that is not available from the test data generated. As shown, the elastic response is within 2% in most cases and less than 5% for all cases. This confirms linearity of the elastic response for all conditions. Since the elastic response is due to stretching of primary bonds in the molecular structure, linearity of the elastic response suggests that radiation and temperature do not affect primary bonds.

3.6 Discussion

3.6.1 Healing Effects

As mentioned in Chapter 1, radiation causes chain scission and can break off radicals from molecular chains. These radicals will recombine over time and form cross-links. As the mobility of the radicals is increased, the rate at which they will recombine also increases. When temperatures near the T_g are reached, these radicals will quickly recombine. This phenomena is called healing of the epoxy resin and it can help us explain many of the test results obtained in this study.

Table 4. Bulk Resin Elastic Response

	Elastic Response			
	Bulk Resin Coupons			
Coupon	Load Level	Instantaneous Strain Upon Loading	Instantaneous Strain Upon Recovery	% Change
NR-BR	1	0.243	0.249	2.41%
	2	0.477	0.484	1.45%
	3	0.742	0.737	0.68%
	4	0.994	1.005	1.10%
IR-BR	1	0.324	0.323	0.31%
	2	0.575	0.573	0.35%
	3	0.823	0.825	0.24%
	4	1.096	1.098	0.18%
NE-BR	1	0.387	0.390	0.77%
	2	0.742	0.738	0.54%
	3	1.109	1.105	0.36%
	4	1.489	1.503	0.93%
IE-BR	1	0.407	0.400	1.75%
	2	-	-	-
	3	-	-	-
	4	-	-	-

Table 5. 10° Elastic Response

	Elastic Response			
	10° Coupons			
Coupon	Load Level	Instantaneous Strain Upon Loading	Instantaneous Strain Upon Recovery	% Change
NR-10	1	0.062	0.062	0.00%
	2	0.127	0.127	0.00%
	3	0.197	0.197	0.00%
	4	0.267	0.268	0.37%
IR-10	1	0.067	0.065	3.08%
	2	0.129	0.129	0.00%
	3	0.194	0.193	0.52%
	4	0.259	0.260	0.39%
NE-10	1	0.059	0.057	3.51%
	2	0.095	0.094	1.06%
	3	0.130	0.132	1.52%
	4	0.169	0.171	1.17%
IE-10	1	0.071	0.069	2.90%
	2	0.107	0.105	1.91%
	3	0.108	0.106	1.89%
	4	0.139	0.140	0.71%

Table 6. 45° Elastic Response

	Elastic Response			
	45° Coupons			
Coupon	Load Level	Instantaneous Strain Upon Loading	Instantaneous Strain Upon Recovery	% Change
NR-45	1	0.258	0.261	1.15%
	2	0.369	0.372	0.81%
	3	0.477	0.488	2.25%
	4	-	-	-
IR-45	1	0.252	0.248	1.61%
	2	0.347	0.348	0.29%
	3	-	-	-
	4	-	-	-
NE-45	1	0.224	0.217	3.23%
	2	0.351	0.353	0.57%
	3	0.412	0.403	2.23%
	4	-	-	-
IE-45	1	0.100	0.096	4.17%
	2	0.121	0.120	0.83%
	3	0.147	0.140	5.00%
	4	0.169	0.160	5.63%

Table 7. 90° Elastic Response

	Elastic Response			
	90° Coupons			
Coupon	Load Level	Instantaneous Strain Upon Loading	Instantaneous Strain Upon Recovery	% Change
NR-90	1	0.083	0.080	3.75%
	2	0.163	0.160	1.88%
	3	0.246	0.245	0.41%
	4	0.327	0.327	0.00%
IR-90	1	0.081	0.078	3.85%
	2	0.157	0.161	2.48%
	3	0.250	0.247	1.22%
	4	0.336	0.333	0.90%
NE-90	1	0.106	0.104	1.92%
	2	0.202	0.201	0.50%
	3	0.301	0.298	1.01%
	4	0.338	0.335	0.90%
IE-90	1	0.112	0.111	0.90%
	2	0.140	0.143	2.10%
	3	0.200	0.202	1.00%
	4	0.235	0.236	0.42%

The IE results in all cases seem to bear out this healing effect. As shown, the first loading always exhibited the greatest creep behavior while subsequent loadings exhibited a relative decrease in the creep behavior. Additionally, the recovery data shows large permanent strains. At + 250 °F, the broken chains in the epoxy are quite mobile and will slide, twist, and uncurl rapidly. Also at this temperature, radiation induced radicals in the epoxy are quite mobile and begin to recombine. As the specimen is strained, the radicals are moved and form new cross-links in the strained condition. Cross-linking in this fashion is an on-going process. Upon recovery, the epoxy is in a different state than when the load was applied. In this state, more cross-links now exist, many of which were formed in the strained state. This would create apparent permanent strain in the specimen. Upon subsequent loadings, the structure is more cross-linked, more rigid, and more resistant to creep. This would explain the decrease in creep behavior and the decrease in permanent strains seen upon subsequent loadings.

To verify this healing effect, some additional tests were run. Since cross-links are continually being reformed in the IE condition, some irradiated 10° specimens were tested after being pre-soaked at + 250 °F for varying amounts of time. Figure 44 shows the creep response of these tests. As shown, the longer the specimen is exposed to + 250 °F, the less creep behavior is seen. After eight hours at + 250 °F, the creep response of the 10° off-axis specimen is approaching the NR creep response of the material. This suggests that healing is taking place while the temperature is held at + 250 °F.

The linearity of the elastic response for the IE condition coupled with the healing of the time-dependent response suggests that radiation is only affecting secondary bonds of the epoxy network. It also suggests that the healing process is only concerned with secondary bonds and does not affect the primary bonds of the structure. Upon loading, the stretching of primary bonds is instantaneous and is evidenced in the elastic response of a test specimen. Twisting, uncurling, and sliding of secondary bonds is time-dependent and is evidenced in the viscoelastic response of a test specimen. Radiation and healing seem to affect only the viscoelastic response of the tested specimens and not the elastic response.

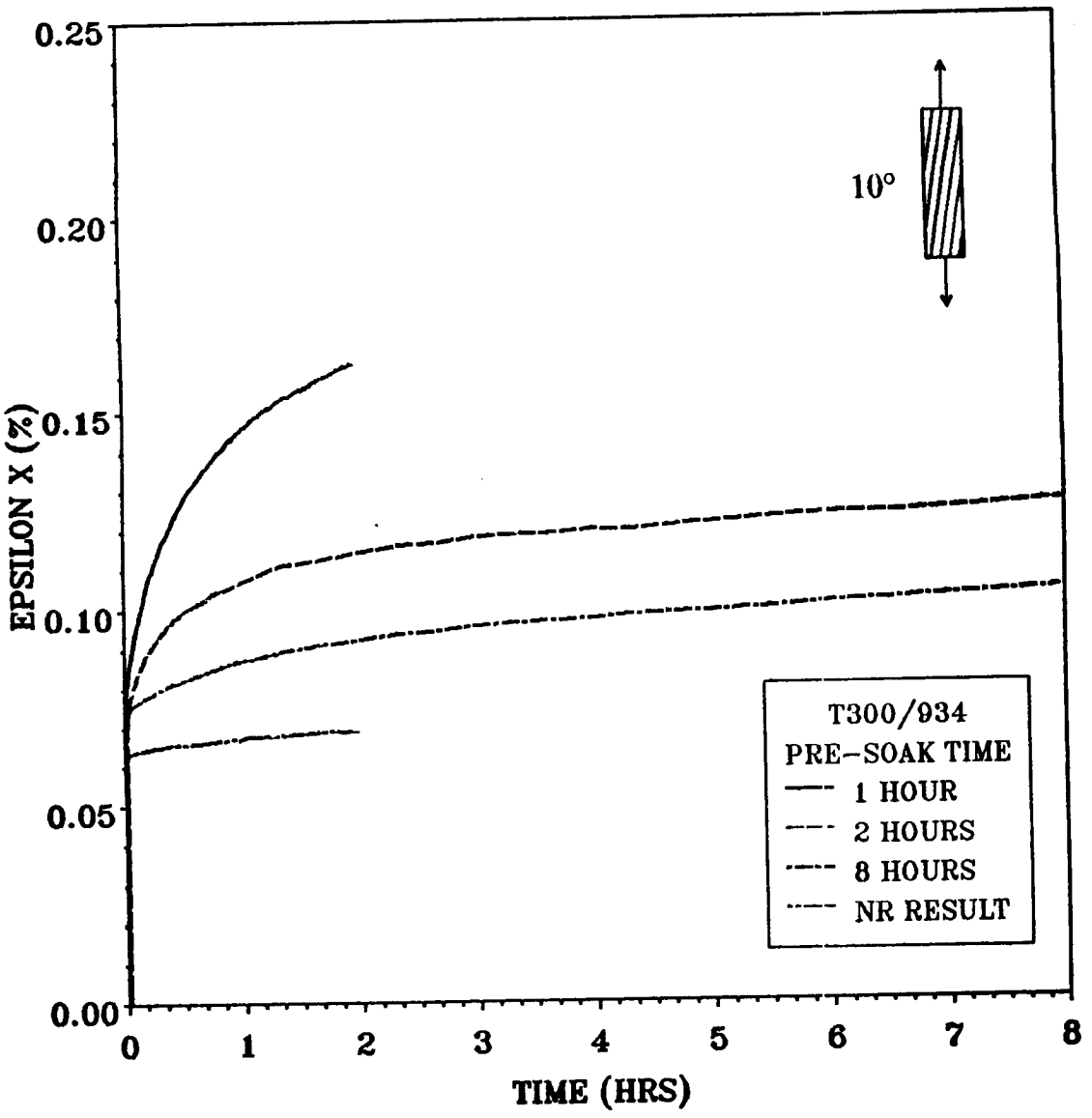

Figure 44. Effect of Pre-Soak Time at 250 °F on Creep Response

3.6.2 IE Linearity

Because of the healing process, the evaluation of linearity in the IE bulk resin is a complicated task. Viscoelastic linearity, as it has been assumed in this study, is dependent on stress, strain, and time. The healing process appears to be dependent on temperature and pre-soak time, both of which are parameters not commonly associated with linear viscoelasticity. These additional parameters introduce apparent nonlinearities into both the IE bulk resin response and the IE composite response. The healing process constantly changes the state of the material. Since viscoelastic linearity is a *material* property, as the material changes through healing, so does the linearity of the material. This manifests itself as apparent nonlinearity of the material. Although the IE material may be linear at any given time, linearity in the general sense cannot be assumed for this condition.

3.6.3 90° Recovery Discussion

T300/934 graphite epoxy is a +350 °F cure epoxy system. Upon curing, cross-linking occurs at +350 °F to make the epoxy a rigid structure. Upon cooling, the epoxy in an unconstrained state contracts isotropically while the unconstrained graphite fibers expand slightly in the longitudinal direction. Because of constraints present in the composite, tensile residual stresses in the fiber direction are present in the matrix and compressive residual stresses in the fiber direction are present in the fibers. The residual stresses in the fiber and matrix increase as the graphite/epoxy composite is cooled from +350 °F. In other words, the residual stresses in the composite at room temperature would be greater than the residual stresses at +250 °F. This phenomena may explain the differences in the recovery responses of the 90° room temperature coupons and the 90° elevated temperature coupons.

Tensile residual stresses in the fiber direction that are present in the room temperature graphite/epoxy material can be quite significant. A typical graphite/epoxy composite may have

tensile residual stresses in the matrix as high as 80-90% of the ultimate strength of the epoxy resin [34]. Upon applying a tensile load to a 90° specimen, fibers and matrix contract transversely in accordance with the composite Poisson's response. Under uniaxial loading, the unconstrained matrix would contract more than a transversely loaded, unconstrained graphite fiber. Due to constraints in the composite, however, tensile residual stresses in the matrix in the fiber direction are further increased. In a room temperature composite, this increases the already significant tensile residual stresses in the matrix which may then become high enough to cause damage in the epoxy. Damage would restrict the recovery of the coupon.

At +250 °F, tensile residual stresses in the fiber direction that are present in the matrix would be quite small. These tensile residual stresses in the matrix at +250 °F will be on the order of only 20-30% of the ultimate strength of the epoxy resin [34]. Applying a tensile load to a 90° specimen would create a tensile load in the matrix in the fiber direction. Since tensile residual stresses in the matrix are minimal to begin with, residual stresses caused by uniaxial loading would not be significant enough to cause damage and the epoxy would creep in the direction of the tensile residual stress. Any permanent strain resulting from the creep of the epoxy would manifest itself in an increased width of the specimen. An increased width of the specimen would create a decreased length in accordance with the Poisson's response. This can explain the recovery dipping below zero for the elevated temperature results.

4.0 Analytical Model

This chapter will discuss the formulation of the analytical prediction tool developed in this study. The goal of the analytical formulation was to modify existing micromechanical models, now formulated to predict elastic response, to have the capability to predict viscoelastic response as well. This modification is accomplished by use of the Correspondence Principle.

A discussion of linear viscoelasticity and the principles behind it will first be presented along with a discussion of the Correspondence Principle and its application to problems in linear viscoelasticity. The micromechanics models will then be presented and discussed in addition to how the Correspondence Principle can be applied to these models. A discussion will follow on the viscoelastic modeling of the matrix and how the various viscoelastic parameters to be used with the model formulation were evaluated. This chapter will end with a presentation and discussion of sample results obtained from this predictive model formulation for glass reinforced epoxy.

4.1 Linear Viscoelasticity

For a perfectly elastic material, the stress and strain is related by Hooke's Law. This law states that

$$\sigma_{ij} = E_{ijkl}\,\varepsilon_{kl} \tag{4.1}$$

or,

$$\varepsilon_{ij} = D_{ijkl}\,\sigma_{kl} \tag{4.2}$$

where σ_{ij} and ε_{ij} represent the stress and strain respectively. E_{ijkl} is known as the elasticity tensor and D_{ijkl} is known as the compliance tensor. A perfectly elastic material is characterized by stresses and strains that are not dependent on time.

The response of a viscoelastic material is not only dependent on the present state of body forces and surface tractions, but also on the entire history of such forces. Linear viscoelasticity is concerned with materials whose time-dependent displacements and strains are small and can be superimposed in time according to the Boltzmann superposition principle. Assuming a homogeneous material and a stress and strain field that are not space dependent, the Boltzmann superposition principle states that

$$\sigma_{ij}(t) = \int_{-\infty}^{t} C_{ijkl}\,(t-\tau)\frac{d\varepsilon_{kl}}{d\tau}\,d\tau \tag{4.3}$$

or,

$$\varepsilon_{ij}(t) = \int_{-\infty}^{t} S_{ijkl}\,(t-\tau)\frac{d\sigma_{kl}}{d\tau}\,d\tau \tag{4.4}$$

where the $C_{ijkl}(t)$ and $S_{ijkl}(t)$ are response functions which define the given material behavior. The $C_{ijkl}(t)$ are known as the relaxation moduli and the $S_{ijkl}(t)$ are known as the creep compliances. The same symmetry conditions hold for these tensors as for the corresponding elastic tensors. In order to determine these functions, we proceed in the following fashion. First define a step function strain such that

$$\varepsilon_{ij}(t) = \varepsilon_{ij}^{o} H(t) \tag{4.5}$$

where

$$H(t) = \begin{cases} 0 & t < 0 \\ 1 & t \geq 0 \end{cases} \tag{4.6}$$

is defined as the unit step function.

The derivative of H(t) is the delta function $\delta(t)$ defined as

$$\delta(t) = \begin{cases} 0 & |t| > 0 \\ 1 & t = 0 \end{cases} \tag{4.7}$$

Inserting (4.5) into (4.3) gives

$$\sigma_{ij}(t) = C_{ijkl}(t)\, \varepsilon_{kl}^{o} \tag{4.8}$$

Similarly, imposing a step function stress

$$\sigma_{ij}(t) = \sigma_{ij}^{o} H(t) \tag{4.9}$$

results in

$$\varepsilon_{ij}(t) = S_{ijkl}(t)\, \sigma_{kl}^{o} \tag{4.10}$$

Equations (4.8) and (4.10) provide a convenient experimental method to determine $C_{ijkl}(t)$ and $S_{ijkl}(t)$. To determine the creep compliance $S_{ijkl}(t)$, for example, a step function stress is applied. By monitoring the strain $\varepsilon_{ij}(t)$ as a function of time and dividing through by the stress level σ^{o}_{kl}, the creep compliance $S_{ijkl}(t)$ is evaluated. A similar procedure is followed in evaluating the relaxation moduli $C_{ijkl}(t)$.

In the laboratory, measurements can only be made when the experiment begins, which leads to the assumption

$$\varepsilon_{ij}(-\infty, t) = \begin{cases} 0 & t < 0 \\ \varepsilon_{ij}(t) & t \geq 0 \end{cases} \tag{4.11}$$

This expression contains a discontinuity at $t = 0$ which gives

$$\varepsilon_{ij}(-\infty, t) = \varepsilon_{ij}(0)\, H(t) + \varepsilon'_{ij}(t) \tag{4.12}$$

where ε'_{ij} is continuous and vanishes for t < 0. The derivative of the strain is therefore

$$\frac{d\varepsilon_{ij}}{dt} = \varepsilon_{ij}(0)\delta(t) + \frac{d\varepsilon'_{ij}}{dt} \tag{4.13}$$

Inserting this into (4.3) we get

$$\sigma_{ij}(t) = C_{ijkl}(t)\, \varepsilon_{kl}(0) + \int_{0_+}^{t} C_{ijkl}(t-\tau)\frac{d\varepsilon_{kl}}{d\tau}\, d\tau \tag{4.14}$$

Taking the same approach with a suddenly applied stress gives

$$\varepsilon_{ij}(t) = S_{ijkl}(t)\, \sigma_{kl}(0) + \int_{0_+}^{t} S_{ijkl}(t-\tau)\frac{d\sigma_{kl}}{d\tau}\, d\tau \tag{4.15}$$

Equations (4.14) and (4.15) can be simplified by writing

$$\sigma_{ij}(t) = \int_0^t C_{ijkl}(t-\tau)\frac{d\varepsilon_{kl}}{d\tau}\,d\tau \tag{4.16}$$

$$\varepsilon_{ij}(t) = \int_0^t S_{ijkl}(t-\tau)\frac{d\sigma_{kl}}{d\tau}\,d\tau \tag{4.17}$$

assuming that these integral expressions take jump discontinuities into account.

4.2 *Correspondence Principle*

4.2.1 Laplace Transform Conversion

The Laplace transform is a useful tool in the field of viscoelasticity. The Laplace transform of a function $\phi(t)$ is defined as:

$$\mathcal{L}[\phi(t)] = \bar{\phi}(s) = \int_0^\infty e^{-st}\,\phi(t)dt \tag{4.18}$$

The convolution theorem is also useful here. The convolution of the Laplace transform is

$$\mathcal{L}\left[\int_0^\infty \phi(t-\tau)\,\psi(\tau)d\tau\right] = \bar{\phi}(s)\,\bar{\psi}(s) \tag{4.19}$$

The Laplace Transform of a derivative is

$$\mathcal{L}\left[\frac{d\phi}{dt}\right] = s\,\bar{\phi}(s) - \phi(0) \tag{4.20}$$

Using these expressions with $\phi(0) = 0$ and taking equations (4.16) and (4.17) and the Laplace transforms of each gives

$$\bar{\sigma}(s) = s\,\bar{C}_{ijkl}(s)\,\bar{\varepsilon}_{kl}(s) \tag{4.21}$$

$$\bar{\varepsilon}(s) = s\,\bar{S}_{ijkl}(s)\,\bar{\sigma}_{kl}(s) \tag{4.22}$$

It can be seen from relations (4.21) and (4.22) that if it is allowed that

$$s\,\bar{C}_{ijkl}(s) = \Gamma_{ijkl}(s) \tag{4.23}$$

$$s\,\bar{S}_{ijkl}(s) = \mathrm{K}_{ijkl}(s) \tag{4.24}$$

then

$$\bar{\sigma}_{ij}(s) = \Gamma_{ijkl}(s)\,\bar{\varepsilon}_{kl}(s) \tag{4.25}$$

$$\bar{\varepsilon}_{ij}(s) = \mathrm{K}_{ijkl}(s)\,\bar{\sigma}_{kl}(s) \tag{4.26}$$

These equations are similar to an elastic stress-strain law. $\Gamma_{ijkl}(s)$ and $\mathrm{K}_{ijkl}(s)$ are known as the transform domain moduli and compliances respectively.

4.2.2 Boundary Value Problems

Now consider a viscoelastic body in the presence of body forces. Ignoring the inertia terms, the equilibrium equations are

$$\sigma_{ij,\,j}(\underline{x}, t) = 0 \tag{4.27}$$

To obtain the differential equations for the displacements, substitute (4.16) into (4.27) to get

$$\frac{\partial^2}{\partial x_i \partial x_j}\left[\int_0^t C_{ijkl}(t-\tau)\frac{\partial u_k(\underline{x},\tau)}{\partial \tau}\,d\tau\right] = 0 \tag{4.28}$$

The boundary conditions on the surface S can be of the type

$$u_i(S,t) = u_i^o \quad on\ S_u \tag{4.29}$$

$$T_i(S,t) = T_i^o \quad on\ S_T \tag{4.30}$$

where S_u denotes the part of the surface over which the displacements are prescribed and S_T denotes the part of the surface over which the tractions are prescribed. If the body is heterogeneous then (4.29) and (4.30) must be satisfied in each phase and the additional boundary interface conditions

$$\left.\begin{matrix} u_i(\underline{x},t) \\ T_i(\underline{x},t) \end{matrix}\right\} \quad continuous\ on\ S_{interface} \tag{4.31}$$

will be imposed where $S_{interface}$ denotes all interface boundaries.

This boundary value problem is quite complicated in the space-time domain. If, however, the transforms of equations (4.28) through (4.31) are taken to the Laplace transform domain, the problem becomes

$$s\,\overline{C}_{ijkl}\,u_{k,lj} = 0 \tag{4.32}$$

$$\overline{u}(S,s) = \overline{u}_i^o \quad on\ S_u \tag{4.33}$$

$$\overline{T}(S,s) = \overline{T}_i^o \quad on\ S_T \tag{4.34}$$

$$\left.\begin{matrix} \overline{u}_i(\underline{x},s) \\ \overline{T}_i(\underline{x},s) \end{matrix}\right\} \quad continuous\ on\ S_{interface} \tag{4.35}$$

where

$$\overline{T}_i = s\,\overline{C}_{ijkl}\,\overline{u}_{k,l}\,n_j \tag{4.36}$$

Examination of equations (4.32) through (4.36) shows that these equations are analogous to a formulation of an elasticity problem if the transform domain moduli $s\,\overline{C}_{ijkl} = \Gamma_{ijkl}$ assume the role of the elastic moduli. A convenient method of solving linear quasi-static viscoelastic problems, therefore, is to solve the associated elastic problem, substitute in the transform domain moduli for the elastic moduli, and obtain the transforms $\overline{u}_i(\underline{x}, s)$ and $\overline{\sigma}_{ij}(\underline{x}, s)$ of the viscoelastic solution. Inversion of the Laplace transform then gives the viscoelastic solution. This is known as the Correspondence Principle [35].

4.3 *Micromechanical Models*

Since the advent of composite materials, scientists and engineers have attempted to develop effective methods for predicting their properties. Since composites are generally composed of two separate materials whose material properties are known, it seems advantageous to develop models to predict properties of the composite using the properties of the individual constituents. This would allow the designer to look at many different combinations of materials to find the one that best meets his needs. The study dealing with this subject is that of micromechanics. The basic goal of micromechanics is to model a "representative cell" consisting of, in the case of continuous fiber reinforced composites, a single fiber and the surrounding matrix material. The objective is to analyze the representative cell with the implication that this cell is "representative" of the total composite. Micromechanics can not only be useful as a predictive tool but can also help us understand composites at the "micro" scale of a single fiber.

Two micromechanical models that are being used today will now be discussed. The Composite Cylinder Assemblage (CCA) model proposed by Hashin [36] will first be discussed. The Composite

Cylinder Assemblage model is widely accepted in the field today. A relatively new model proposed by Aboudi [37] will also be discussed.

4.3.1 Hashin Model

Hashin [36] developed a micromechanical model called the Composite Cylinder Assemblage (CCA) model. This model assumes that the composite can be modeled as a single cylindrical fiber surrounded by a matrix sleeve. This is shown in Figure 45. The fiber volume fraction is used in this model to calculate the ratio of the fiber radius to the matrix sleeve radius. Different sizes of these composite-matrix cylinders with the same radii ratios can be assembled to fill up the free space and model the total composite. Figure 46 shows the composite cylinder assemblage.

If we make these assumptions, the problem of determining the properties of a continuous fiber reinforced material reduces to that of solving the much simpler problem of a single composite cylinder as shown in Figure 45. The single composite cylinder with the given radii ratio is considered a representative cell. This turns out to be a fairly simple boundary value problem. The details of this problem along with the solutions can be found in Hashin [36].

This boundary value problem can give us exact solutions of the model for the longitudinal Young's modulus (E_{11}), the Poisson's response (E_{12}), and the axial shear modulus (G_{12}). Due to the geometry of the composite cylinder, however, exact solutions of the model for the transverse properties of the composite cannot be formulated. As a result, the Hashin model resorts to energy methods to give upper and lower bounds for the transverse Young's modulus (E_{22}), and the transverse shear modulus (G_{23}). In order to completely characterize a transversely isotropic composite, all five properties must be evaluated.

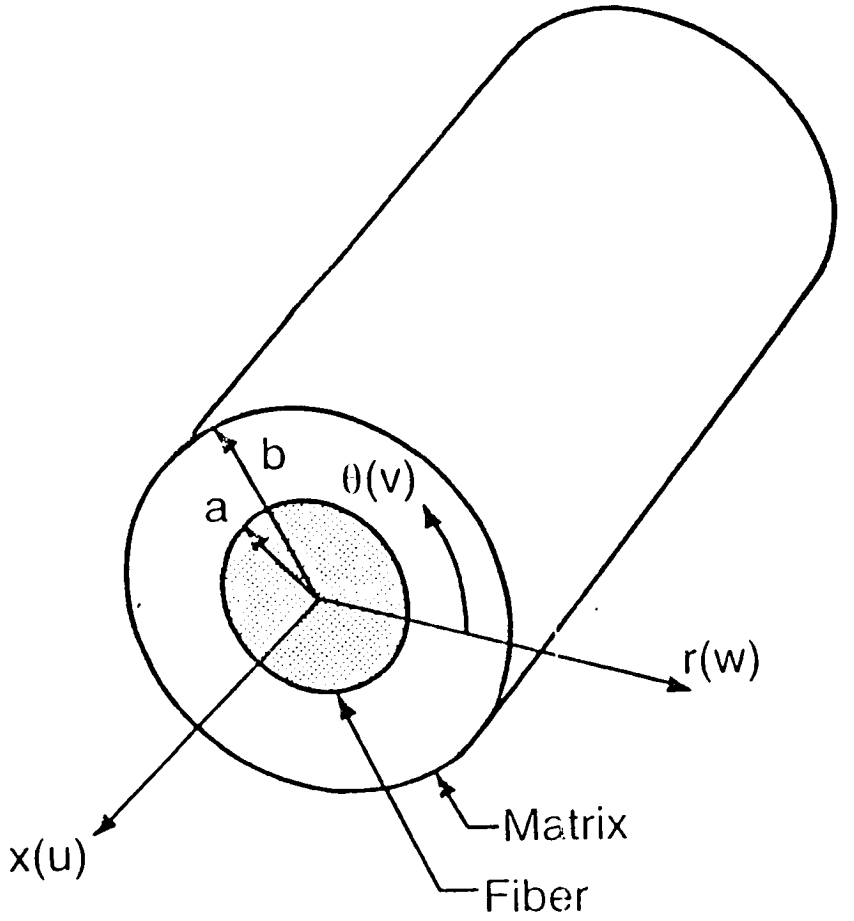

Figure 45. Single Composite Cylinder

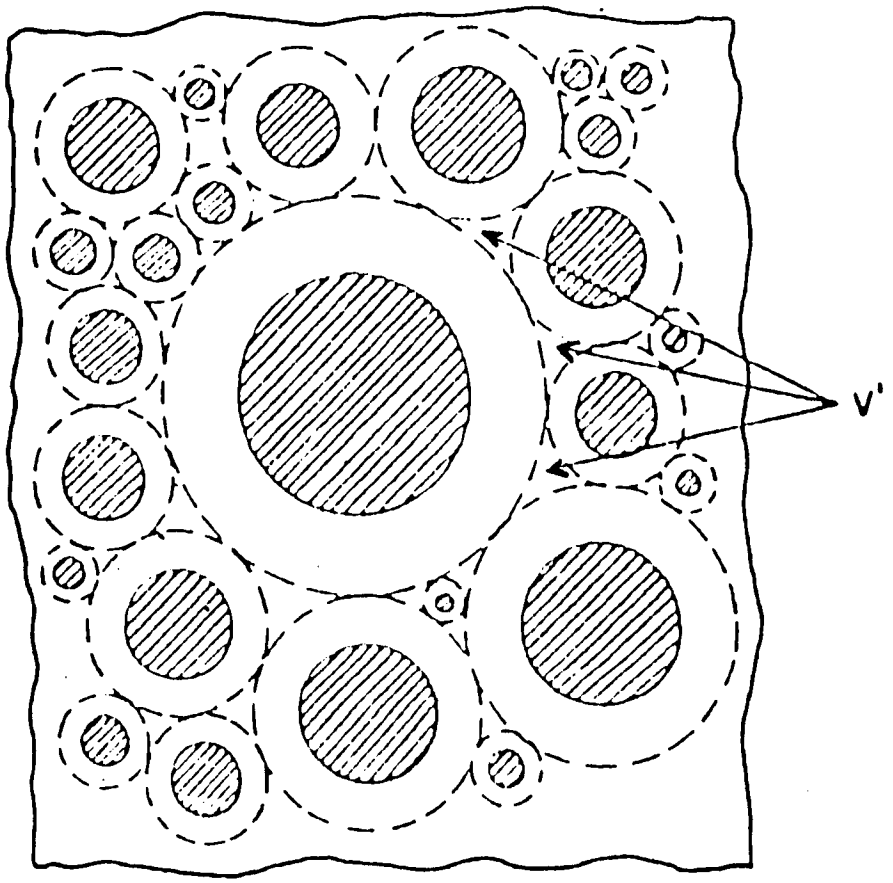

Figure 46. Hashin Composite Cylinder Assemblage Model: [36]

4.3.2 Aboudi Model

The Aboudi [37] model is based on a repeating unit cell consisting of a square fiber embedded in a matrix phase which is divided into three subcells. A representation of the repeating unit cell is shown in Figure 47. A first order displacement expansion is employed in each of the subcells in the course of calculating the effective elastic properties. Continuity of tractions and displacements across the boundaries of the individual subcells of the representative volume element is imposed in an average sense. Closed form expressions have been derived which relate the overall applied stresses to the stresses in the fiber phase and the individual subcells of the matrix phase. This, in turn, allows generation of the effective elastic response of the composite under arbitrary loading in a straight-forward fashion [37-40]. Due to the geometry of the Aboudi model, an exact formulation for the transverse moduli (E_{22}, G_{23}) is obtained. This is in contrast to the Hashin model with gives upper and lower bounds for the transverse moduli.

4.4 Application of Correspondence Principle

A micromechanical model predicts the elastic moduli of a composite in terms of the elastic moduli of the individual constituents. Taking the tensor elastic modulus C_{11} as an example,

$$C_{11} = g\,(C^{f}_{\alpha\beta},\ C^{m}_{\alpha\beta}) \tag{4.37}$$

where f denotes fiber properties and m denotes matrix properties. Since micromechanical models are boundary value problems of the type discussed in Section 4.2.2, the Correspondence Principle may be employed to predict the viscoelastic response of a composite consisting of linearly viscoelastic phases. To use this principle we must substitute the transform domain constituent moduli into the elastic solution. Doing this gives

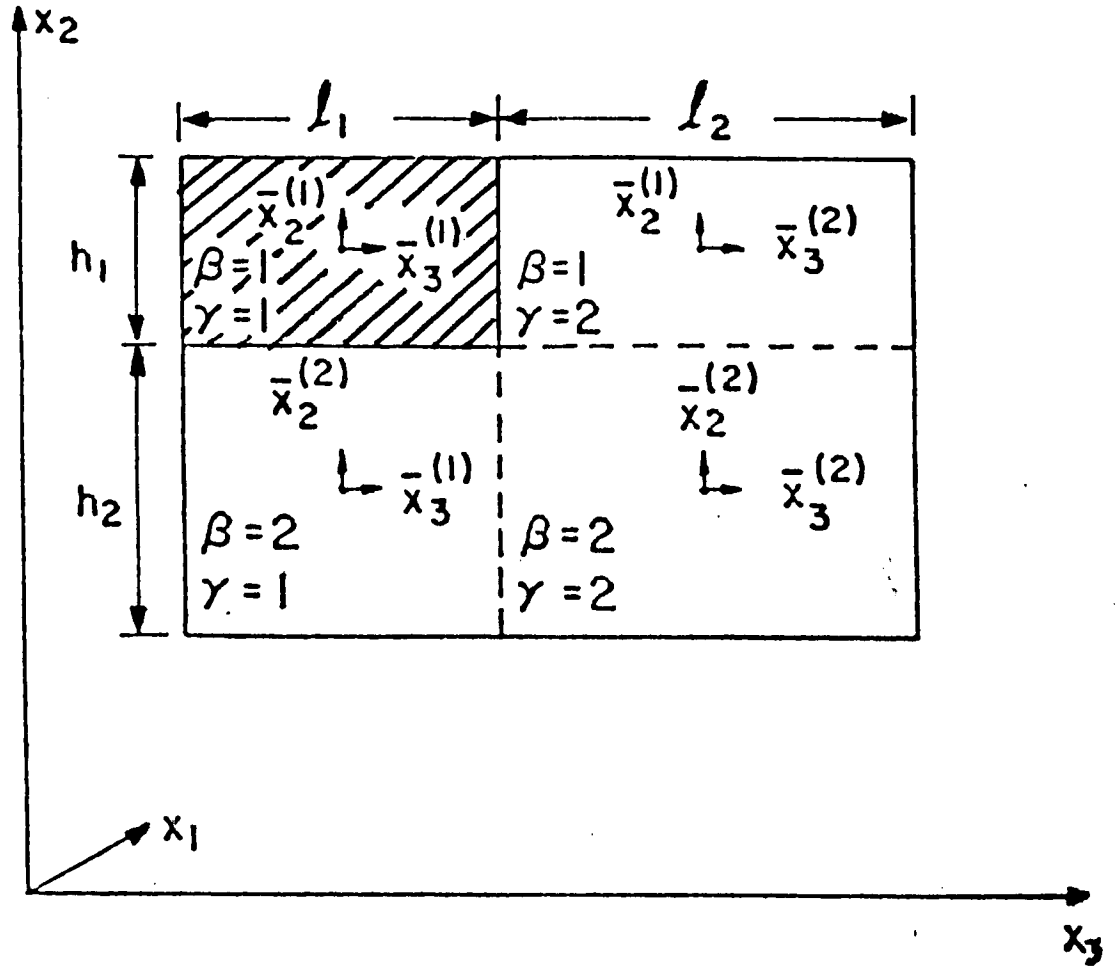

Figure 47. Aboudi Micromechanical Model: [37]

$$s\,\overline{C}_{11} = g\,(s\,\overline{C}^{f}_{\alpha\beta},\ s\,\overline{C}^{m}_{\alpha\beta}) \tag{4.38}$$

Now dividing through by s gives

$$\overline{C}_{11} = \frac{1}{s} g\,(s\,\overline{C}^{f}_{\alpha\beta},\ s\,\overline{C}^{m}_{\alpha\beta}) \tag{4.39}$$

The Laplace transform of the composite modulus is now given as a function of s, the Laplace transform variable. Inverting this expression back into the time domain gives the time domain viscoelastic solution of the micromechanical model. These expressions for the composite moduli in the Laplace transform domain are quite complicated and simple methods for inverting the Laplace transform are difficult to use in this case. A numerical technique developed by Bellman [41] gives a fairly simple procedure for inverting the Laplace transform assuming that the time domain function is smooth. Since the viscoelastic response of a material is an assumed smooth function of time, this method works quite well.

Bellman uses Legendre polynomials to invert a known function of s to its corresponding function of time. The result of this formulation is a matrix that when multiplied by the values of the Laplace transform function at given values of s gives the desired result. A more detailed description of this formulation is given by Bellman [41] and in Appendix A.

4.5 *Matrix Modeling*

In order to determine the viscoelastic properties of the composite, the viscoelastic properties of the constituents must be determined. Assuming that the fibers are perfectly elastic, an effective way to model the matrix is all that is needed. Two models are used here. The first model is the Power-Law model and it assumes that the viscoelastic response can be modeled as a constant compliance

term plus a power law expression in t. The isotropic creep compliance, $S(t)$, for the Power-Law model is given by

$$S(t) = D_0 + Ct^n \tag{4.40}$$

where D_0 is the initial elastic compliance, C and n are measured parameters, and t is time. A graphical representation of this viscoelastic model is given in Figure 48.

The second model is a Four-Parameter model. This is a mechanical model consisting of springs and dashpots. The model has a Kelvin element in parallel with a Maxwell element as shown in Figure 49. The isotropic creep compliance, $S(t)$, for the Four-Parameter model is given by

$$S(t) = \frac{1}{E_0} + \frac{1}{E_1}(1 - e^{-\lambda t}) + \frac{t}{\mu_0} \tag{4.41}$$

where

$$\lambda = \frac{\mu_1}{E_1} \tag{4.42}$$

Since the epoxy matrix which will be modeled in this study is isotropic, these isotropic creep compliances are all that is needed if it is assumed that the Poisson's ratio remains constant with time. From the experimental results, this assumption was shown to be valid and was therefore used in this study.

In order to use the Correspondence Principle, the Laplace transforms of the creep compliances will be needed. For the Power-Law model,

$$\bar{S}(s) = \frac{D_0}{s} + \frac{C\,\Gamma(n+1)}{s^{n+1}} \tag{4.43}$$

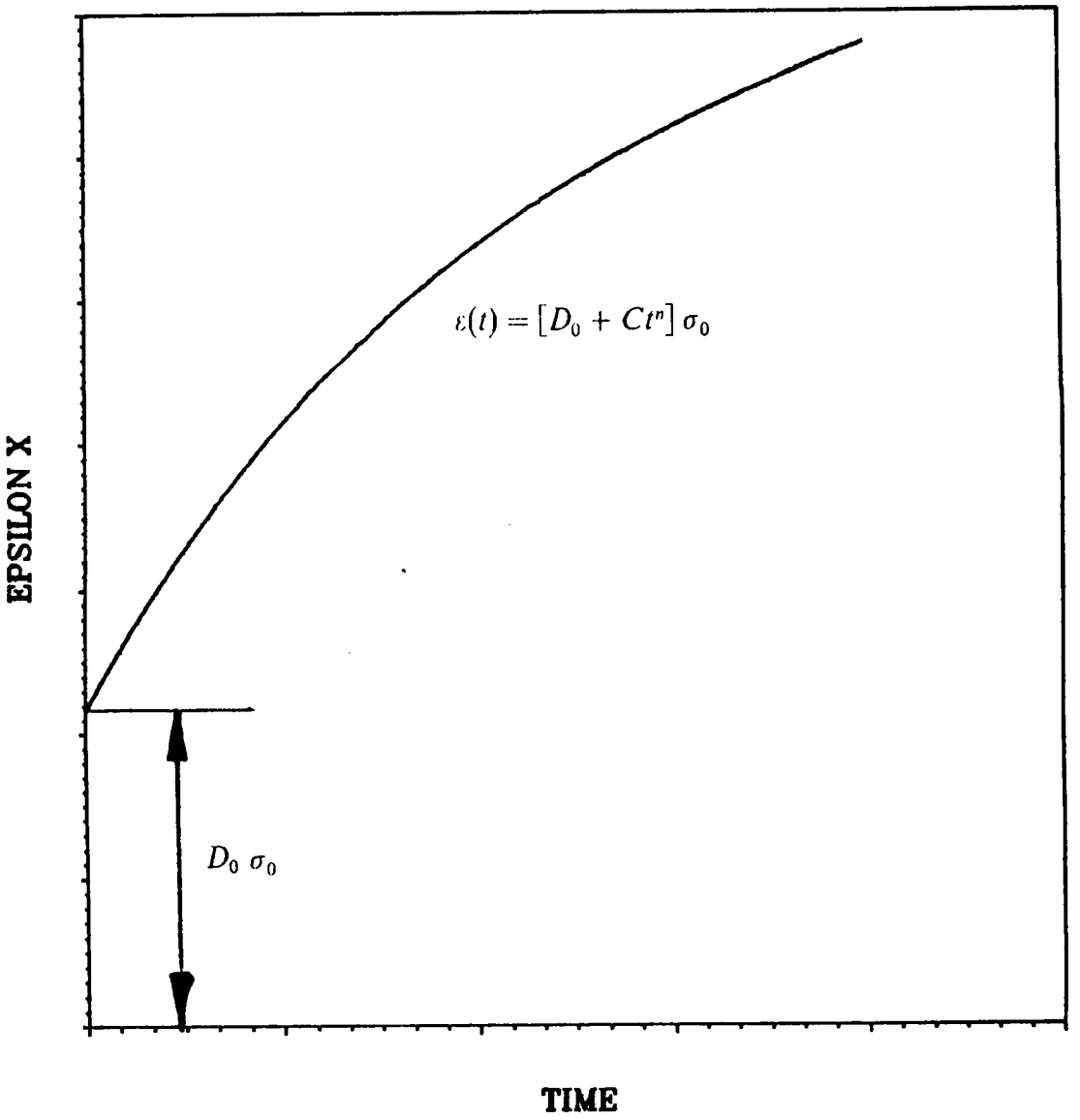

Figure 48. Power Law Graphical Representation

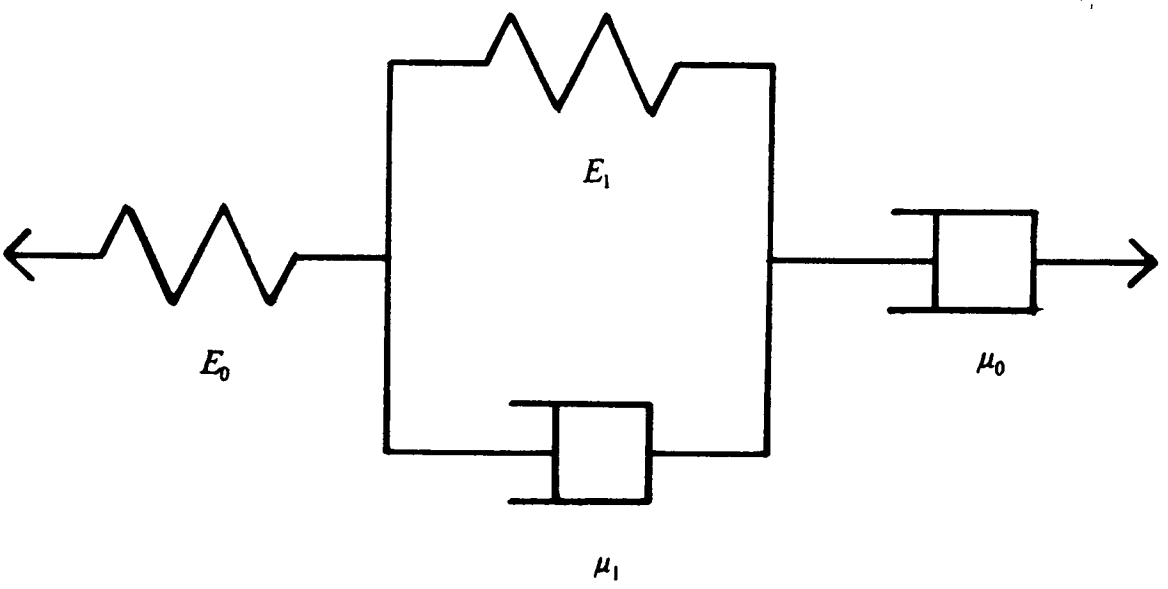

Figure 49. Mechanical Representation of Four-Parameter Model

where $\Gamma(n+1)$ is the Gamma function for $(n+1)$. Values for the Gamma function can be found in [42].

For the Four-Parameter model,

$$\overline{S}(s) = \frac{(1/E_0)}{s} + \frac{(1/E_1)}{s} - \frac{(1/E_1)}{s+\lambda} + \frac{(1/\mu_0)}{s^2} \tag{4.44}$$

Since the two micromechanical models are calculated in terms of moduli rather than compliances, $\overline{S}(s)$ is converted to $\overline{C}(s)$, the Laplace transform of the relaxation modulus, by

$$\overline{C}(s) = \frac{1}{s^2\,\overline{S}(s)} \tag{4.45}$$

4.5.1 Parameter Evaluation

In order to use the previously outlined micromechanical models, the parameters to be used in either the Power-Law model or the Four-Parameter model must be evaluated. The methods used in this study to determine the needed parameters are outlined below.

For the Power-Law model, the creep compliance is

$$S(t) = D_0 + Ct^n \tag{4.46}$$

Subtracting the elastic compliance from the creep compliance gives the portion of the creep compliance which is time-dependent. This will be called $B(t)$ such that

$$B(t) = Ct^n \tag{4.47}$$

Taking the base 10 logarithm of both sides gives

$$\log B(t) = \log C + n \log t \tag{4.48}$$

In the above expression, $\log B(t)$ can be seen as a linear function of $\log t$. The experimental data normalized with respect to stress level gives the creep compliance. Subtracting the elastic compliance from the creep compliance and plotting the base 10 logarithm of this function versus the base 10 logarithm of time should approximate a straight line. The slope of this line gives us the exponent n. Choosing any point on the line and using its coordinates gives the solution for $\log C$ which completes the determination of the two unknown parameters C and n. This process is illustrated in Figure 50.

For the Four-Parameter model, the evaluation of the unknown parameters is somewhat more arbitrary. Many combinations of the unknown parameters can yield a satisfactory solution. Choosing a method is therefore more important for the sake of consistency than for accuracy. The method used in this study is outlined below.

The creep compliance for the Four-Parameter model is

$$S(t) = \frac{1}{E_0} + \frac{1}{E_1}(1 - e^{-\lambda t}) + \frac{t}{\mu_0} \tag{4.49}$$

The spring constant E_0 is simply the elastic modulus of the material. This value was evaluated from the initial elastic response of the matrix. The elastic compliance was subtracted from the compliance at $t = 2\,hours$ and multiplied by $(1 - 1/e)$. Adding this to the elastic compliance results in a value hereafter called S_1 defined as

$$S_1 = (S_{2hrs} - S_{elastic})(1 - \frac{1}{e}) + S_{elastic} \tag{4.50}$$

The value of time at that value of the compliance (S_1) was taken as the time constant $\tau = \frac{1}{\lambda}$. This is shown in Figure 51. To solve for E_1 and μ_0, values of the compliance at $t = 30\,min$ and

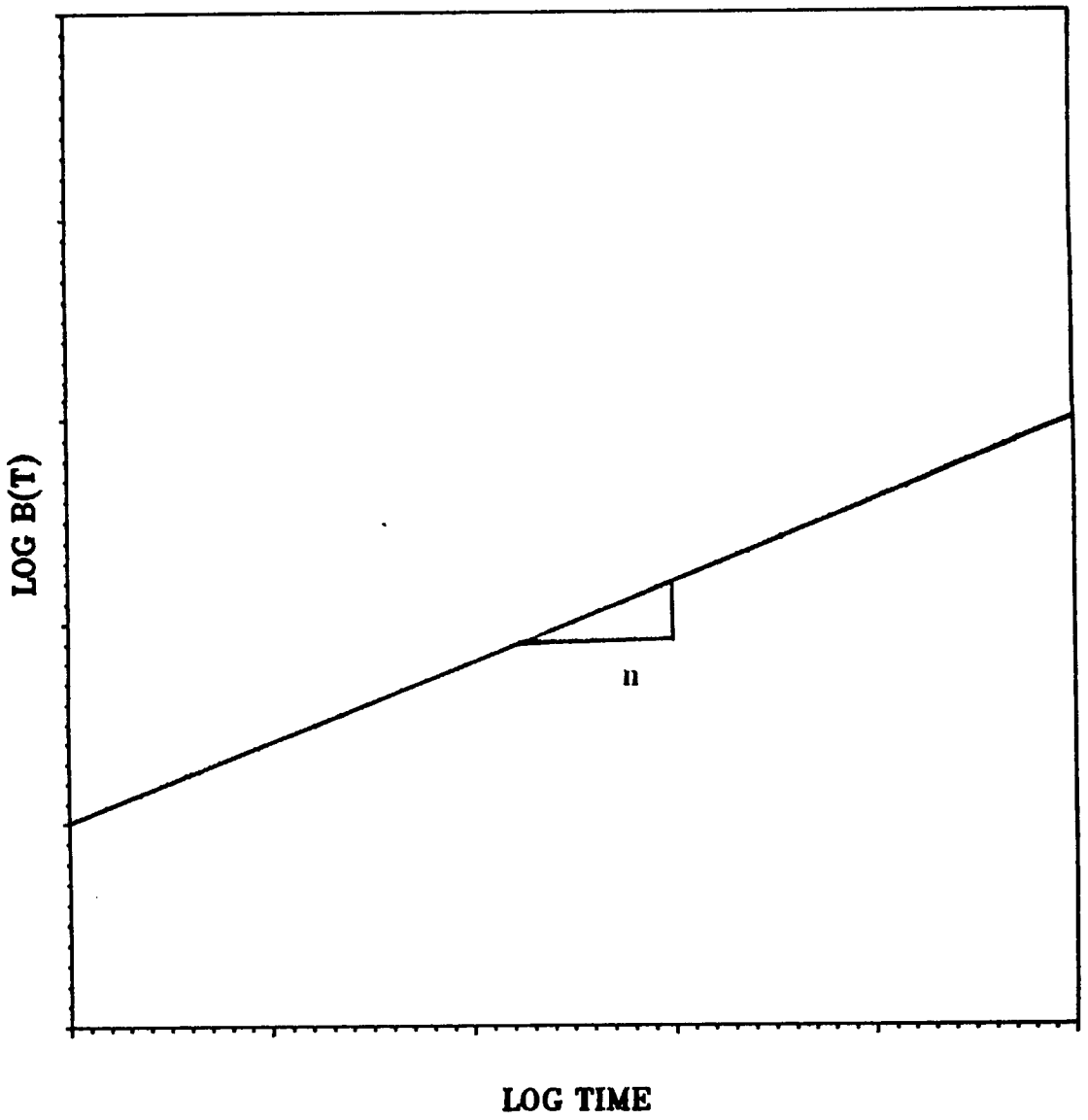

Figure 50. Parameter Determination for Power-Law Model

$t = 2\ hours$ were taken and inserted into equation (4.49). This yields two equations in the two unknowns E_1 and μ_0. These equations are easily solved.

4.6 *Program Verification*

A FORTRAN code known as MICVIS has been written for the MICromechanical VIScoelastic formulation explained in this chapter. The User's Guide to MICVIS can be found in Appendix B. To check the validity of the program, readily available data from glass reinforced epoxy was used with the program [43]. The input parameters were as follows:

- E_0 = 0.563 MSI
- C = .0.188 1/MSI-sec
- n = 0.31
- E_1 = 4.37 MSI
- λ = 0.641 1/sec
- μ_0 = 392.5 MSI-sec

The glass fiber properties are as follows:

- E_A^f = 12.4 MSI
- ν_A^f = 0.20
- G_A^f = 5.17 MSI

To verify the program, the transform domain moduli of the matrix were input into the program for not only the matrix, but for the fiber also. In this case, only the isotropic matrix is being modeled. The creep compliance on output from MICVIS should be the same as the creep compliance of the

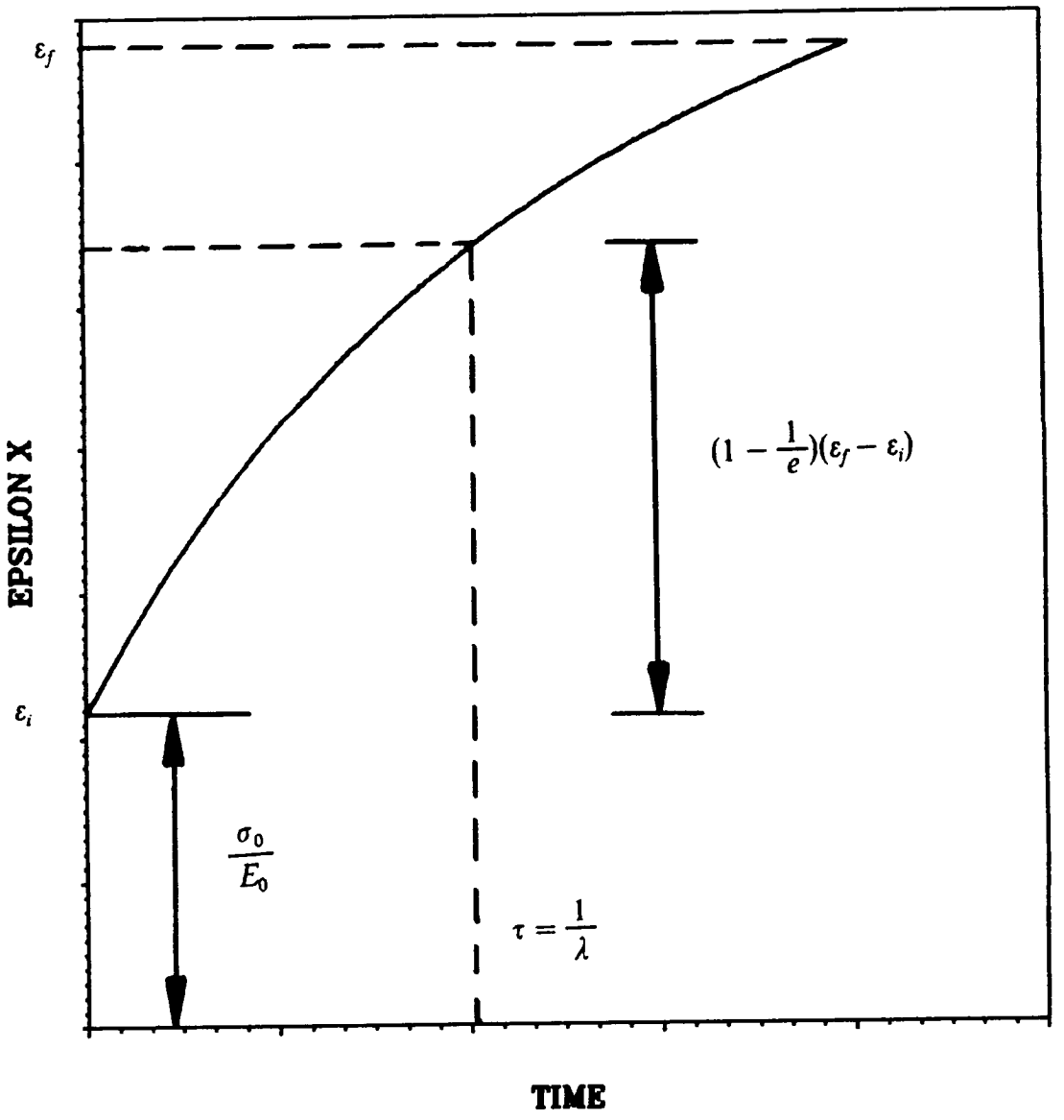

Figure 51. Parameter Determination for Four-Parameter Model.

matrix on input. As shown in Figure 52 and Figure 53, the results from both the Aboudi and Hashin models and the input values are identical.

The case for the viscoelastic epoxy matrix and the perfectly elastic glass fibers was then investigated. The glass fibers were assumed isotropic although this model can accommodate transversely isotropic fibers. The resulting compliances (S_{ij}) are plotted against time in hours. Plots are shown in Figure 54 through Figure 58 for the five independent compliances of the composite, S_{11} , S_{12}, S_{22}, S_{44} , and S_{66} where

- $S_{11} = 1/E_{11}$
- $S_{12} = -\nu_{12}/E_{11}$
- $S_{22} = 1/E_{22}$
- $S_{44} = 1/G_{23}$
- $S_{66} = 1/G_{12}$

A comparison between the Aboudi and Hashin models is given in these figures. These comparisons show the differences in the predictions of the two models under the same conditions. The two models give nearly identical predictions for S_{11} and S_{12} and the models differ only slightly for S_{66}. The predictions for S_{22} and S_{44} give the bounds of the Hashin model. As shown, the Aboudi model prediction lies between the Hashin bounds.

It should be noted that the use of the Correspondence Principle has been mathematically proven for the exact values of moduli, namely E_{11} , ν_{12}, and G_{12}. Difficulty arises, however, when one deals with the bounds on E_{22} and G_{23} . Christensen [44] concludes that the Correspondence Principle will only give the correct bounds on the viscoelastic response under the following conditions:

- A perfectly elastic fiber
- An isotropic viscoelastic matrix
- A time-independent Poisson's ratio for the matrix

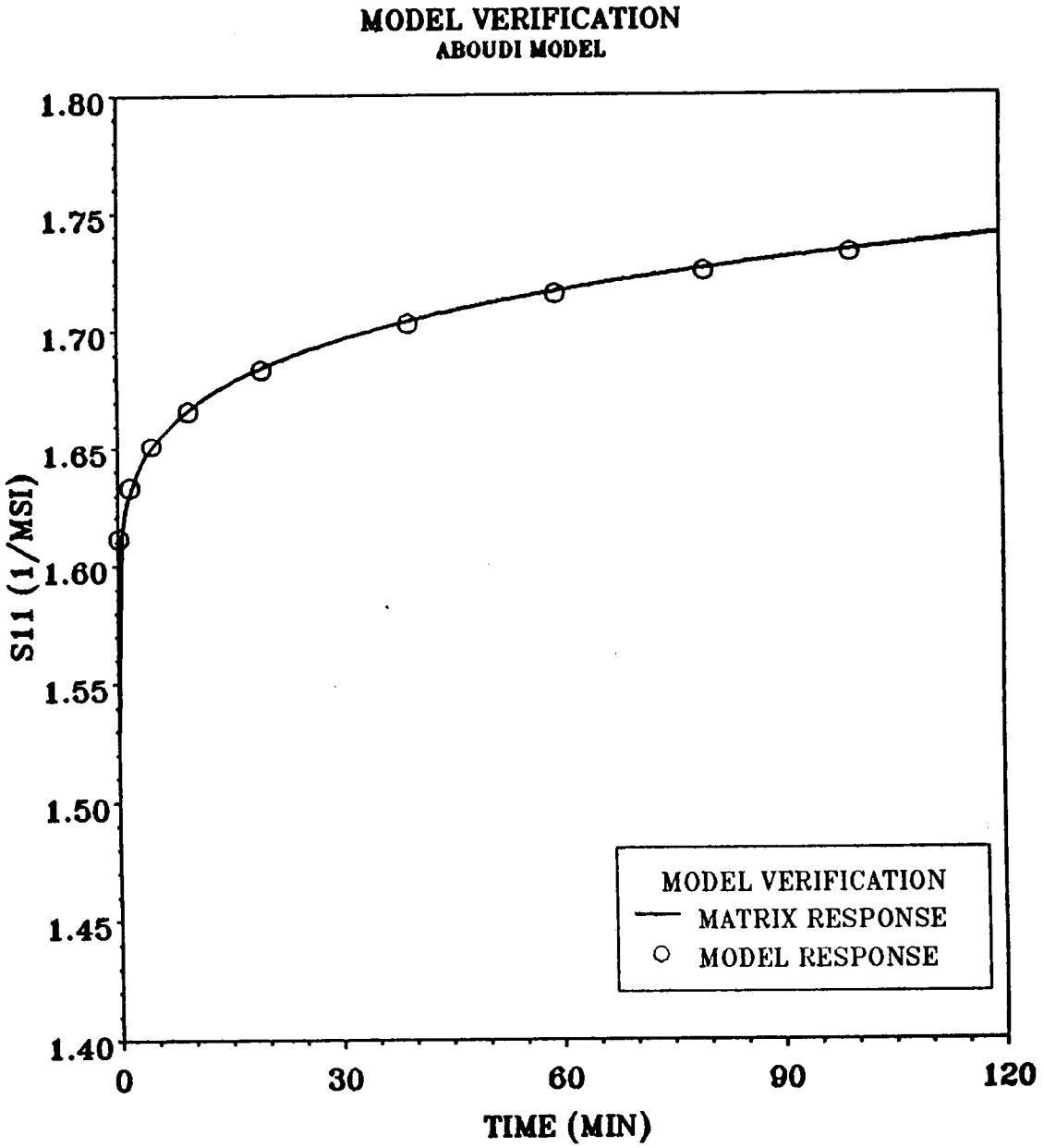

Figure 52. MICVIS Aboudi Model Prediction and Exact Value

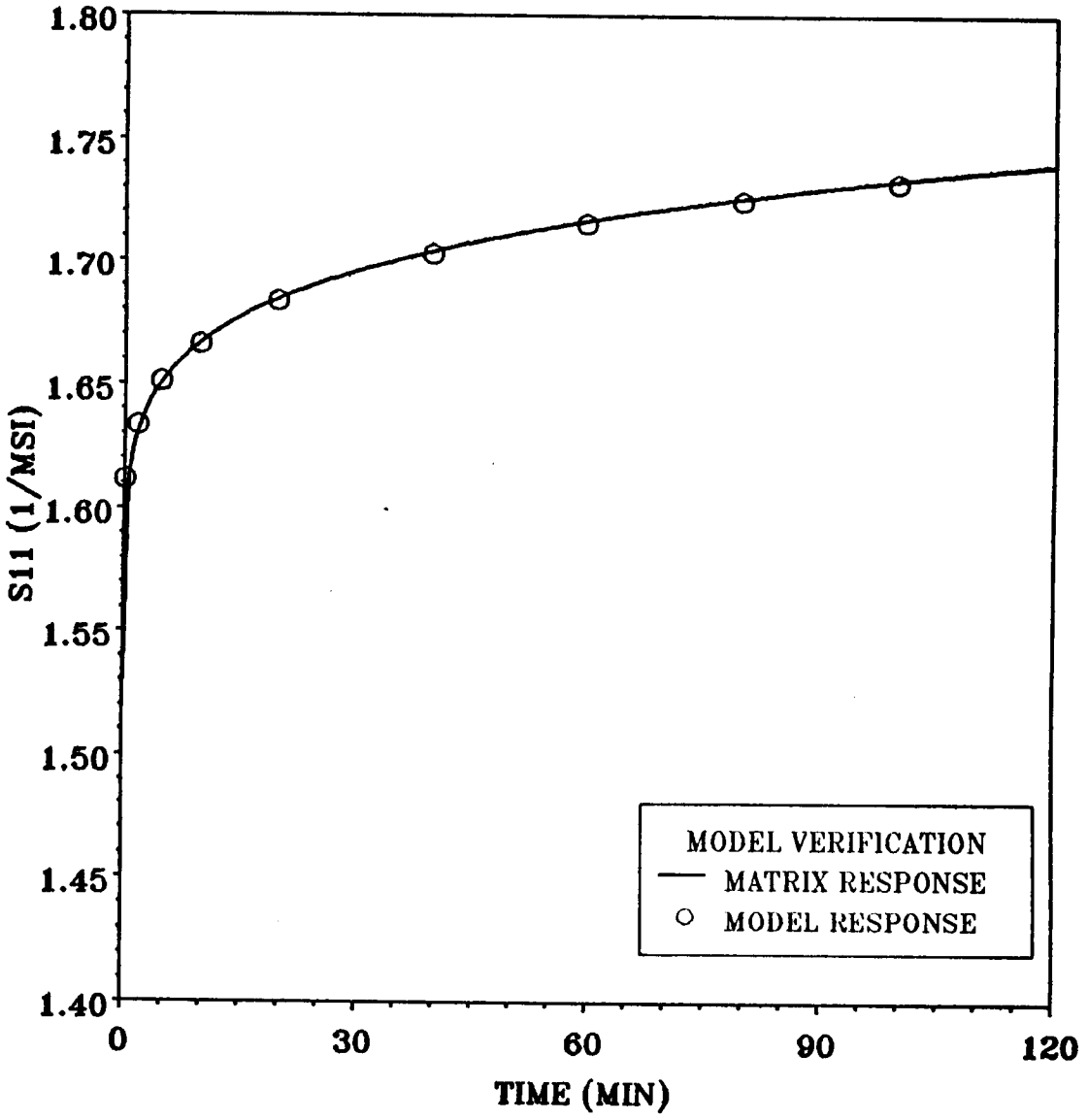

Figure 53. MICVIS Hashin Model Prediction and Exact Value

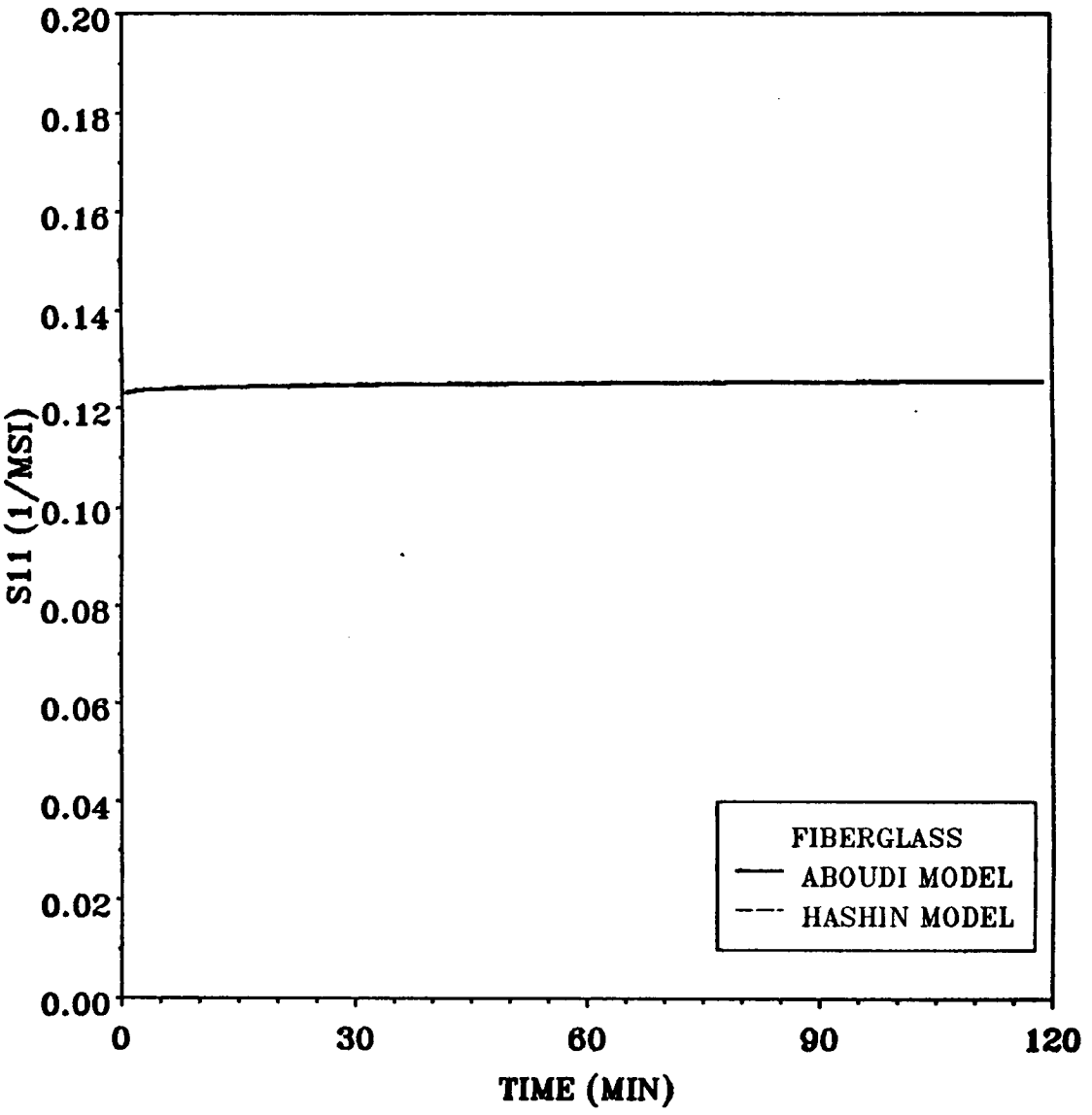

Figure 54. S11 Compliance vs. Time

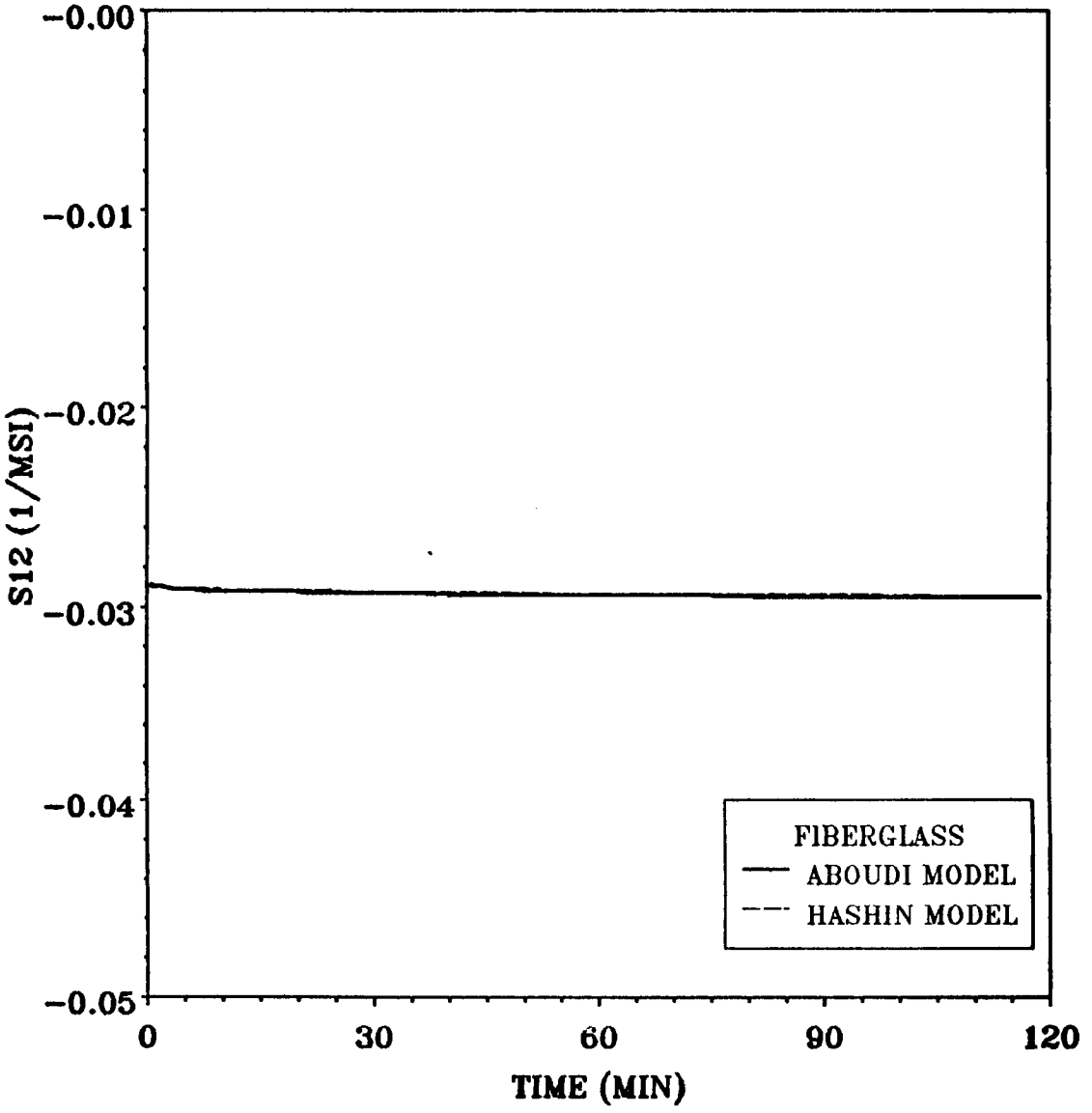

Figure 55. S12 Compliance vs. Time

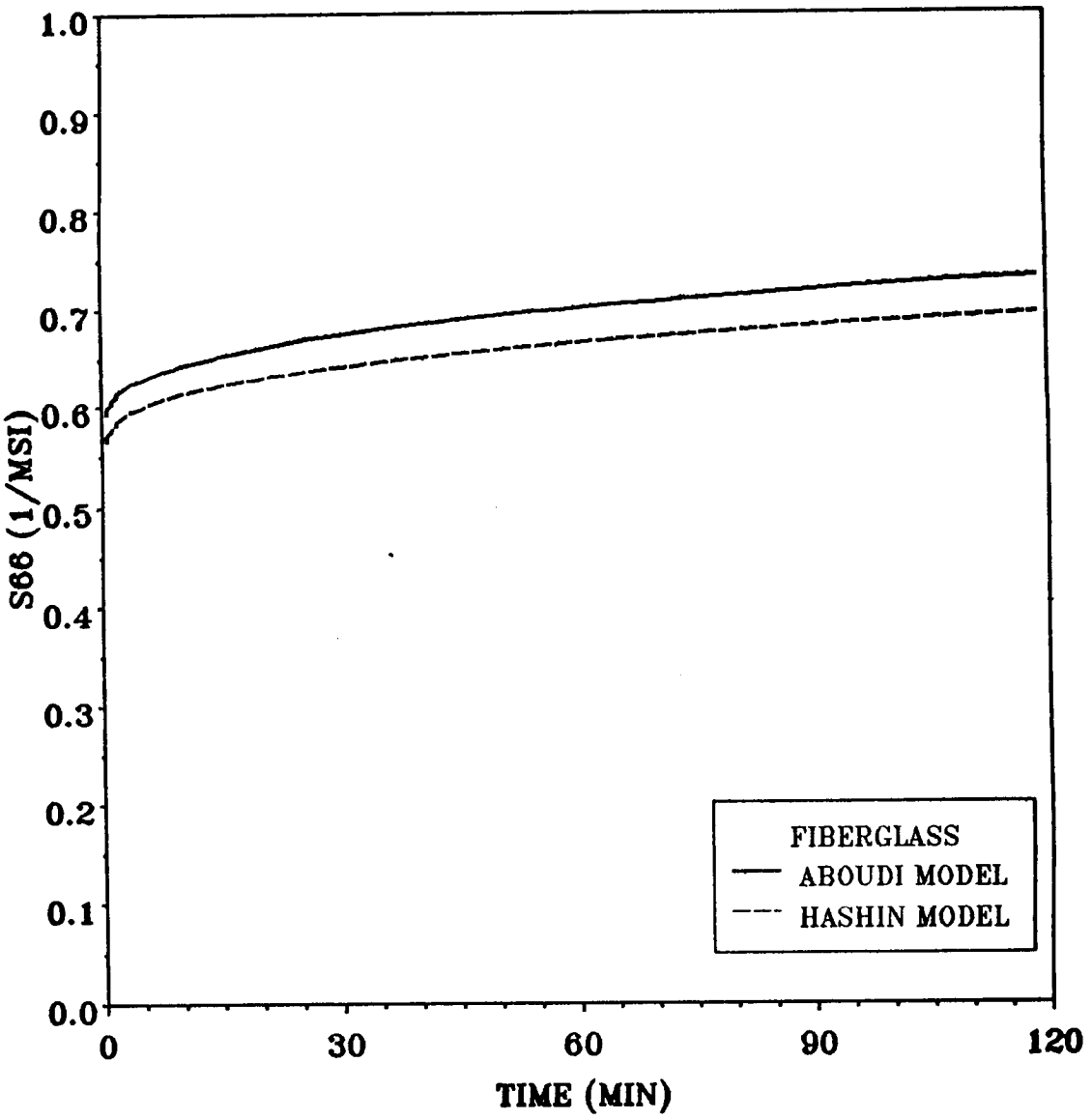

Figure 56. S66 Compliance vs. Time

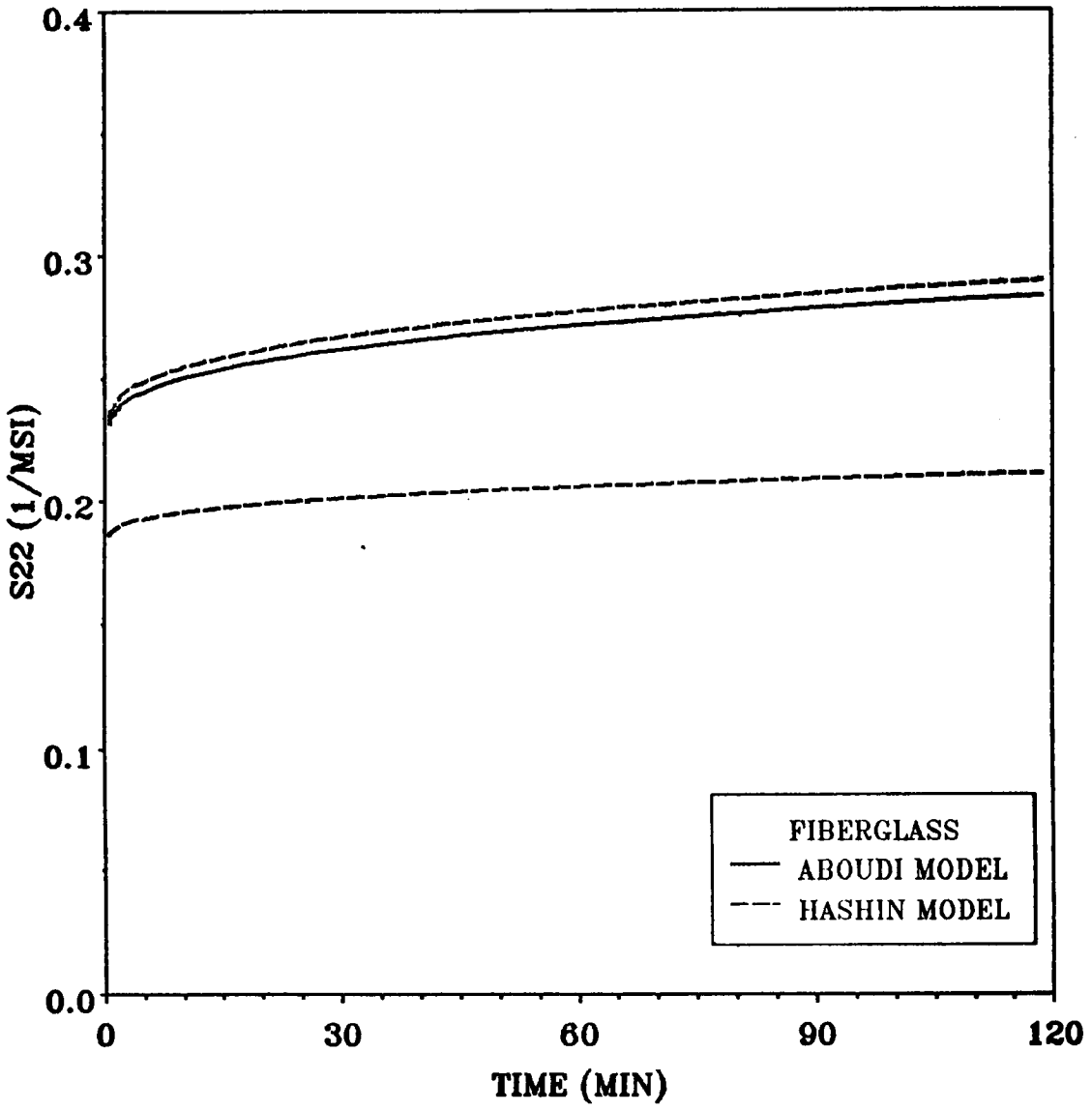

Figure 57. S22 Compliance Bounds vs. Time

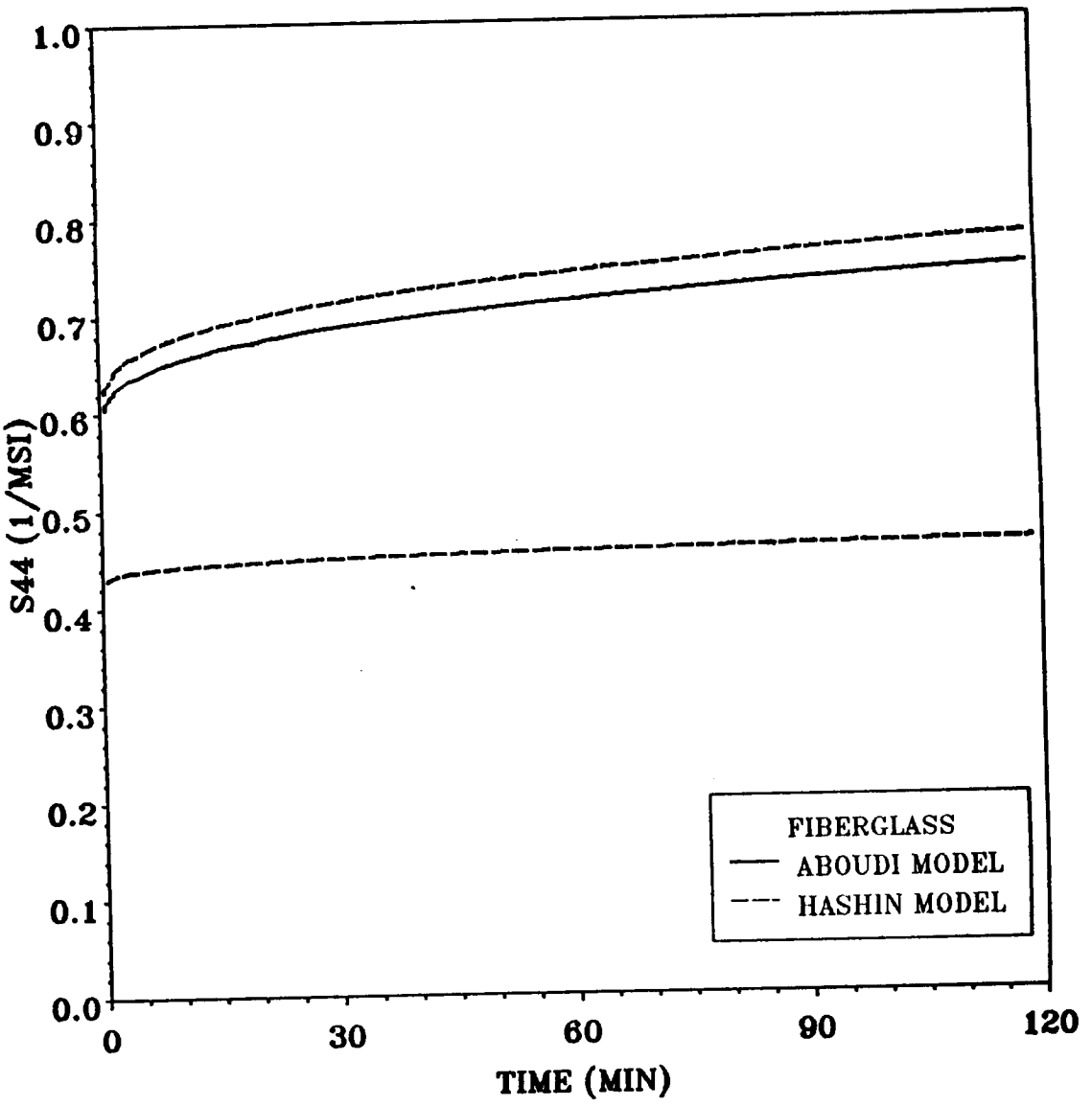

Figure 58. S44 Compliance Bounds vs. Time

In this example, all of these conditions are met.

5.0 Experimental-Analytical Correlation

This chapter compares the predictions of the analytical model developed in Chapter 4.0 with the experimental data presented in Chapter 3.0. Elastic and viscoelastic properties are evaluated for both the T300 graphite fibers and the 934 epoxy resin. These properties are then used in MICVIS to predict the viscoelastic response of the graphite/epoxy composite under the various conditions tested. These predictions are compared with the experimental data.

5.1 Matrix Modeling

The bulk resin results were modeled using both the Power-Law and Four-Parameter models described in Section 4.5. As shown in Section 3.5, the NR, IR, and NE results are very nearly linear. The IE results for the initial loading were modeled using both the Power-Law and Four-Parameter model, although linearity cannot be assumed. Plots showing the model approximations to the experimental data are shown in Figure 59 through Figure 62. Both models do reasonably well in approximating the experimental data. The Power-Law model seems to do the best job in fitting the NR, IR, and NE results. The Four-Parameter model seems to do the best job in fitting the IE

results. Table 8 shows the parameters used for the various models. It should be noted that the power-law exponent, n, evaluated for the NR condition is the identical exponent evaluated by Hiel and Brinson [45] in their study on the creep behavior of 934 resin.

5.2 *Model Comparison*

In this section, comparison between the model predictions and the experimental data is presented. The results are given for compliance vs. time where the experimental compliances are computed by taking the experimental strains and dividing by the stress level. The results from the second loading were used for the NR, IR, and NE compliance calculations. The results from the initial loading were used for the IE compliance calculations.

5.2.1 Back Calculation

Isotropic fibers such as glass and boron have measurable properties. Transversely isotropic fibers such as graphite, on the other hand, have properties that are difficult to experimentally measure. The fiber elastic properties for graphite fibers, therefore, were determined by back calculation through the Aboudi micromechanical model. In the case of transversely isotropic fibers, this is an acceptable method for determination of the fiber elastic properties [34]. Composite properties and bulk resin properties determined from experiment were used to calculate the fiber elastic properties. The composite and bulk resin properties for each condition are shown in Table 9. Appendix C shows the comparison of these elastic values with results obtained by Milkovich, et al. [16], Reed, et al. [23], and Fox, et al. [26]. For the composite properties, the axial Young's modulus and axial Poisson's ratio were taken from the 0° tensile test, the transverse Young's modulus was taken from the 90° test, and the axial shear modulus was taken from the 45° off-axis test [46].

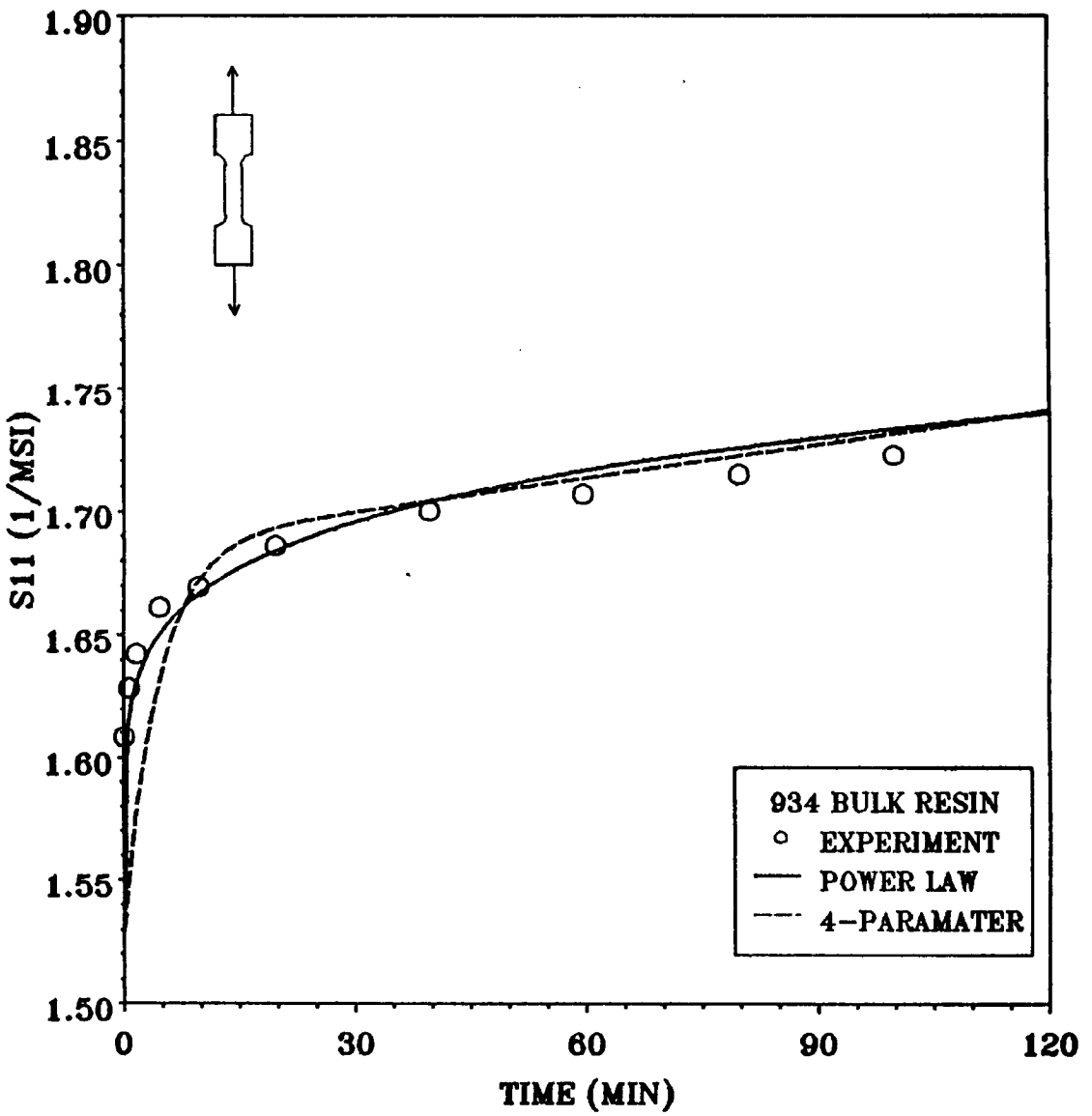

Figure 59. Linear Viscoelastic Model Approximations to NR Bulk Resin Data

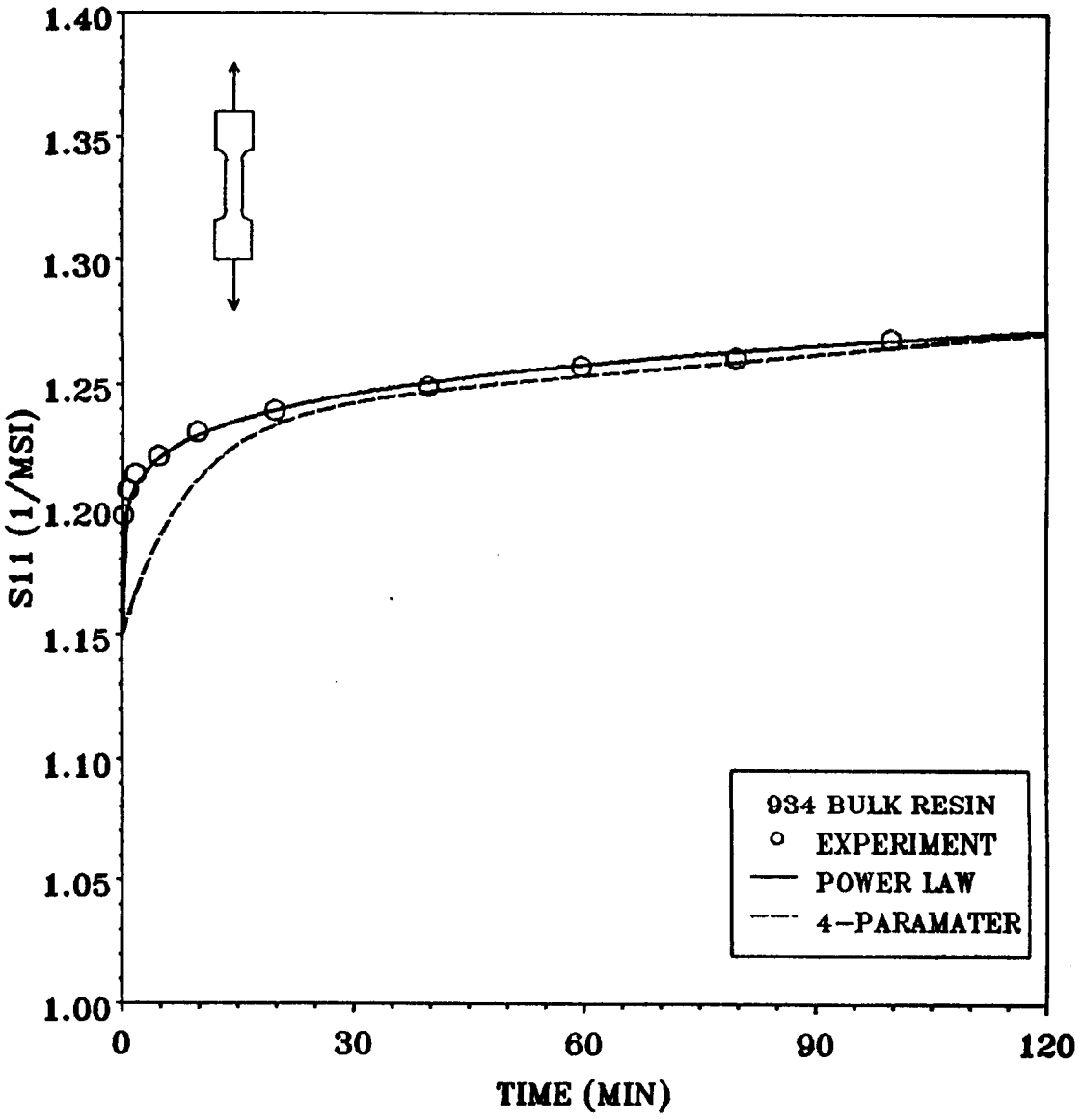

Figure 60. Linear Viscoelastic Model Approximations to IR Bulk Resin Data

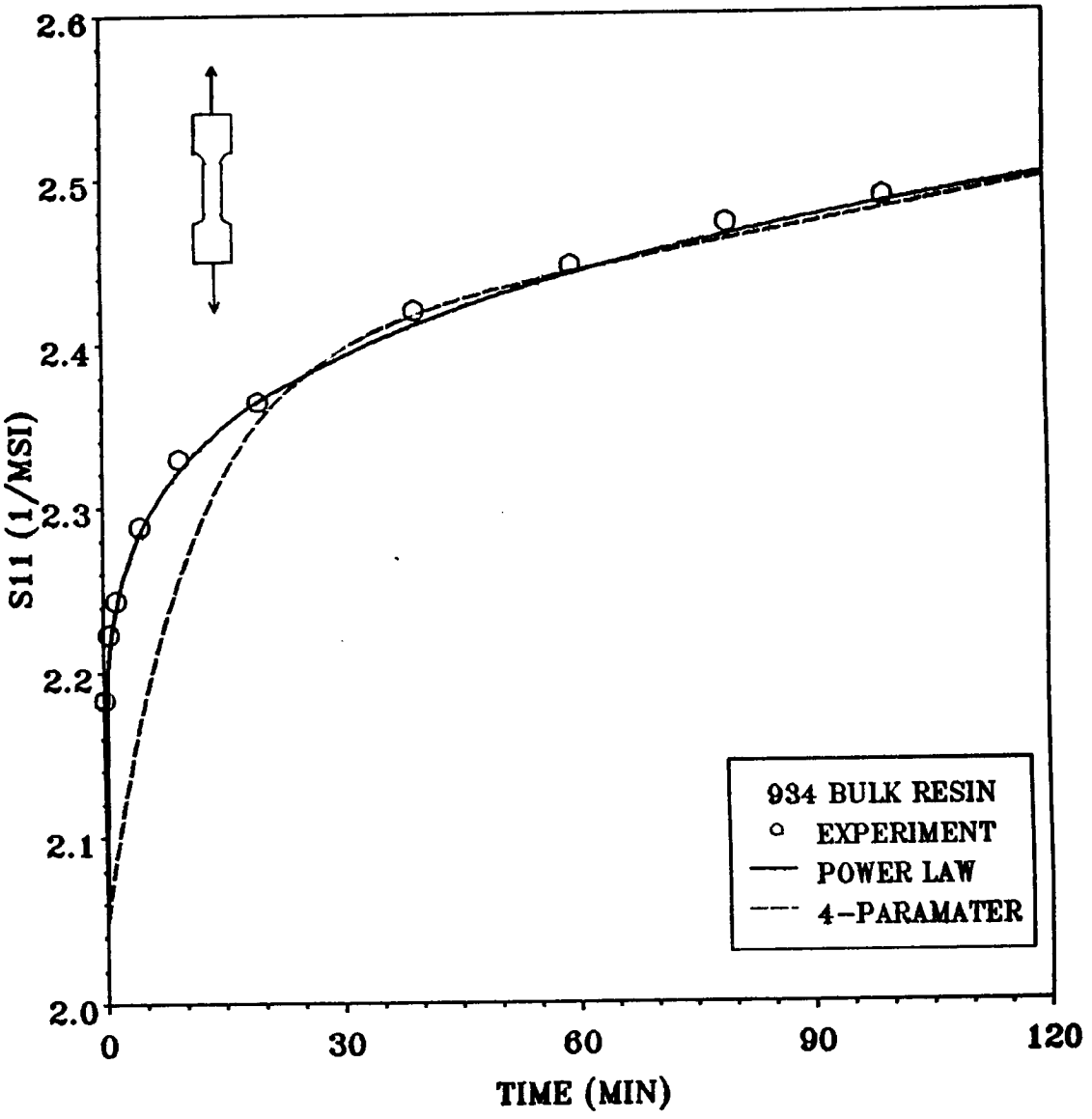

Figure 61. Linear Viscoelastic Model Approximations to NE Bulk Resin Data

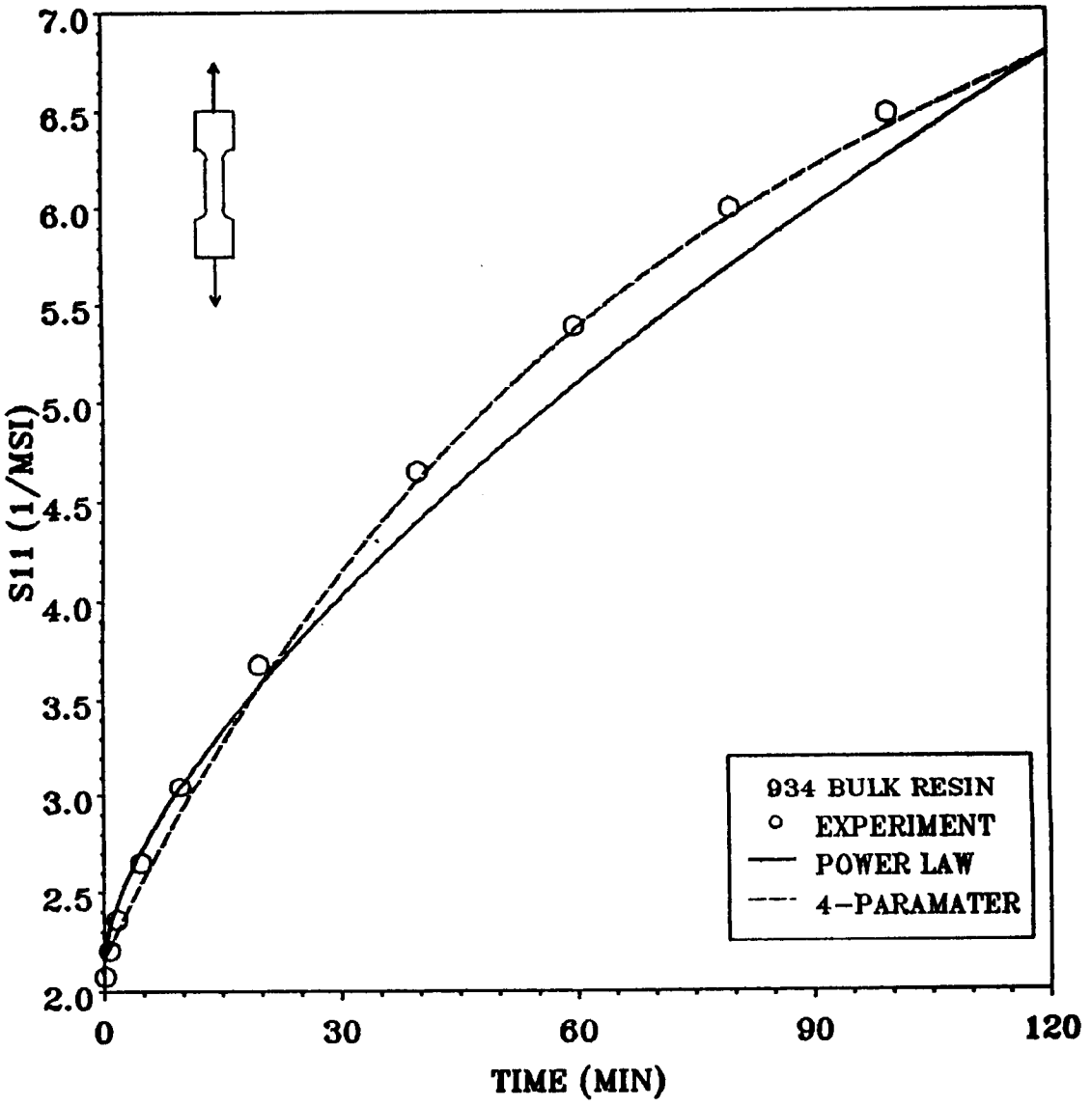

Figure 62. Linear Viscoelastic Model Approximations to IE Bulk Resin Data

Table 8. Linear Viscoelastic Model Parameters

	Viscoelastic Parameters			
	Four-Parameter Model			
Condition	E_0 (MSI)	E_1 (MSI)	λ (1/sec)	μ_0 (MSI-sec)
NR	0.654	6.407	0.222	2208.0
IR	0.870	11.561	0.118	3463.0
NE	0.488	2.940	0.091	1113.0
IE	0.461	0.256	0.019	108.1

	Viscoelastic Parameters		
	Power Law Model		
Condition	D_0 (1/MSI)	C (1/MSI-sec)	n
NR	1.53	0.093	0.17
IR	1.15	0.054	0.17
NE	2.05	0.173	0.20
IE	2.17	0.196	0.66

Table 9. Composite and Bulk Resin Properties

	Composite Properties			
	Condition			
Property	NR	IR	NE	IE
Axial Modulus (MSI)	18.55	18.01	19.55	19.53
Axial Poisson's	0.399	0.361	0.400	0.400
Transverse Modulus (MSI)	1.60	1.46	1.14	1.16
Axial Shear Modulus (MSI)	0.792	0.880	0.687	0.650

	Bulk Resin Properties			
	Condition			
Property	NR	IR	NE	IE
Axial Modulus (MSI)	0.654	0.870	0.488	0.461
Axial Poisson's	0.311	0.407	0.317	0.328
Axial Shear Modulus (MSI)	0.225	0.309	0.185	0.174

Fiber properties were backed out for each condition and the corresponding fiber elastic properties are shown in Table 10. It can be seen that the fiber properties vary somewhat under the various conditions. Reed, et al. [28] did show that radiation does not affect the axial modulus of the graphite fibers. The significant differences in the backed out fiber properties between the various conditions are most pronounced for the axial shear modulus and the transverse modulus. These variations may indicate changes in the axial shear and transverse modulus of the graphite fiber or may also be an indication of changes in the fiber-matrix interface under conditions of radiation and temperature.

Fiber properties were also backed out from the Hashin model. These fiber properties are also given in Table 10. Two properties are given for the transverse modulus to correlate with the upper and lower bounds for the transverse properties given by the Hashin model. The back calculated fiber properties from the Hashin model are different from the back calculated fiber properties of the Aboudi model. It is interesting to note that the back calculated value for the fiber transverse modulus from the Aboudi model does not fall between the fiber transverse modulus as calculated from the Hashin model. There also exists large differences in the fiber axial shear modulus obtained from the two models.

The problem with using the fiber properties from the Hashin model is deciding which bound to use for the transverse modulus. As shown in Figure 54 through Figure 58, the bounded solutions from the Hashin model follow fairly similar trends. Choosing a particular bound to use in the experimental-analytical correlation may indicate a proper trend but give no information on the proper elastic response. This is obviously a critical parameter to be evaluated. We don't encounter this problem with the Aboudi model. Due to the difficulties associated with the Hashin bounds, the model comparison to follow is done only for the Aboudi model.

Table 10. Backed Out Fiber Properties

	Backed Out Fiber Properties (Aboudi)			
	Condition			
Property	NR	IR	NE	IE
Axial Modulus (MSI)	29.42	28.38	31.09	31.07
Axial Poisson's	0.443	0.330	0.450	0.443
Transverse Modulus (MSI)	3.67	1.75	2.15	2.43
Transverse Poisson's	0.05	0.05	0.05	0.05
Axial Shear Modulus (MSI)	6.40	2.78	9.89	9.89

	Backed Out Fiber Properties (Hashin)			
	Condition			
Property	NR	IR	NE	IE
Axial Modulus (MSI)	29.42	28.38	31.09	31.07
Axial Poisson's	0.443	0.330	0.450	0.443
Transverse Modulus UB (MSI)	2.71	0.83	1.10	1.30
Transverse Modulus LB (MSI)	1.56	0.82	0.87	0.93
Transverse Poisson's	0.05	0.05	0.05	0.05
Axial Shear Modulus (MSI)	4.05	2.39	4.70	4.60

5.2.2 Experimental-Analytical Correlation Results

Figure 63 through Figure 67 show the experimental-analytical correlation for the NR and NE conditions. Since the NR and IR results are nearly identical for all cases, only the NR experimental-analytical correlation is detailed in the following figures. The instantaneous elastic responses of the 90° results and the 45° shear results agree exactly since the composite elastic properties used for back calculation were taken from these tests. For the 10° off-axis shear result, an error from the experimental results is present. Pindera and Herakovich [46] observe that the measured shear strain in a 10° off-axis test is influenced by constraints resulting from the grips. The calculated error for the 10° tests with an aspect ratio of 8 used in this study is approximately 40%. This correction was made in the comparison of the 10° shear results. The 10° longitudinal results shown in Figure 63 compare favorably with the model and the 10° shear results in Figure 64 show good correlation when the Pindera-Herakovich correction is made. The 45° longitudinal results in Figure 65 correlate well except for a slight difference in the magnitude of the elastic response. The 45° shear results in Figure 66 correlate well where no correction factor was used. The 90° results in Figure 67 also compare well with the model. The transverse response is critical in the formulation of micromechanical models and it is shown that the Aboudi model predicts the elastic and viscoelastic response quite well.

5.2.3 IE Results

As discussed in Section 3.6.2, linearity of the IE response cannot be assumed due to the healing process. The analytical model developed in Chapter 4.0 assumes linearity of the viscoelastic material. Disregarding this fact, however, the initial response of the IE bulk resin test was modeled using the Power-Law and Four-Parameter models. Using the results for the Power-Law model in MICVIS, the IE composite viscoelastic response is predicted. Sample comparisons with the various

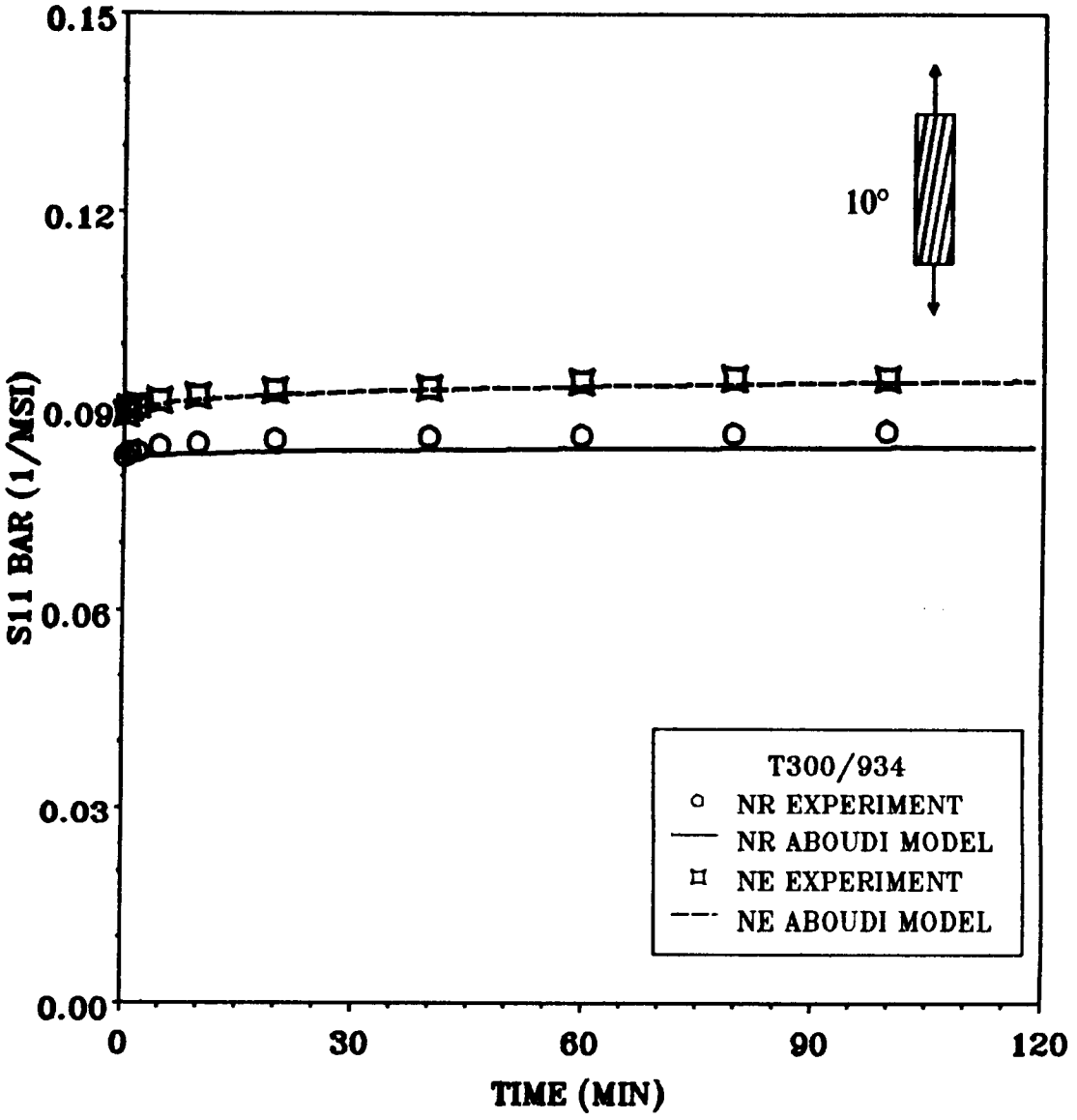

Figure 63. 10° Longitudinal Experimental-Analytical Correlation

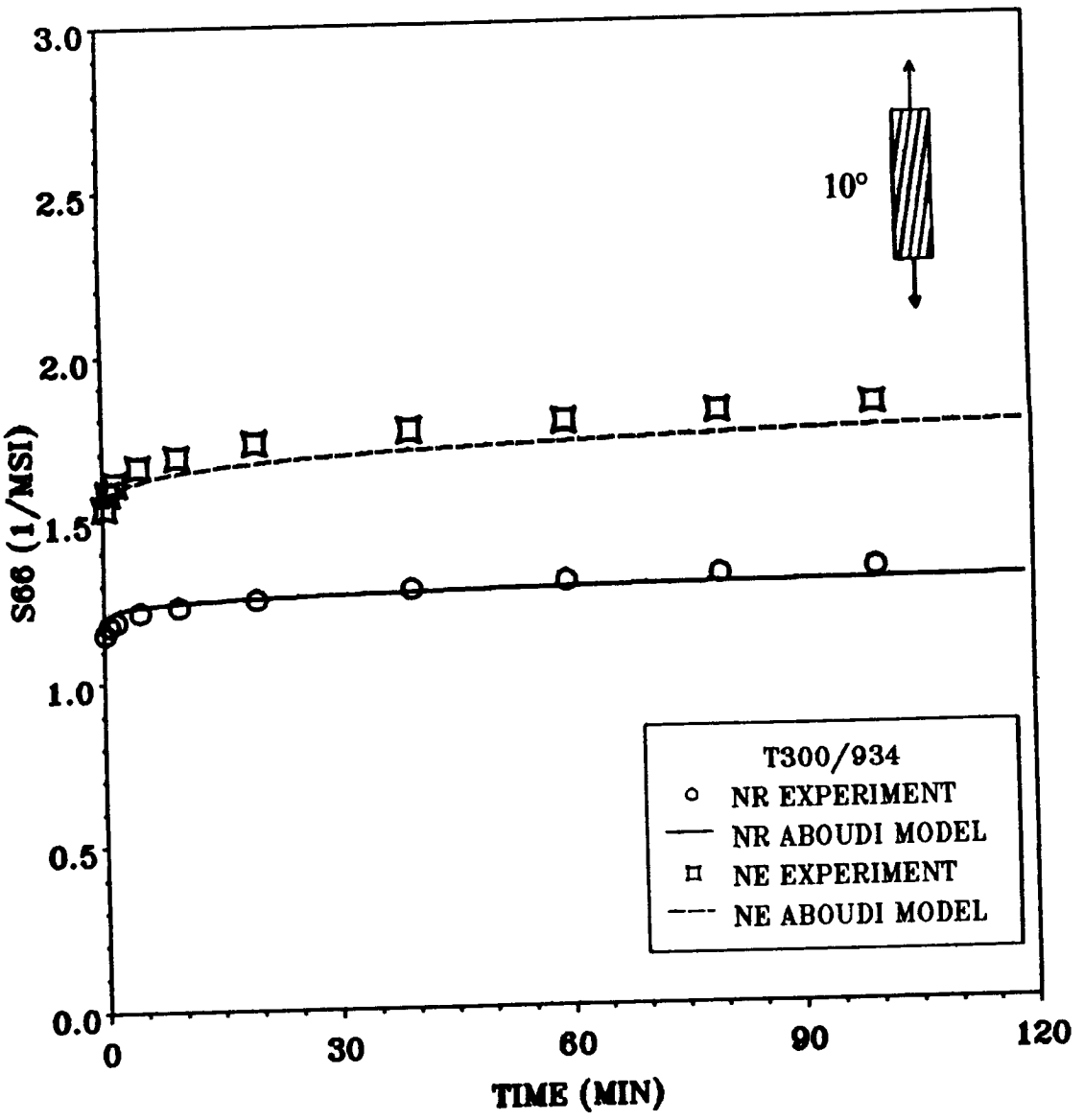

Figure 64. 10° Shear Experimental-Analytical Correlation

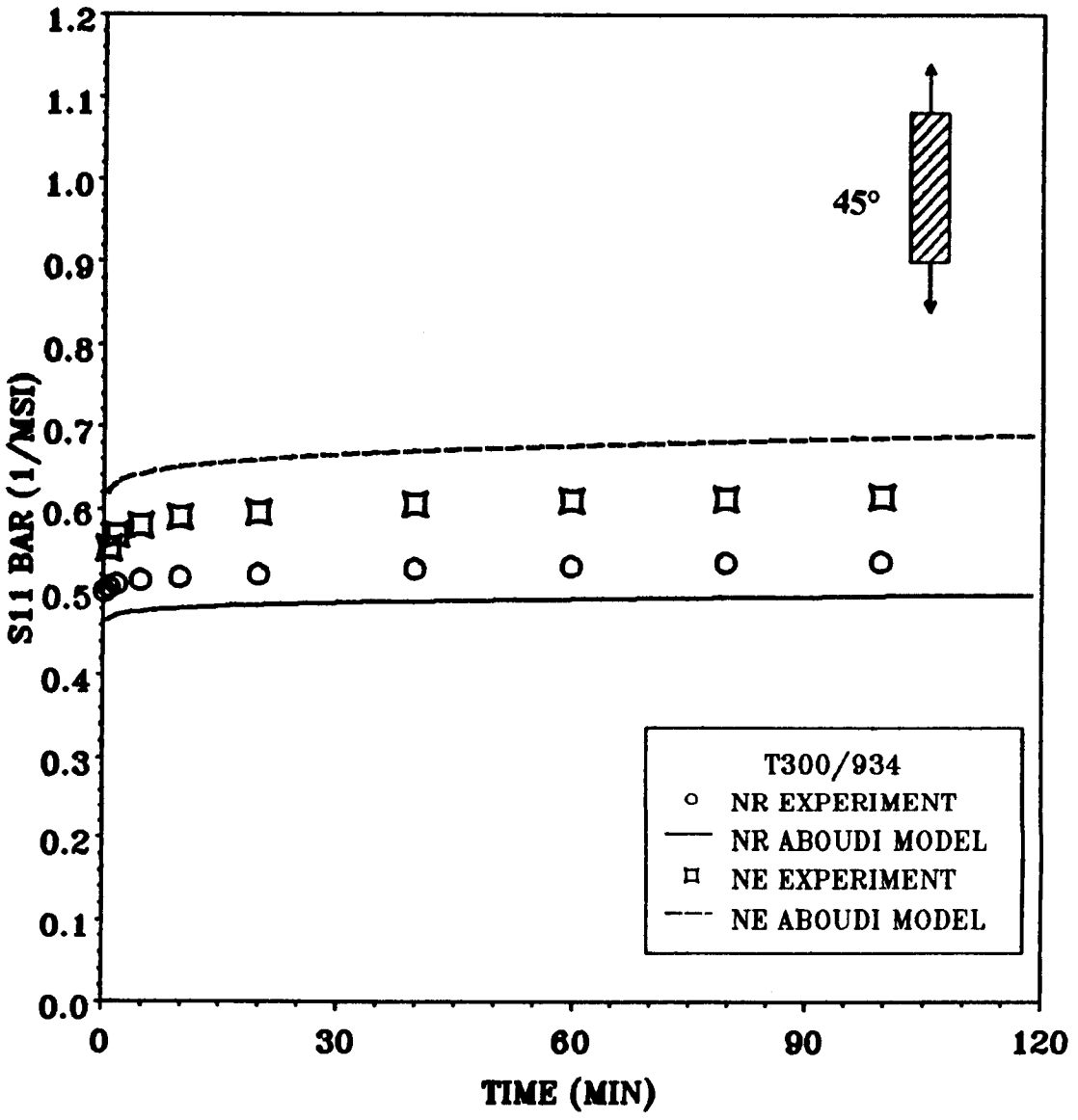

Figure 65. 45° Longitudinal Experimental-Analytical Co·relation

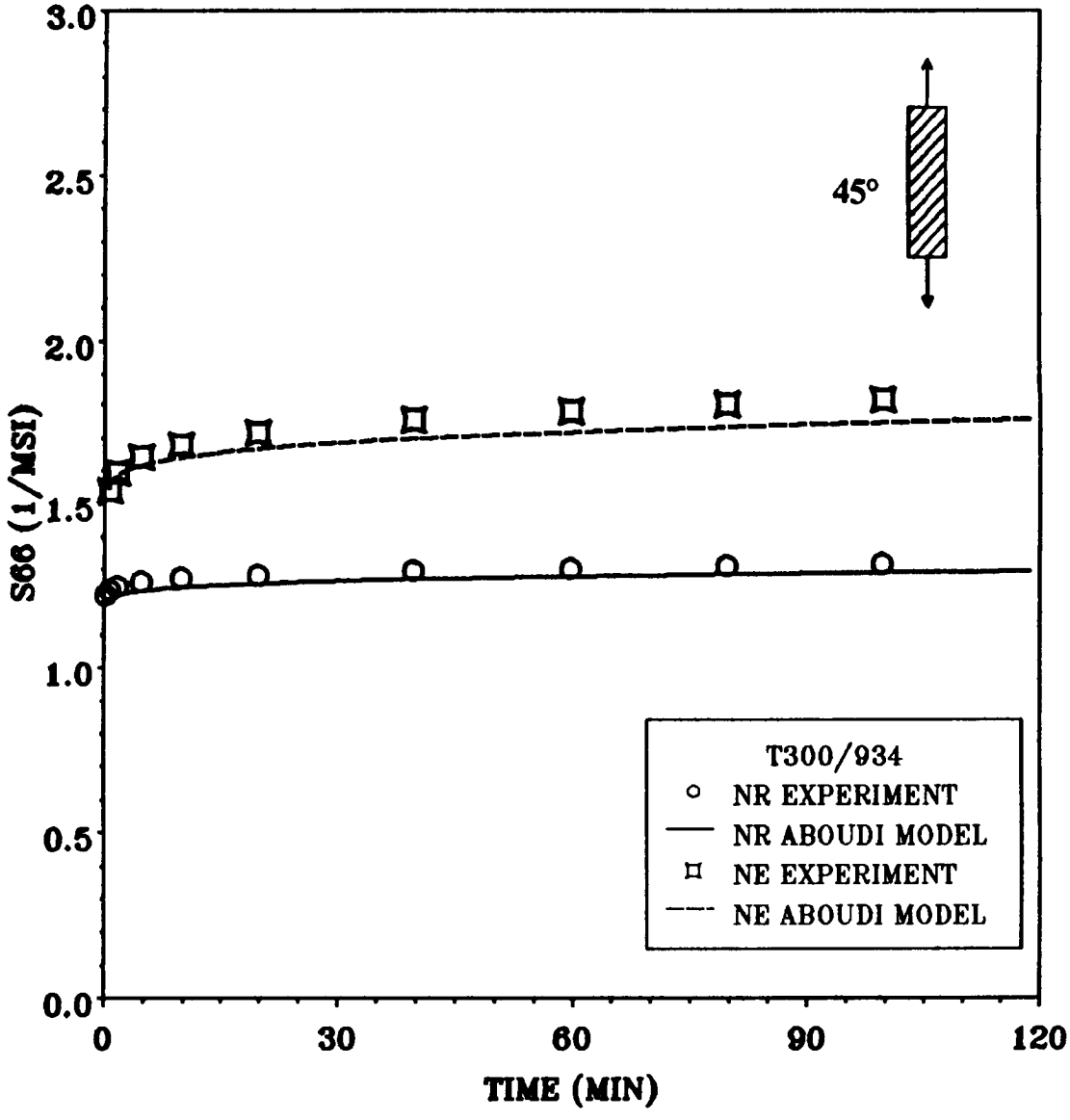

Figure 66. 45° Shear Experimental-Analytical Correlation

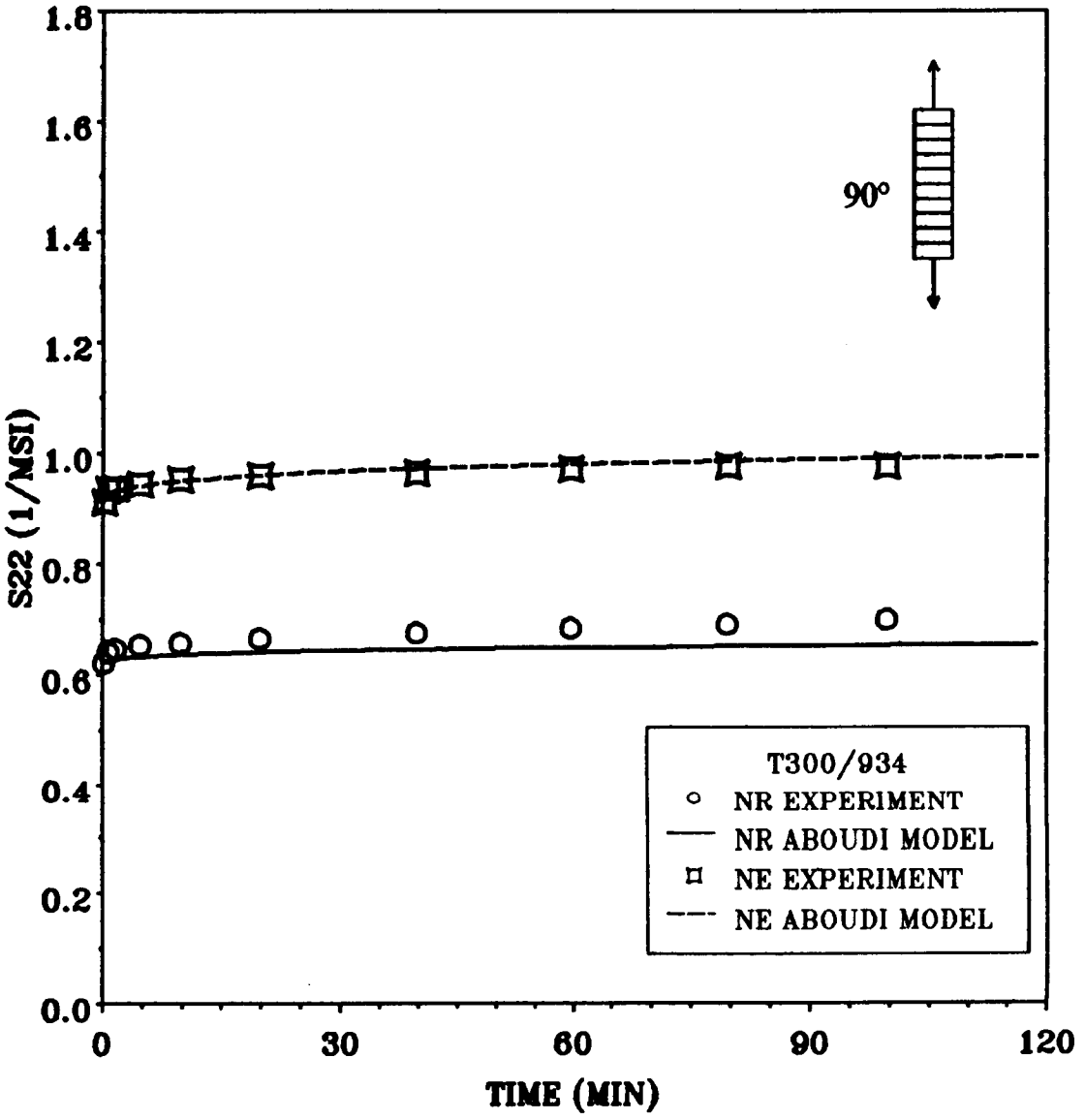

Figure 67. 90° Longitudinal Experimental-Analytical Correlation

tests are shown in Figure 68 through Figure 70. The 10° longitudinal results in Figure 68 show a reasonable correlation between experiment and the analytical model although it is not as good a correlation as seen for the NR and NE results. The 45° shear results in Figure 69 show a less accurate correlation between theory and experiment. The 90° longitudinal results in Figure 70 show a very poor correlation. In this case, the model significantly over-predicts the experimental result. The poor correlation may be due to the healing process which introduces complications in the assumption of linear viscoelasticity. The poor correlation may also be an indication that the rate of healing in the bulk resin is different than the rate of healing in the composite.

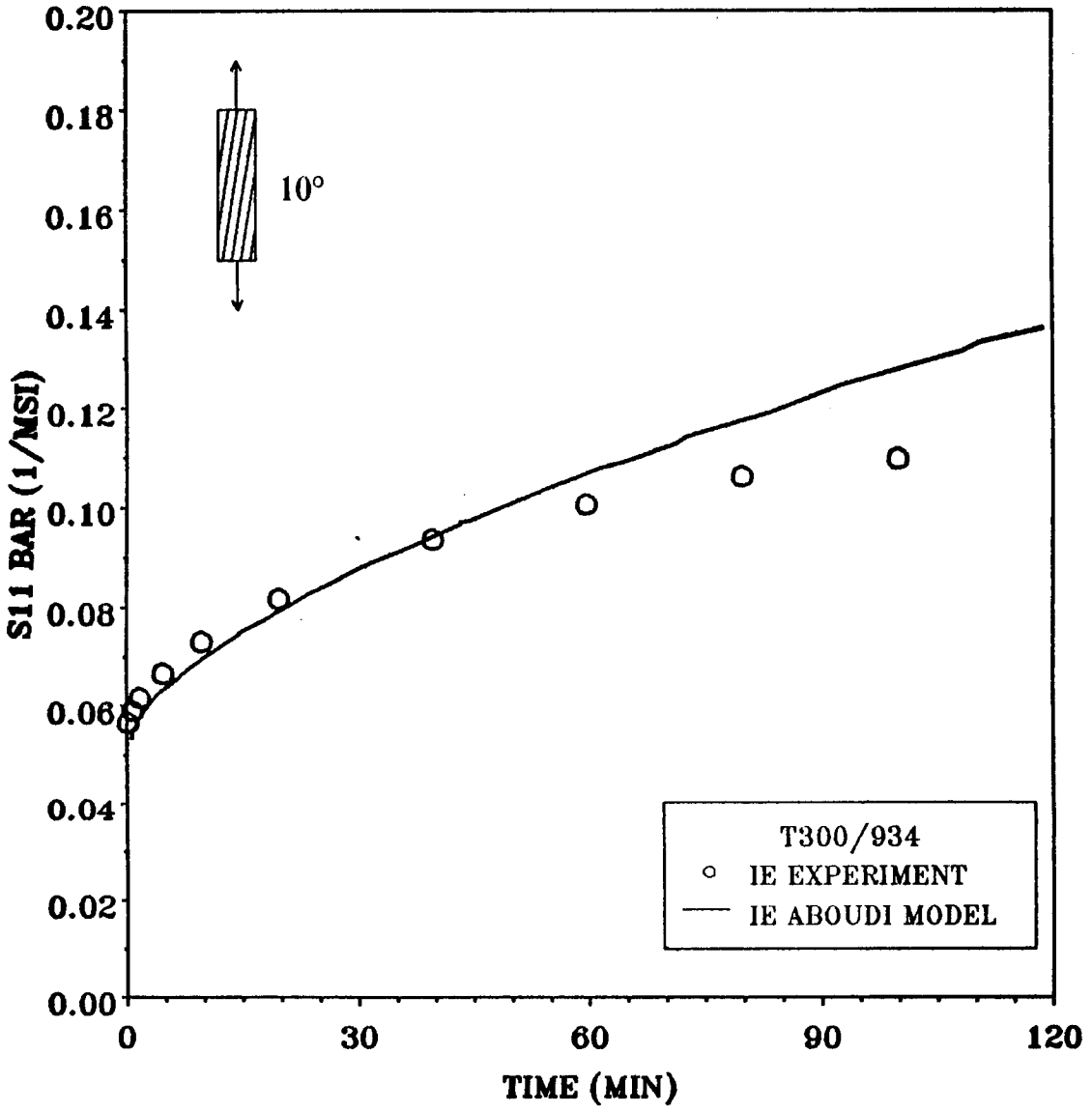

Figure 68. 10° IE Longitudinal Experimental-Analytical Correlation

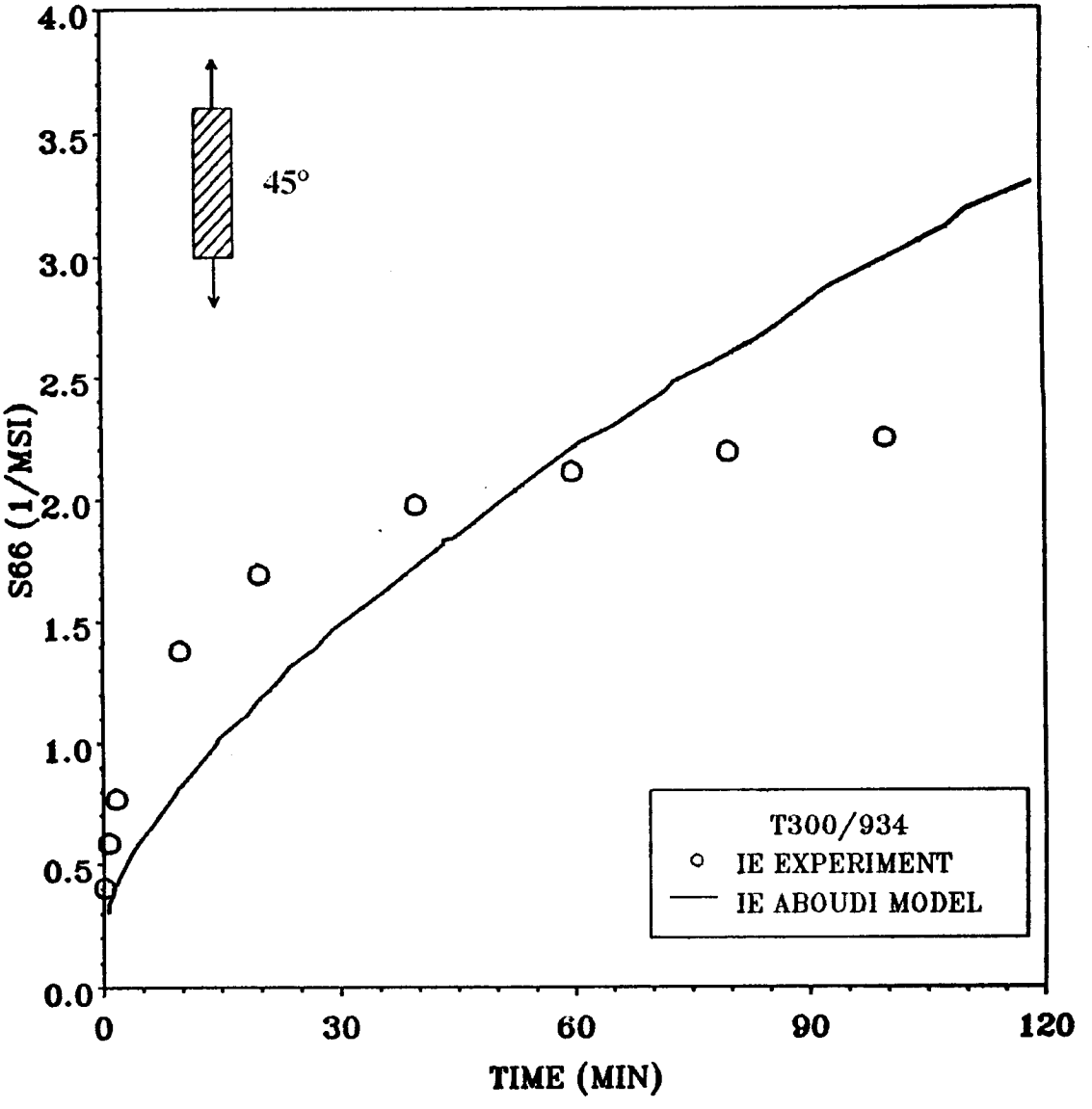

Figure 69. 45° IE Shear Experimental-Analytical Correlation

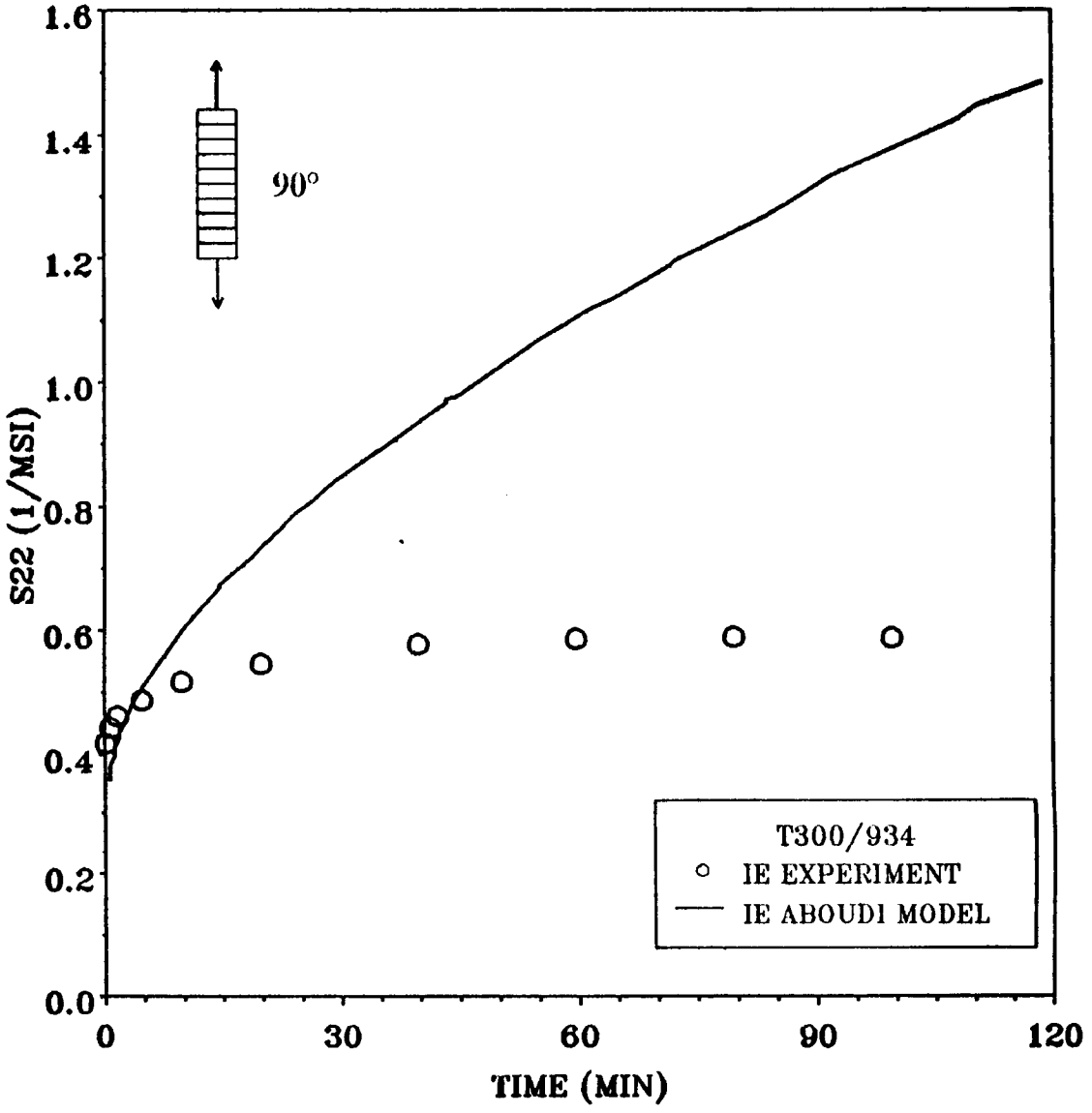

Figure 70. 90° IE Longitudinal Experimental-Analytical Correlation

6.0 Conclusions and Recommendations

The results of this study indicate that electron radiation has a significant effect on the time-dependent response of T300/934 graphite/epoxy at +250 °F, a temperature very near the glass transition temperature of the irradiated composite. Radiation-induced chain scission of the epoxy network allows for increased chain mobility near the glass transition temperature. Chain mobility increases the viscoelastic behavior of the composite and also permits free radicals and ionic centers broken off from molecular chains during irradiation to recombine and form cross-links. Over time, this recombination or healing restricts further chain mobility and therefore decreases subsequent viscoelastic behavior of the composite.

The following list summarizes the significant conclusions of this study.

- Radiation has little effect on the creep response of T300/934 graphite/epoxy at 72 °F.
- Radiation has a significant effect on the creep response of T300/934 graphite/epoxy at +250 °F.
- Healing of radiation induced chain scission in the 934 resin structure is observed at +250 °F.

- Only the the time-dependent behavior of the irradiated composite at + 250 °F is affected by healing. The elastic response is linear with time. It is hypothesized that radiation and healing affect only secondary bonds in the epoxy molecular network and that these conditions have no effect on the primary bonds of the molecular structure.

- Trends in the creep response of the bulk 934 resin are similar to the creep response of T300/934 graphite/epoxy under various conditions of temperature and radiation exposure.

- Creep is most pronounced in off-axis orientations of unidirectional T300/934 graphite/epoxy where a 1-2 shear stress is present.

- The micromechanical approach to viscoelasticity formulated in this study gives accurate predictions of the viscoelastic response for unidirectional fiber reinforced composites. The model correlates best with linearly viscoelastic behavior with relatively small creep strains. The model breaks down for the IE response when healing is present.

The following list outlines recommendations for further work in this area.

- Further evaluate the healing process in the irradiated 934 epoxy resin. Stress, temperature, and time dependence of healing effects need to be quantified by conducting additional tests under various conditions of the above parameters.

- Model the healing process to better predict the time-dependent response of the IE condition.

- Modify MICVIS to incrementally predict nonlinear viscoelastic behavior of fiber reinforced composite materials.

- Implement the Correspondence Principle with the Bellman Method to predict viscoelastic behavior of additional composite configurations such as laminates and tubes.

7.0 References

1. Tenney, D.R., Sykes, G.F., and Bowles, D.E., "Composite Materials for Space Structures", Proceedings of the Third European Symposium on Spacecraft Materials in Space Environments, October 1985, pp. 9-21.

2. Tenney, D.R., "Spacecraft Materials Research - A NASA Perspective", *Large Space Antenna Systems Technology - 1982*, Part 1, NASA CP-2269, pp. 213-239.

3. Lubin, G. and Dastin, S.J., "Aerospace Applications of Composites", *Handbook of Composites* G. Lubin, Ed., Von Nostland Reinhold Company, Inc., New York, pp. 722-743.

4. Hillesland, H.L., "Advance Composites Hardware Utilized on the Intelsat V Spacecraft", *SAMPE Symposium/Exhibition*, Vol. 24, pp. 202-211.

5. Archer, J.S. "High Performance Parabolic Antenna Reflectors", Proceedings AIAA 7th Communications Satellite Systems Conference, San Diego, CA, 24-27 April 1978, AIAA Paper No. 78-593, pp. 442-447.

6. Grounder, R.N., "Advanced Composite Antenna Reflectors for Communication Satellites", *SAMPE Journal* 19(3), pp. 11-14.

7. Qualls, J.P., "Graphite Epoxy Satellite Structure Development Program", National SAMPE Technical Conference, Vol. 14, pp. 513-520.

8. Ginty, C.A. and Chamis, C.C., "Select Fiber Composites for Space Applications : A Mechanistic Assessment", SAMPE 29th National Symposium, 3-5 April 1984, pp. 979-993.

9. Leung, C.L., "Space Environmental Effects on Graphite/Epoxy Composites", *Composites For Extreme Environments*, ASTM STP 768, N.R. Adsit, Ed., American Society for Testing and Materials, 1982, pp. 110-117.

10. Sykes, G.F., Slemp, W.S., "Space Radiation Effects on an Elastomer-Toughened Epoxy-Graphite Composite", 30th National Symposium/Exhibition Society for the Advancement of Materials and Process Engineering, 19-21 March, 1985, Anaheim, CA.

11. Sykes, G.F., Funk, J.G., and Slemp, W.S., "Assessment of Space Environment Induced Microdamage in Toughened Composite Materials", 18th International Technical Conference, Society for the Advancement of Materials and Process Engineering, 7-9 October, 1986, Seattle, WA.

12. Alfrey, T. Jr., *Mechanical Behavior of High Polymers*, Interscience Publishers, New York, 1948.

13. Turner, A. and Gurnee, E.F., *Organic Polymers*, Prentice-Hall Series in Materials Science, Englewood Cliffs, NJ, 1967.

14. Doolittle, A.K. and Doolittle, D.B., *Journal of Applied Physics*, Vol. 28, p. 373, 1957.

15. Ferry, J.D., *Viscoelastic Properties of Polymers*, John Wiley and Sons, New York, 1970.

16. Milkovich, S.M., Herakovich, C.T., and Sykes, G.F., "Space Radiation Effects on the Thermo-Mechanical Behavior of Graphite-Epoxy Composites", *Journal of Composite Materials*, Vol. 20, November 1986.

17. Bowles, D.E., Tompkins, S.S., and Sykes, G.F., "Electron Radiation Effects on the Thermal Expansion of Graphite/Resin Composites", AIAA 19th Thermophysics Conference, 25-28 June 1984, AIAA-84-1704.

18. Haskins, J.F., "Advanced Composite Design Data for Spacecraft Structural Applications", SAMPE 12th National Technical Conference, 7-9 October, 1980.

19. Tompkins, S.S., Sykes, G.F., and Bowles, D.E., "The Thermal and Mechanical Stability of Composite Materials for Space Structures", IEEE/ASM/ASME/SME Space Tech Conference, 23-25 September 1985, Anaheim, CA.

20. Chapiro, A., "Radiation Induced Polymerizations in the Vicinity of Glass Transition Temperatures", Proceedings of the Twenty-Second Nobel Symposium, 20-22 June 1972, Sodergarn, Lidingo, Sweden.

21. Tenney, D.R., Sykes, G.F., and Bowles, D.E., "Space Environmental Effects on Materials", AGARD Environmental Effects on Materials for Space Applications, Toronto, Canada, 22-24 September 1982.

22. Garrett, H.B., "Review of the Near-Earth Spacecraft Environment", SPIE, Vol. 216, Optics in Adverse Environments, 1980, pp. 109-115.

23. Reed, S.M., Herakovich, C.T., and Sykes, G.F., "Influence of Electron Radiation and Temperature on the Cyclic, Matrix Dominated Response of Graphite-Epoxy", *Journal of Composite Materials*, Vol. 21, July 1987.

24. Hagiwara, M., and Kagiya, T., "High Energy Degradation and Stabilization of Polymers", *Degradation and Stabilization of Polymers*, Jellinek, H.H.G., Ed., Elsevier, New York, 1983.

25. Fox, T.G., "Polymer Flow in Concentrated Solutions and Melts", *Structure and Properties of Polymers*, Tobolsky, A.F., Ed., John Wiley Interscience Publishers, New York, 1965.

26. Fox, D.J., Herakovich, C.T., and Sykes, G.F., "Degradation of Graphite-Epoxy Due to Electron Radiation", *ASME Journal of Engineering Materials Technology*, (in press 1988).

27. Milkovich, S.M., Sykes, G.F., and Herakovich, C.T., "Space Radiation Effects on Graphite/Epoxy Composite Materials", Interim Report 45, The NASA-Virginia Tech Composites Program, VPI-E-84-20, June 1984.

28. Reed, S.M., Herakovich, C.T., and Sykes, G.F., "The Effects of Space Radiation on a Chemically Modified Graphite/Epoxy Composite Material", Interim Report 60, The NASA-Virginia Tech Composites Program, VPI-E-86-19, October 1986.

29. Fox, D.J., Sykes, G.F., and Herakovich, C.T., "Space Environmental Effects on Graphite/Epoxy Compressive Properties and Epoxy Tensile Properties", Interim Report 63, The NASA-Virginia Tech Composites Program, VPI-E-87-13, July 1987.

30. D638-82a, "Standard Test Method for Tensile Properties of Plastics", *1984 Annual Book of ASTM Standards*, Section 8, Vol. 08.01, American Society for Testing and Materials, 1984, Philadelphia.

31. Micro-Measurements, M-Line Accessories, Instruction Bulletin B-137-11.

32. Signor, L.L., "The Effect of Temperature on the Creep Response of 934 Epoxy Resin", Senior Project Final Report, VPI, June 1987.

33. Hidde, J.S., Beuth, J.L. Jr., and Herakovich, C.T., "MATPACO v2.0: A PC-Based Software Package for Materials Testing", January 1988.

34. Tsai, S.W., *Composites Design*, Third Edition, Think Composites Publishers, Dayton, Ohio, 1987.

35. Christensen, R.M., *Theory of Viscoelasticity: An Introduction*, Second Edition, Academic Press, New York, 1982.

36. Hashin, Z., "Theory of Fiber-Reinforced Materials", NASA Contractor Report 1974, March 1972.

37. Aboudi, J., "A Continuum Theory For Fiber-Reinforced Elastic-Viscoplastic Composites", *International Journal of Engineering Science*, Vol. 20, No. 5, pp. 605-621, 1982.

38. Aboudi, J., "Closed Form Constitutive Equations for Metal Matrix Composites", *International Journal of Engineering Science*, Vol. 25, No. 9, pp. 1229-1240, 1987.

39. Pindera, M-J, and Aboudi, J., "Micromechanical Analysis of Yielding of Metal Matrix Composites", *International Journal of Plasticity* (1988 in press).

40. Pindera, M-J, Aboudi, J., and Herakovich, C.T., "Nonlinear Response of Boron/Aluminum Under Combined Loading", IUTAM/ICM Symposium on Yielding, Damage, and Failure of Anisotropic Solids, Grenoble, France, August 1987.

41. Bellman, R., Kalaba, R.E., and Lockett, J.A., *Numerical Inversion of the Laplace Transform*, American Elsevier Publishing Company, Inc., New York, 1966.

42. Hilldebrand, F.B., *Advanced Calculus for Applications*, Second Edition, Prentice-Hall, Inc., Englewood Cliffs, NJ, 1976.

43. Pindera, M-J, Lazarus, B.E., "Program User's Guide for VISCO: Evaluation of Effective Viscoelastic Properties", MSC TIR 1311, Materials Science Corporation, November 1982.

44. Christensen, R.M., *Mechanics of Composite Materials*, John Wiley and Sons, New York, 1979.

45. Hiel, C., Brinson, H.G., "The Nonlinear Viscoelastic Response of Resin Matrix Composite Laminates," VPI-E-83-6, Virginia Polytechnic Institute and State University, June 1984.

46. Pindera, M-J and Herakovich, C.T. "Shear Characterization of Unidirectional Composites with the Off-Axis Tension Test", *Experimental Mechanics*, Vol. 26, No. 1, pp. 103-112, March 1986.

Appendix A. Bellman Method

As discussed in Section 4.2, use of the Correspondence Principle can lead to a wide range of viscoelastic solutions from the corresponding elastic solutions. The difficulty arises in inverting the given expression in the Laplace Transform domain to the time domain. Except for very simple problems, the function

$$\bar{\sigma}_{ij}(s) = s\,\bar{C}_{ijkl}(s)\,\bar{\varepsilon}_{kl}(s) \tag{A.1}$$

will be a very complicated function of s. Inverting this is difficult and thus an approximate means of inverting these expressions to the time domain is typically employed. A method proposed by Bellman [41] has been chosen in this investigation. It is briefly outlined below.

A function u(t) is desired such that

$$F(s) = \int_0^\infty e^{-st} u(t)\,dt \tag{A.2}$$

where F(s) is a known function of the Laplace transform variable s. First, the integral in (A.2) is expressed as a finite sum of the form

$$\int_a^b f(x)dx \cong \sum_{i=1}^{N} w_i f(x_i) \tag{A.3}$$

where $f(x_i)$ are values of the function f(x) at the points x_i and w_i are the corresponding weight factors.

The next step is to express the function f(x) as a finite sum such that

$$f(x) = \sum_{k=0}^{N} b_k P_k(x) \tag{A.4}$$

where $P_k(x)$ are some known functions of x. The choice of $P_k(x)$ is the key here. Choosing $P_k(x)$ to be the Legendre polynomials of order k which are orthogonal polynomials helps to solve the problem. On the interval $[-1,1]$ this orthogonality condition states that

$$\int_{-1}^{1} P_m P_n dx = 0 \quad m \neq n \tag{A.5}$$

$$\int_{-1}^{1} P_n^2(x)dx = \frac{2}{(2n+1)} \tag{A.6}$$

Multiplying the function f(x) by $P_l(x)$ and integrating from $[-1,1]$ gives

$$\int_{-1}^{1} f(x)P_l(x)dx = \int_{-1}^{1} \left[\sum_{k=0}^{N} b_k P_k(x) P_l(x) \right] dx \tag{A.7}$$

By the orthogonality condition of (A.5) and (A.6) this reduces to

$$\int_{-1}^{1} f(x)P_l(x)dx = b_l \int_{-1}^{1} P_l^2(x)dx \qquad (A.8)$$

This gives

$$b_l = \frac{(2l+1)}{2}\int_{-1}^{1} f(x)P_l(x)dx \qquad (A.9)$$

Assuming now that the integration in (A.3) is evaluated on the interval $[-1,1]$ gives w_i and x_i. It is required that (A.3) be exact for *any* polynomial of degree less than or equal to 2N - 1 by a procedure proposed by Gauss.

Letting $f(x) = x^k P_N(x)$ in (A.2) gives

$$\int_{-1}^{1} x^k P_N(x)dx = \sum_{i=1}^{N} w_i x_i^k P_N(x_i) \qquad (A.10)$$

For k < N,

$$\int_{-1}^{1} x^k P_N(x)dx = 0 \qquad (A.11)$$

This results in

$$\sum_{i=1}^{N} w_i x_i^k P_N(x_i) = 0 \qquad (A.12)$$

For (A.12) to hold true, assuming that the x_i are distinct and the w_i are non-zero, the x_i must be the zeroes of $P_N(x)$. The zeroes of a Legendre polynomial are distinct.

To determine the weight factors, w_i , let the function f(x) in (A.3) be

$$f(x) = \frac{P_N(x)}{(x - x_i)P'_N(x_i)} \tag{A.13}$$

It can be seen that

$$f(x_j) = 0 \quad j \neq i \tag{A.14}$$

$$f(x_i) = 1 \quad j = i$$

Substituting this into (A.3) gives

$$w_i = \int_{-1}^{1} \frac{P_N(x)}{(x - x_i)P'_N(x_i)} \tag{A.15}$$

Using (A.15) gives a solution for $u(t)$ in (A.2). First, a change of variables is performed in (A.2) where $x = e^{-t}$. This results in

$$F(s) = \int_0^1 x^{s-1} u(-\log x)dx \tag{A.16}$$

Since the evaluation of the weights and zeroes of the Legendre polynomials are on the interval $[-1,1]$, a shifting to the interval $[0,1]$ is desired. This shifting is accomplished by simply letting

$$P^*_N(x) = P_N(1 - 2x) \tag{A.17}$$

where $P^*_N(x)$ are the shifted Legendre polynomials. This gives

$$x^*_i = 2(x_i - 1) \tag{A.18}$$

$$w^*_i = 2w_i \tag{A.19}$$

This shifting is done since the Legendre polynomials on the interval $[-1,1]$ are readily available [42].

Now applying the quadrature formula of (A.3) while setting the interval $[a,b]$ to [0,1] gives

$$\int_0^1 x^{s-1} u(-\log x)dx = \sum_{i=1}^{N} w_i x^{s-1} g(x_i) \qquad (A.20)$$

where $g(x_i) = u(-\log x)$. The x_i are the zeroes of the shifted Legendre polynomial of order N and the w_i are the weight factors as determined by (A.15) and (A.19). Since F(s) is a known function of s, u(t) can be evaluated by the formula

$$F(s) = \sum_{i=1}^{N} w_i x^{s-1} g(x_i) \qquad (A.21)$$

Letting s assume N different values, say s = 1,2,....,N, yields a linear system of equations in the N unknowns, $g(x_i)$, i = 1,2,....N. This system of equations can be readily solved.

Bellman further develops this approach by obtaining an explicit inversion formula. This eliminates the need to invert the N by N matrix obtained by (A.21) for each specific solution. This procedure can be studied in more detail in Bellman [41]. Bellman obtains the N by N matrix Q_{ij} so that

$$g(x_i) = Q_{ij} F(j) \quad i, j = 1,2,3,....,N \qquad (A.22)$$

The values for this matrix Q_{ij} have been calculated to sixteen places by Bellman and are listed in Bellman [41].

Since this method is restricted to the time scale of $t = -\log x_i$, a multiplicative factor can be used such that

$$\frac{F(s/a)}{a} = \sum_{i=1}^{N} w_i x^{s-1} u(-a \log x_i) \qquad (A.23)$$

This allows one to obtain the values of u(t) at any given time t and still use the same inversion matrix Q_{ij}, thus eliminating the need to repeat the entire procedure from the beginning.

Appendix B. MICVIS User's Guide

B.1 Introduction

MICVIS is a FORTRAN program written to evaluate the effective viscoelastic properties of a unidirectional composite material. These properties are calculated using the properties of the constituent materials as input assuming a perfectly elastic, transversely isotropic fiber and an isotropic, viscoelastic matrix with a time-independent Poisson's ratio. The program can be easily modified to take into account a viscoelastic fiber and/or a varying Poisson's ratio. These properties, however, were not needed for the problem this program was intended to solve and the reader can modify this program if so desired to meet these conditions.

The user needs to have the following information for input:

Fiber

- E_A = Axial Young's Modulus
- E_T = Transverse Young's Modulus
- ν_A = Axial Poisson's Ratio

- v_T = Transverse Poisson's Ratio
- G_A = Axial Shear Modulus

Matrix

- E_A = Axial Young's Modulus
- v_A = Axial Poisson's Ratio
- C , n = Parameters for Power-Law Model
- E_1 , λ , μ_0 = Parameters for Four-Parameter Model

Other Input

- V_f = Fiber Volume Fraction
- Γ = Gamma Function evaluation for exponent n

The output of the program gives the effective creep compliances of the composite:

Output

- $S_{11}(t)$ = *Axial Creep Compliance*
- $S_{12}(t)$ = *Axial Poisson Creep Compliance*
- $S_{22}(t)$ = *Transverse Creep Compliance*
- $S_{44}(t)$ = *Transverse Shear Creep Compliance*
- $S_{66}(t)$ = *Axial Shear Creep Compliance*

This program is based on the elastic-viscoelastic Correspondence Principle. Two elastic micromechanical models developed by Aboudi [37] and Hashin [36] respectively are converted to the viscoelastic time domain by use of the Correspondence Principle [35]. A Laplace Transform inversion scheme developed by Bellman is used to make this conversion. Two different models are employed to characterize the viscoelastic behavior of the matrix, namely the Power-Law Model and the Four-Parameter Model. These procedures can be found in Chapter 4.0.

MICVIS calls one of two subroutines, ABOUDEXP or HASHEXP. ABOUDEXP is the Aboudi Model and calls the subroutine ABOUDI. HASHEXP is the Hashin Model and calls the subroutine HASHIN. ABOUDEXP and HASHEXP are very similar but ABOUDI and HASHIN are not. ABOUDI and HASHIN contain the mathematical formulations of the respective models.

B.2 Input Description

Following is a description of each line of input that must be entered into a data file before running MICVIS. Figure 71 shows a sample input file.

Line 1 Composite Material Description (50 characters long)

Line 2 Volume Fraction Description (50 characters long)

Line 3 Date (50 characters long)

Line 4 IMULT - Multiplication factor 'a' to determine to what time increment to calculate u(t). Gives the maximum 'a' used in equation (A.23) and also the number of times this process should be carried out for a = 1,2,....,IMULT.

Line 5 IOPT - Option to use Power-law model or Four-parameter model.

IOPT = 0 - Power-Law Model

IOPT = 1 - Four-Parameter Model

Line 6 N - order of Legendre polynomial to be used. N = 5,10,15.

Line 7 VF - Fiber Volume Fraction, $0 < VF < 1$

Line 8 EAF , GNUAF , ETF , GNUTF , GAF

EAF = Fiber Axial Young's Modulus

GNUAF = Fiber Axial Poisson's Ratio

ETF = Fiber Transverse Young's Modulus

GNUTF = Fiber Transverse Poisson's Ratio

GAF = Fiber Axial Shear Modulus

Line 9 D0 , EXP1 , C , GNUAM

D0 = D_0 in Power-Law Model

EXP1 = n in Power-Law Model

C = C in Power-Law Model

GNUAM = Matrix Poisson's Ratio

Line 10 GAMMA - Gamma function evaluated for (n + 1)

Line 11 E11M , LAM , MU10

E11M = E_1 in Four-Parameter Model

LAM = λ in Four-Parameter Model

MU10 = μ_0 in Four-Parameter Model

Line 12 + First the poles of the Legendre polynomial of order N and then the elements of the matrix Q_{ij} entered by row with each row preceded by the row number. Parameters used with Bellman Method.

```
**  GLASS FIBERS AND EPOXY MATRIX                **
**  FIBER VOLUME FRACTION (VF) = 0.6             **
**  14 OCTOBER 1987                              **
5
1
5
6.0D-01
1.24D+07  2.0D-01  1.24D+07  2.0D-01  5.16667D+06
5.6313D-07  3.10D-01  1.881D-07  3.0D-01
8.96D-01
4.37D+06  6.405D-01  3.9246D+08
4.6910077030668073E-02
2.3076534494715854E-01
5.0000000000000000E-01
7.6923465505284136E-01
9.5308992296933192E-01
1
 1.3096091215873584E+01
-1.1370836617381254E+02
 3.2621455387960418E+02
-3.7977104240584473E+02
 1.5481333922979571E+02
2
-3.7321558320700493E+00
 9.5791727360612028E+01
-3.6864824974282344E+02
 4.9250461742576776E+02
-2.1703556145201710E+02
3
 1.8750000000000001E+00
-5.2500000000000000E+01
 2.8874999999999997E+02
-4.7249999999999996E+02
 2.3624999999999998E+02
4
-1.1196222405308258E+00
 3.2133165655799880E+01
-1.9334776617762277E+02
 3.7563762838230071E+02
-2.1703556145201714E+02
5
 6.4457574561629890E-01
-1.8660971287044596E+01
 1.1578146204084460E+02
-2.3948231451333832E+02
 1.5481333922979571E+02
```

Figure 71. Sample Input File for MICVIS

B.3 Output Description

The output comes with a Program Identification Block, a Problem Identification Block, and the values for the calculated compliances at the given times. A sample output for the Hashin Model is shown in Figure 72. A U or an L appearing after the compliance value denotes an upper and lower bound respectively. Figure 73 gives a sample output for the Aboudi Model.

```
**************************************************
**                    MICVIS                    **
**                  HASHIN MODEL                **
**        VISCOELASTIC CREEP COMPLIANCES        **
**             LAPLACE INVERSION BY             **
**              THE BELLMAN METHOD              **
**                                              **
**                PROGRAMMED BY                 **
**              ROBERT N. YANCEY                **
**                OCTOBER 1987                  **
**************************************************
```

```
**************************************************
**  GLASS FIBERS AND EPOXY MATRIX               **
**  FOUR-PARAMETER MODEL                        **
**  FIBER VOLUME FRACTION (VF) = 0.6            **
**  14 OCTOBER 1987                             **
**************************************************
```

EFFECTIVE CREEP COMPLIANCES IN (1/MSI)

TIME	S11	S12	S22U	S22L	S44U	S44L	S66
0.05	0.1228	-.0288	0.1820	0.2261	0.5996	0.4228	0.5465
0.10	0.1230	-.0288	0.1829	0.2280	0.6049	0.4243	0.5509
0.14	0.1231	-.0288	0.1838	0.2299	0.6102	0.4256	0.5553
0.19	0.1232	-.0289	0.1847	0.2318	0.6153	0.4269	0.5596
0.24	0.1233	-.0289	0.1855	0.2336	0.6202	0.4282	0.5638
0.26	0.1234	-.0289	0.1859	0.2342	0.6220	0.4287	0.5653
0.52	0.1239	-.0290	0.1900	0.2429	0.6461	0.4347	0.5855
0.69	0.1242	-.0291	0.1923	0.2479	0.6601	0.4380	0.5972
0.79	0.1243	-.0291	0.1934	0.2501	0.6664	0.4396	0.6025
1.05	0.1246	-.0292	0.1963	0.2563	0.6836	0.4435	0.6170
1.31	0.1249	-.0292	0.1987	0.2616	0.6983	0.4467	0.6293
1.39	0.1250	-.0293	0.1994	0.2631	0.7026	0.4476	0.6329
1.47	0.1250	-.0293	0.1999	0.2642	0.7056	0.4483	0.6354
2.08	0.1254	-.0294	0.2038	0.2731	0.7306	0.4532	0.6563
2.77	0.1257	-.0294	0.2066	0.2798	0.7491	0.4565	0.6718
2.93	0.1257	-.0294	0.2070	0.2806	0.7515	0.4569	0.6738
3.06	0.1258	-.0294	0.2076	0.2822	0.7559	0.4575	0.6775
3.47	0.1258	-.0294	0.2085	0.2842	0.7614	0.4585	0.6821
4.40	0.1259	-.0295	0.2098	0.2876	0.7708	0.4598	0.6899
5.87	0.1260	-.0295	0.2111	0.2908	0.7800	0.4611	0.6976
6.12	0.1260	-.0295	0.2116	0.2920	0.7832	0.4615	0.7003
7.33	0.1261	-.0295	0.2119	0.2927	0.7853	0.4617	0.7020
9.18	0.1261	-.0295	0.2130	0.2955	0.7930	0.4629	0.7085
12.24	0.1262	-.0295	0.2140	0.2981	0.8002	0.4640	0.7145
15.30	0.1263	-.0296	0.2150	0.3005	0.8070	0.4651	0.7202

Figure 72. Sample Output for Hashin Model

```
**********************************************
**                  MICVIS                    **
**                ABOUDI MODEL                **
**        VISCOELASTIC CREEP COMPLIANCES      **
**             LAPLACE INVERSION BY           **
**              THE BELLMAN METHOD            **
**                                            **
**                PROGRAMMED BY               **
**              ROBERT N. YANCEY              **
**                OCTOBER 1987                **
**********************************************
```

```
**********************************************
**  GLASS FIBERS AND EPOXY MATRIX             **
**  FOUR-PARAMETER MODEL                      **
**  FIBER VOLUME FRACTION (VF) = 0.6          **
**  14 OCTOBER 1987                           **
**********************************************
```

EFFECTIVE CREEP COMPLIANCES IN (1/MSI)

TIME	S11	S12	S22	S44	S66
0.05	0.1228	-.0288	0.2230	0.5831	0.5708
0.10	0.1229	-.0288	0.2249	0.5880	0.5757
0.14	0.1230	-.0289	0.2267	0.5929	0.5805
0.19	0.1231	-.0289	0.2284	0.5976	0.5852
0.24	0.1232	-.0289	0.2301	0.6021	0.5897
0.26	0.1233	-.0289	0.2307	0.6038	0.5913
0.52	0.1238	-.0291	0.2390	0.6259	0.6134
0.69	0.1241	-.0291	0.2438	0.6387	0.6261
0.79	0.1242	-.0291	0.2459	0.6446	0.6319
1.05	0.1246	-.0292	0.2518	0.6603	0.6476
1.31	0.1249	-.0293	0.2568	0.6737	0.6610
1.39	0.1249	-.0293	0.2582	0.6777	0.6649
1.47	0.1250	-.0293	0.2593	0.6804	0.6676
2.08	0.1254	-.0294	0.2678	0.7032	0.6905
2.77	0.1256	-.0294	0.2740	0.7201	0.7073
2.93	0.1257	-.0295	0.2749	0.7222	0.7095
3.06	0.1257	-.0295	0.2764	0.7262	0.7135
3.47	0.1258	-.0295	0.2782	0.7313	0.7186
4.40	0.1259	-.0295	0.2814	0.7398	0.7271
5.87	0.1260	-.0295	0.2845	0.7481	0.7355
6.12	0.1260	-.0295	0.2856	0.7510	0.7384
7.33	0.1260	-.0295	0.2863	0.7529	0.7403
9.18	0.1261	-.0295	0.2889	0.7599	0.7474
12.24	0.1262	-.0296	0.2914	0.7664	0.7539
15.30	0.1263	-.0296	0.2937	0.7726	0.7601

Figure 73. Sample Output for Aboudi Model

Appendix C. Elastic Properties

Following are a list of tables showing the composite and bulk resin elastic properties as evaluated in this study. Also given are tables showing the elastic properties as determined by Milkovich, et al. [16], Reed, et al. [23], and Fox, et al. [26]. It should be kept in mind that the resin system used by Reed is slightly different than the resin system used in this study or in Milkovich, et al. [16].

Table 11. Composite Elastic Properties

	Composite Properties (Yancey)			
	Condition			
Property	NR	IR	NE	IE
Axial Modulus (MSI)	18.55	18.01	19.55	19.53
Axial Poisson's	0.399	0.361	0.400	0.400
Transverse Modulus (MSI)	1.60	1.46	1.14	1.16
Axial Shear Modulus (MSI)	0.792	0.880	0.687	0.650

	Composite Properties (Milkovich)			
	Condition			
Property	NR	IR	NE	IE
Axial Modulus (MSI)	18.88	19.31	19.03	19.76
Axial Poisson's	0.314	0.283	0.345	0.397
Transverse Modulus (MSI)	1.38	1.52	1.24	1.06
Axial Shear Modulus (MSI)	0.688	0.777	0.563	0.397

	Composite Properties (Reed)			
	Condition			
Property	NR	IR	NE	IE
Axial Modulus (MSI)	21.00	20.60	22.20	23.60
Axial Poisson's	0.345	0.312	0.355	0.371
Transverse Modulus (MSI)	1.23	1.51	1.18	0.88
Axial Shear Modulus (MSI)	0.683	0.752	0.569	0.422

Table 12. Bulk Resin Elastic Properties

	Bulk Resin Properties (Yancey)			
	Condition			
Property	NR	IR	NE	IE
Axial Modulus (MSI)	0.654	0.870	0.488	0.461
Axial Poisson's	0.311	0.407	0.317	0.328
Axial Shear Modulus (MSI)	0.225	0.309	0.185	0.174

	Bulk Resin Properties (Fox)			
	Condition			
Property	NR	IR	NE	IE
Axial Modulus (MSI)	0.674	0.799	0.489	0.501
Axial Poisson's	0.363	0.373	0.341	0.368
Axial Shear Modulus (MSI)	0.247	0.291	0.182	0.183

BIBLIOGRAPHIC DATA SHEET	1. Report No. CCMS-88-02; VPI-E-88-5	2.	3. Recipient's Accession No.

4. Title and Subtitle
RADIATION AND TEMPERATURE EFFECTS ON THE TIME-DEPENDENT RESPONSE OF T300/934 GRAPHITE/EPOXY

5. Report Date March 1988

6.

7. Author(s)
Robert N. Yancey and Marek-Jerzy Pindera

8. Performing Organization Rept. No. VPI-E-88-5

9. Performing Organization Name and Address
Virginia Polytechnic Institute & State University
Dept of Engineering Science and Mechanics
Blacksburg, Virginia 24061-0219

10. Project/Task/Work Unit No.

11. Contract/Grant No. NAG-1-343

12. Sponsoring Organization Name and Address
Applied Materials Branch
National Aeronautics and Space Administration
Langley Research Center
Hampton, Virginia 23665

13. Type of Report & Period Covered

14.

15. Supplementary Notes

16. Abstracts
A time-dependent characterization study was performed on T300/934 graphite-epoxy in a simulated space environment. Creep tests on irradiated and non-irradiated graphite/epoxy and bulk resin specimens were carried out at temperatures of 72°F and 250°F. Irradiated specimens were exposed to dosages of penetrating electron radiation equal to 30 years exposure at GEO-synchronous orbit. Radiation was shown to have little effect on the creep response of both the composite and bulk resin specimens at 72°F while radiation had a significant effect at 250°F. A healing process was shown to be present in the irradiated specimens where broken bonds in the epoxy due to radiation recombined over time to form cross-links in the 934 resin structure. An analytical, micromechanical model was also developed to predict the viscoelastic response of fiber reinforced composite materials. The model was shown to correlate well with experimental results for linearly viscoelastic materials with relatively small creep strains.

17. Key Words and Document Analysis. 17a. Descriptors

composites, graphite/epoxy, radiation, temperature, time-dependent, viscoelasticity, creep, recovery, healing, micromechanics, Correspondence Principle, Laplace Transform

17b. Identifiers/Open-Ended Terms

17c. COSATI Field/Group

18. Availability Statement	19. Security Class (This Report) UNCLASSIFIED	21. No. of Pages 168
	20. Security Class (This Page UNCLASSIFIED	22. Price